



**HAL**  
open science

# Analytic application of the mean crossover function to the description of the isothermal compressibility of xenon

Yves Garrabos, Carole Lecoutre-Chabot, Fabien Palencia

## ► To cite this version:

Yves Garrabos, Carole Lecoutre-Chabot, Fabien Palencia. Analytic application of the mean crossover function to the description of the isothermal compressibility of xenon. 2007. hal-00165475

**HAL Id: hal-00165475**

**<https://hal.science/hal-00165475>**

Preprint submitted on 26 Jul 2007

**HAL** is a multi-disciplinary open access archive for the deposit and dissemination of scientific research documents, whether they are published or not. The documents may come from teaching and research institutions in France or abroad, or from public or private research centers.

L'archive ouverte pluridisciplinaire **HAL**, est destinée au dépôt et à la diffusion de documents scientifiques de niveau recherche, publiés ou non, émanant des établissements d'enseignement et de recherche français ou étrangers, des laboratoires publics ou privés.

# Analytic application of the mean crossover function to the description of the isothermal compressibility of xenon

Yves Garrabos, Carole Lecoutre, Fabien Palencia

*Equipe du Supercritique pour l'Environnement, les Matériaux et l'Espace  
- Institut de Chimie de la Matière Condensée de Bordeaux - UPR 9048,  
Centre National de la Recherche Scientifique - Université Bordeaux I - 87,  
avenue du Docteur Schweitzer, F 33608 PESSAC Cedex, France*

(Dated: 24 July 2007)

We use the mean crossover functions [Garrabos and Bervillier, Phys. Rev. E **74**, 021113 (2006)] estimated from the bounded results of the Massive Renormalization scheme applied to the  $\Phi_d^4(n)$  model in three dimensions ( $d = 3$ ) and scalar order parameter ( $n = 1$ ) [Bagnuls and Bervillier, Phys. Rev. E **65**, 066132 (2002)], to represent the singular behavior of the isothermal compressibility of xenon along the critical isochore in the homogeneous preasymptotic domain. The validity range and the Ising nature of the crossover description are discussed in terms of a single scale factor whose value can be analytically estimated *beyond* the Ising-like preasymptotic domain.

PACS numbers: 64.60.Ak., 05.10.Cc., 05.70.Jk, 65.20.+w

## 1. INTRODUCTION

The Ising-like nature of the universal features of the one-component fluids close to their vapor-liquid critical point is now well-established (author?) [1]. These universal features can be estimated by using a renormalization approach (author?) [2] of the classical-to-critical crossover behavior (author?) [3] for three-dimensional (3D) Ising-like systems with a symmetrical order parameter density. Especially, the massive renormalization scheme (author?) [4, 5, 6] applied to the  $\Phi_{d=3}^4(n = 1)$  model ( $d$  and  $n$  are the dimensions of the space and order parameter density, respectively), has been recently revisited (author?) [7] to provide max and min crossover functions which include updated estimations (author?) [8] of the universal values for exponents and amplitude combinations. Subsequently, a related paper (author?) [9] has provided a unique universal form of the mean crossover functions, which enabled asymptotic description of the universal features valid within the *Ising-like preasymptotic domain* exactly, by eliminating the increasing uncertainties associated with the asymptotic error-bar propagation in the initial min and max estimations of the critical exponents.

These crossover functions have been used to analyze for example, the singular behavior of the correlation length of seven pure fluids in their homogeneous domain (author?) [10] or the singular behavior of the squared capillary length of twenty pure fluids in their non-homogeneous domain (author?) [11]. For both cases, it was shown that the scale dilatation method proposed by one of us (author?) [12, 13, 14, 15, 16] gives a corresponding master singular behavior for the one-component fluid subclass which agrees with a description by an appropriate modification of the theoretical function (author?) [17] within the Ising-like preasymptotic domain. As a matter of fact, such an exact behavior of each theoretical function, approximated by a two-term Wegner-like expansion (author?) [18] close to the non-

trivial fixed point, is an essential tool to provide better understanding of the basic relations between the “measured” asymptotic amplitudes and the unknown (fluid-dependent) scale factors introduced by linear approximations between bare fields and physical fields (author?) [19]. From the analogy with the scale dilatation method which relates the master fields to the physical fields introducing two well-defined critical parameters of each fluid, it was then recently proposed (author?) [17] an unambiguous modification of the mean theoretical functions to represent the master crossover for the one-component fluid subclass (labeled  $\{1f\}$ ) in conformity with the corresponding universal features of the Ising-like universality class (labeled  $\Phi_3(1)$ ). In the following, the theoretical functions (valid for any three-dimensional Ising-like system) estimated in Ref. (author?) [9] are called *mean* crossover functions and the related reference (author?) [9] is labeled I, while their modification (only valid for the one-component fluids) proposed in Ref. (author?) [17] are called *master* crossover functions and the related Ref. (author?) [17] is labeled II.

The validity range of the mean crossover functions is theoretically funded only *within* the Ising-like preasymptotic domain (i.e. for  $t \lesssim \mathcal{L}_{\text{PAD}}^{\text{Ising}}$ , where  $t$  is the thermal-like field along the critical isochore, i.e. for  $h = 0$ , where  $h$  is the magnetic-like field, see II). Especially, the uniqueness of the asymptotic scale factor, which acts as a crossover parameter along the critical isochore, has never been clearly demonstrated for the effective extended asymptotic domain where the mean crossover functions fit correctly the experimental results. The main goal of the present paper addresses to the explicit calculation of this single crossover parameter using the mean crossover functions *beyond* the Ising-like preasymptotic domain.

We consider in detail the singular behavior of the isothermal compressibility  $\kappa_T(\Delta\tau^*)$  and the correlation length  $\xi(\Delta\tau^*)$  of xenon as a function of the reduced temperature distance  $\Delta\tau^* = \frac{T-T_c}{T_c}$ , along the critical

isochore, in the homogeneous domain  $T > T_c$ , [ $T$  ( $T_c$ ) is the temperature (critical temperature)]. Xenon is here selected as a standard “critical fluid” in the sense that the present work only uses quantities which originate from theoretical arguments, now well-understood, to link three independent dimensionless amplitudes to the needed three scale factors (author?) [20]. As a matter of fact, the fit of susceptibility and correlation length data obtained by Güttinger and Cannell (author?) [21] from their precise turbidity measurements in the temperature range  $0.028 K \leq T - T_c \leq 29 K$ , can then be used as representative of an “ideal” result in order to check carefully the temperature range where the value (and its attached uncertainty) of the scale factor characteristic of the thermal field is effectively determined. This singular behavior was first analyzed (author?) [22], jointly with singular behaviors of the correlation length (author?) [21] and the heat capacity (author?) [23], using precisely the initial estimations (author?) [4] of the crossover functions from the massive renormalization scheme. In addition to the experimental critical temperature  $T_c$  ( $\simeq 289.74 K$ ), pressure  $p_c$  ( $\simeq 5.84 MPa$ ), and density  $\rho_c$  ( $\simeq 1110 kg m^{-3}$ ), for the first time a minimal quantity made of three Ising-like non-universal parameters of xenon was introduced as a set of a single critical wavelength (noted  $g_0$ ) and two dimensionless scale factors (noted  $\vartheta$  and  $\psi$ ) for the thermal-like ( $t$ ) and magnetic-like ( $h$ ) fields, respectively, with the analytical relations  $t = \vartheta \Delta\tau^*$  and  $h = \psi_\rho \Delta\tilde{\mu}$  valid for the asymptotic limits  $t \rightarrow 0$  and  $h \rightarrow 0$  (author?) [19, 22].  $\Delta\tilde{\mu}$  is the standard notation of the dimensionless ordering field in the fluid case (author?) [24], which is related to the chemical potential difference to the critical chemical potential [see below Eq. (16)]. In the following, when we refer to this initial result obtained by fitting the experimental data with the (max) crossover functions estimated for the sixth-order, we will use the label MR6<sub>max</sub> (author?) [4, 5].

Now, using the updated mean crossover functions given in I, the main objective is to replace the fitting adjustment of the fluid-dependent parameters  $g_0$ ,  $\vartheta$ , and  $\psi_\rho$ , by their exact asymptotical values defined in II, only introducing three master numbers (noted  $\Theta^{\{1f\}}$ ,  $\mathbb{L}^{\{1f\}}$ , and  $\Psi^{\{1f\}}$ ) which are characteristics of the  $\{1f\}$ -subclass (see II). In that scheme,  $g_0$ -,  $\vartheta$ -, and  $\psi_\rho$ -values originate from calculations of the three fluid-dependent amplitudes  $\xi_0^+$ ,  $\Gamma^+$ , and  $a_\chi^+$  (in standard notations (author?) [24, 25]), using the scale dilatation method where each fluid is characterized by only four well-defined critical point coordinates. Such results account for the master singular behavior of the  $\{1f\}$ -subclass observed *within* the Ising-like preasymptotic domain bounded by a known limit (defined as  $\mathcal{L}_{PAD}^{\{1f\}} = \frac{\mathcal{L}_{PAD}^{Ising}}{\Theta^{\{1f\}}}$  in II), in conformity with the two-scale factor-universality of the  $\Phi_3$  (1)-universality class. As a main result explicited below [see Eqs. (35) and (40)], we unambiguously probe that the temperature range  $\Delta\tau_{min}^* < \Delta\tau^* < \Delta\tau_{max}^*$  covered by the Güttinger and Cannell’s experiments is beyond the Ising-like preasymptotic

domain, i.e.  $\Delta\tau_{min}^* (\simeq 10^{-4}) > \frac{\mathcal{L}_{PAD}^{Ising}}{\vartheta}$ .

Moreover, after the initial analysis of Ref. (author?) [22], the Güttinger and Cannell’s xenon data were also used (author?) [26, 27, 28, 29, 30] in support for discussion of several theoretical (author?) [31, 32, 33, 34, 35] and phenomenological (author?) [36, 37, 38, 39, 40] approaches of the crossover phenomena. As an essential common result, a single temperature-like crossover parameter seems appropriate for a complete characterization of the classical-to-critical crossover in pure fluids, whatever the selected crossover theory or the phenomenological approach (for comparative analyses, see for example Ref. (author?) [1] and references therein). However, the theoretical understanding in terms of a Ising-like critical crossover characterized by the asymptotic value of the scale factor  $\vartheta$  appears limited for two main reasons: i) the fitted data are not within the Ising-like preasymptotic domain; ii) any crossover function is only well-defined within the Ising-like preasymptotic domain  $t \lesssim \mathcal{L}_{PAD}^{Ising}$  (see I and II). Especially for the susceptibility case, such a result cannot be used in comparative analyses which debate on the “correct” shape of the temperature dependence of the effective exponent  $\gamma$  defined as universal functions of a single dimensionless variable (author?) [26, 27, 28, 29, 30, 32, 33, 35, 39, 40].

Our present attention is then mainly focused on the determination of a thermal-like scale factor, noted  $\vartheta_{\mathcal{L}}$ , calculated from the application of the mean crossover function beyond the preasymptotic domain. Our analytic procedure developed hereafter aims to retrieve the Ising-like universal features only using well-defined *energy* and *length* units, and a well-controlled number (three) of well-defined *dimensionless scale factors* given in a form of a set  $\mathbb{S}_{SF}$  as defined in II [see also Eqs. (25) and (26) below]. We *strictly* avoid adjusting the system-dependent parameters by a minimization of fitting errors to demonstrate that  $\vartheta_{\mathcal{L}} \equiv \vartheta$ . Alternatively, using both estimations of the effective exponent and amplitude values (author?) [41], we calculate the local value of  $\vartheta_{\mathcal{L}} (\Delta\tau^*)$  to verify the uniqueness of the  $\vartheta_{\mathcal{L}}$  value and its identity with the  $\vartheta$  value when  $\Delta\tau^* \rightarrow 0$ . Accordingly, our method offers the great advantage to directly re-use previous results obtained by fitting experimental data with an effective power law valid in a limited temperature range (author?) [24, 42, 43]. Therefore our attention is also focussed on the corresponding analyses of the isothermal compressibility data obtained from  $pVT$  measurements (author?) [44, 45, 46, 47, 48] covering the temperature range  $0.1 K \leq T - T_c \leq 283.41 K$ , light scattering measurements (author?) [21, 49, 50, 51, 52, 53] covering the temperature range  $2.6 mK \leq T - T_c \leq 29 K$ , and interferometry measurements (author?) [54, 55, 56] covering the temperature range  $-0 \lesssim T - T_c \leq 29 K$ , extending then significantly the temperature range investigated by the present study. We simultaneously provide the effective reduced temperature range of the extended asymptotic domain, bounded by a limit noted  $\mathcal{L}_{EAD}^X$ , with

$\mathcal{L}_{\text{EAD}}^{\text{Xe}} > \mathcal{L}_{\text{PAD}}^{\text{Xe}} = \frac{\mathcal{L}_{\text{PAD}}^{\text{Ising}}}{\vartheta(\text{Xe})}$  (see II and below), where isothermal compressibility of xenon is accurately described by the mean crossover function for susceptibility using the single scale factor  $\vartheta(\text{Xe})$  for the thermal-like field. Such a result gives the first complete comparison between experimental results and crossover theories, *de facto* without any adjustable parameters in a relative temperature range covering more than four decades, when the mean crossover functions are appropriately modified to account for master behaviors of the one-component fluid subclass.

The paper is organized as follows.

In Section 2, we recall useful notations and definitions needed to use the mean crossover functions for the correlation length and the isothermal susceptibility in the homogeneous phase of a one-component fluid. In Section 3, the characterization of the Ising-like preasymptotic domain of xenon is analyzed only using the isothermal compressibility fitting result obtained by Güttinger and Cannell, from their turbidity measurements performed outside the Ising-like preasymptotic domain. In Section 4, after the introduction of the three-parameter characterization when the extension of the crossover domain remains undefined, we demonstrate the great advantage of the mean crossover functions to provide unambiguous scaling determination of  $\vartheta_{\mathcal{L}}$  beyond the Ising-like preasymptotic domain.

In Appendix A, we give the basic estimation of the needed amplitudes from application of the scale dilatation method to xenon. All the other measurement methods of the isothermal compressibility are then considered, with a special attention to the data obtained from  $pVT$  and interferometry measurements which infer a practical three point calibration for their relative comparison to the Güttinger and Cannell's data. We finally compare in a detailed manner all the results to the ones calculated with the mean crossover function for susceptibility, then justifying *a posteriori* the exact values of the three scale factors  $g_0$ ,  $\vartheta$ , and  $\psi_{\rho}$  for xenon which are used in this paper.

## 2. MEAN CROSSOVER FUNCTIONS FOR CORRELATION LENGTH AND SUSCEPTIBILITY

### 2.1. Definitions and notations

The dimensionless mean crossover functions  $F_{\ell}(t, h=0) = \frac{1}{\ell_{\text{th}}(t)}$  for the inverse correlation length, and  $F_{\chi}(t, h=0) = \frac{1}{\chi_{\text{th}}(t)}$  for the inverse susceptibility, in the homogeneous phase, read as follows (see I),

$$[\ell_{\text{th}}(t)]^{-1} = \mathbb{Z}_{\xi}^{+} t^{\nu} \prod_{i=1}^3 \left(1 + X_{\xi,i}^{+} t^{D(t)}\right)^{Y_{\xi,i}^{+}} \quad (1)$$

$$[\chi_{\text{th}}(t)]^{-1} = \mathbb{Z}_{\chi}^{+} t^{\gamma} \prod_{i=1}^3 \left(1 + X_{\chi,i}^{+} t^{D(t)}\right)^{Y_{\chi,i}^{+}} \quad (2)$$

where  $t(>0)$  is the thermal field like variable,  $h(=0)$  is the magnetic field like variable.  $D(t)$  is a universal crossover function for the confluent exponents  $\Delta$  and  $\Delta_{\text{MF}}$  given by

$$D(t) = \frac{\Delta_{\text{MF}} S_2 \sqrt{t} + \Delta}{S_2 \sqrt{t} + 1} \quad (3)$$

All the universal exponents  $\nu$ ,  $\gamma$ ,  $\Delta$ ,  $\Delta_{\text{MF}}$ , theoretical amplitudes  $\mathbb{Z}_{\xi}^{+}$ ,  $\mathbb{Z}_{\chi}^{+}$ , and theoretical parameters  $S_2$ ,  $X_{\xi,i}^{+}$ ,  $Y_{\xi,i}^{+}$ ,  $X_{\chi,i}^{+}$ ,  $Y_{\chi,i}^{+}$ , are defined in I. They are also reported in Table I for use in the following numerical estimations.

More generally, the crossover functions estimated in I are only well-defined for the critical line that links the Gaussian fixed point and the non-trivial fixed point. The effects due to the second-order (and higher) analytical contributions and the ones due to the confluent corrections to scaling linked to critical exponents  $\Delta_2$ ,  $\Delta_3$ , ..., have been discarded. As a direct consequence, these functions account exactly for the Ising-like universal features only estimated in the  $t$ -range very close to the non-trivial fixed point, which corresponds the Ising-like preasymptotic domain  $t \leq \mathcal{L}_{\text{PAD}}^{\text{Ising}}$  defined in I [see also below Eq. (9)].

Within the Ising-like preasymptotic domain, the mean crossover functions can be approximated by their restricted (two-term) Wegner like expansion (**author?**) [18]. Then Eqs. (1) and (2) can be replaced by:

$$\ell_{\text{PAD,th}}(t) = \left(\mathbb{Z}_{\xi}^{+}\right)^{-1} t^{-\nu} \left[1 + \mathbb{Z}_{\xi}^{1,+} t^{\Delta}\right] \quad (4)$$

$$\chi_{\text{PAD,th}}(t) = \left(\mathbb{Z}_{\chi}^{+}\right)^{-1} t^{-\gamma} \left[1 + \mathbb{Z}_{\chi}^{1,+} t^{\Delta}\right] \quad (5)$$

where the amplitudes  $\mathbb{Z}_{\xi}^{1,+}$  and  $\mathbb{Z}_{\chi}^{1,+}$  of the first-order term due to the lowest confluent corrections to scaling are given by

$$\mathbb{Z}_{\xi}^{1,+} = -\sum_{i=1}^3 X_{\xi,i}^{+} Y_{\xi,i}^{+} \quad (6)$$

$$\mathbb{Z}_{\chi}^{1,+} = -\sum_{i=1}^3 X_{\chi,i}^{+} Y_{\chi,i}^{+} \quad (7)$$

(see Table I). They are related by the universal ratio (**author?**) [7, 8]

$$\frac{\mathbb{Z}_{\xi}^{1,+}}{\mathbb{Z}_{\chi}^{1,+}} = 0.67919 \quad (8)$$

a	exponent	$Z_\xi^+$	$S_2$	$i$	$X_{\xi,i}$	$Y_{\xi,i}$	b	exponent	$Z_\chi^+$	$S_2$	$i$	$X_{\chi,i}$	$Y_{\chi,i}$
$\nu$	0.6303875	2.121008	22.9007	1	40.0606	-0.098968	$\gamma$	1.2395935	3.709601	22.9007	1	29.1778	-0.178403
$\Delta$	0.50189			2	11.9321	-0.15391	$\Delta$	0.50189			2	11.7625	-0.282241
$\Delta_{\text{MF}}$	0.5			3	1.90235	-0.00789505	$\Delta_{\text{MF}}$	0.5			3	2.05948	-0.0185424
					$Z_\xi^{1,+} =$	5.81623						$Z_\chi^{1,+} =$	8.56347

Table I: Values of the universal exponents and constants of Eqs. (1) to (7), for (a) the dimensionless correlation length and (b) the dimensionless susceptibility, in the homogeneous domain (see Ref. **(author?)** [9]).

The validity domain of Eqs. (4) to (8) corresponds to  $t \leq \mathcal{L}_{\text{PAD}}^{\text{Ising}}$  where

$$\mathcal{L}_{\text{PAD}}^{\text{Ising}} \simeq \left( \frac{0.033}{S_2} \right)^2 \cong 1.9 \times 10^{-6} \quad (9)$$

with  $S_2 = 22.9007$  (see I and Table I)

Finally, any restricted two-term Wegner-like expansions can be estimated only using the following set of three theoretical amplitudes **(author?)** [20],

$$\mathbb{S}_A^{MR} \left( t \leq \mathcal{L}_{\text{PAD}}^{\text{Ising}}; h = 0 \right) = \left\{ Z_\chi^{1,+}; \left( Z_\xi^+ \right)^{-1}; \left( Z_\chi^+ \right)^{-1} \right\} \quad (10)$$

where the subscript  $A$  labels for the amplitude nature of these characteristic parameters.

Beyond the Ising-like preasymptotic domain, i.e.  $t > \mathcal{L}_{\text{PAD}}^{\text{Ising}}$ , we also recall that the theoretical parameter  $S_2$  acts as a convenient sensor to estimate some orders of magnitude of  $t$  which are convenient for the analysis of the crossover. For example, the theoretical crossover temperature  $t_\Delta$ , which corresponds to the value  $D(t_\Delta) = \frac{\Delta + \Delta_{\text{MF}}}{2}$  of the universal confluent function of Eq. (3), is defined by

$$t_\Delta \simeq \left( \frac{1}{S_2} \right)^2 \cong 1.9 \times 10^{-3} \quad (11)$$

For the confluent corrections,  $t_\Delta$  characterizes the universal crossover exchange between predominant Ising-like nature close to the non-trivial fixed point [ $t \ll t_\Delta$ ], to predominant mean field-like nature close to the Gaussian fixed point [ $t \gg t_\Delta$ ]. Indeed,  $t_\Delta$  gives an estimation of the order of magnitude of the  $t_{e_P, \frac{1}{2}}$ -value where each effective exponent  $e_{P,e,\text{th}}(t) = -\frac{\partial \text{Ln}[F_P(t)]}{\partial \text{Ln}(t)}$  **(author?)** [41] crosses its “mean” crossover value  $e_{P, \frac{1}{2}} \left( t_{e_P, \frac{1}{2}} \right) = \frac{e_P + e_{P,\text{MF}}}{2}$  (see Figure 4 in I). In such a “critical-to-classical” crossing range in the homogeneous domain [ $t > 0$ ],  $\ell_{\text{th}} \simeq 20 - 30$  is a typical (dimensionless) order of magnitude for the theoretical correlation length. For example,  $\ell_{\text{th}}(t_\Delta) = 28.8$ ,  $\ell_{\text{th}} \left( t_{\nu, \frac{1}{2}} \right) = 22.2$ , and  $\ell_{\text{th}} \left( t_{\gamma, \frac{1}{2}} \right) = 18.8$ , anticipating the following discussion of the results reported in Table II where the values of Eqs. (1) and (2) are calculated for eight conditions of the effective exponents. Moreover, introducing the practical relations  $\mathcal{L}_{\text{PAD}}^{\text{Ising}} = \varpi t_\Delta$ , with  $\varpi \cong 10^{-3}$  (see I), it is easy to separate the analysis of, either

the Ising-like preasymptotic domain  $t \lesssim \varpi \times t_\Delta$ , or the intermediate “Ising-like” crossover domain  $\varpi t_\Delta < t < t_\Delta$ . Especially considering the selected values of the effective exponent  $\gamma_{e,\text{th}}(t) = -\frac{\partial \text{Ln}[\chi_{\text{th}}(t)]}{\partial \text{Ln}(t)}$  given in line 3 of Table II), we note that the conditions  $\gamma_e \left( t_{\gamma, \frac{1}{2}} \right)$  (column 1) and  $\gamma_e \left( t_{\nu, \frac{1}{2}} \right)$  (column 2) are obtained for  $t > t_\Delta$ , while, obviously, the condition  $\gamma_e(t_\Delta)$  (column 3) is obtained at  $t = t_\Delta$ , where  $\ell_{\text{th}}$  reach a value  $\sim 30$ . For  $\ell_{\text{th}} \gtrsim 30$ , or  $t \lesssim t_{\Delta, \frac{1}{2}}$  (columns 4 and right), we expect to observe the Ising-like universal features of the critical phenomena which are then characterized by the three system-dependent parameters only asymptotically well-defined when  $\ell_{\text{th}} \gtrsim 1916$ , or  $t \lesssim \mathcal{L}_{\text{PAD}}^{\text{Ising}}$  (i.e. within the Ising-like preasymptotic domain). We note that the effective values  $\gamma_e = \gamma_{e,pVT} = 1.16665$  **(author?)** [13], 1.19 **(author?)** [24, 42], 1.211 **(author?)** [43] obtained from  $pVT$  measurements, are precisely in this intermediate Ising-like range  $\mathcal{L}_{\text{PAD}}^{\text{Ising}} < t < t_\Delta$ . So that, we have underlined these three latter conditions in columns 5 to 6, respectively, showing that the value of theoretical correlation length  $\ell_{\text{th}}$  is on the range 50 – 220, i.e.,  $2 \lesssim \frac{\ell_{\text{th}}}{\ell_{\text{th}}(t_\Delta)} \lesssim 8$ . A special attention to the finite “Ising-like” temperature range covered by  $pVT$  experiments is given in Section 4.2 and Appendix A3. Correlatively, within the Ising-like preasymptotic domain  $t \lesssim \mathcal{L}_{\text{PAD}}^{\text{Ising}}$ , the theoretical values reported in lines 7 and 8 of Table II show that the condition  $\ell_{\text{th}} \gtrsim 2000$  (or  $\frac{\ell_{\text{th}}}{\ell_{\text{th}}(t_\Delta)} \gtrsim 70$ ) is satisfied. The expected temperature-like variation of  $\gamma_{e,\text{th}}(t)$ , i.e.,  $\gamma - \gamma_{e,\text{th}} \left( \mathcal{L}_{\text{PAD}}^{\text{Ising}} \right) \leq 0.006$ , is then significantly lower than the typical uncertainty on the asymptotic experimental value  $\gamma_{\text{exp}} \simeq 1.23 \pm 0.02$  **(author?)** [24].

The eight indexations of  $t$  (or  $\ell_{\text{th}}$ ) given by these eight conditions of Table II will be used to label the horizontal (upper) axes of the next figures with corresponding arrows and column numbers.

## 2.2. Fluid-dependent parameters

The introduction of the fluid-dependent parameters to fit the experimental results using the mean crossover functions was detailed in § 3.1 of II. We recall here the main steps to introduce definitions and notations of the needed quantities, fixing the value  $\Lambda_{q_e}^* = 1$  to neglect

(a) \ label	1	2	3	4	5	6	7
<i>Condition</i>	$\gamma_{\frac{1}{2}} = \frac{\gamma + \gamma_{\text{MF}}}{2}$	$\nu_{\frac{1}{2}} = \frac{\nu + \nu_{\text{MF}}}{2}$	$\Delta_{\frac{1}{2}} = \frac{\Delta + \Delta_{\text{MF}}}{2}$	$\gamma_{e,pVT}$ ( <b>author?</b> ) [12]	$\gamma_{e,pVT}$ ( <b>author?</b> ) [42]	$\gamma_{e,pVT}$ ( <b>author?</b> ) [24]	$\mathcal{L}_{\text{PAD}}^{\text{Ising}}$
$\gamma_{e,\text{th}}$	1.1198	1.12776	1.14081	1.16665	1.19	1.211	1.23397
$\nu_{e,\text{th}}$	0.561	0.5652	0.572	0.5862	0.5994	0.612	0.6266
$\Delta_{e,\text{th}}$	0.500768	0.500834	0.500945	0.501176	0.501396	0.501601	0.50183
$t$	$4.06 \times 10^{-3}$	$3.056 \times 10^{-3}$	$1.907 \times 10^{-3}$	$7.033 \times 10^{-4}$	$2.392 \times 10^{-4}$	$6.22 \times 10^{-5}$	$1.907 \times 10^{-5}$
$\ell_{\text{th}}$	18.76	22.0	28.8	51.32	97.29	220.1	1916
$Z_{\chi,e}^+$	0.73735	0.70492	0.65161	0.54730	0.45641	0.37810	0.29363
(b)							
$\Delta\tau^* = \frac{t}{\vartheta}$	0.193	0.145	0.0905	$0.0334 \gtrsim \mathcal{L}_{\text{EAD}}^{\chi_e}$	0.01135	0.00295	$0.905 \times 10^{-1}$
$\frac{\xi}{\alpha_c} = \frac{\ell_{\text{th}}}{\mathbb{L}^{\{1f\}}}$	0.730	0.857	1.12	1.997	3.786	8.564	74.56
$\Gamma_{e,\text{th}}^+$	0.099601	0.098193	0.095456	0.088586	0.080842	0.072626	0.061629

Table II: (a): Calculated theoretical values of the effective exponents  $\gamma_{e,\text{th}}$  (line 3),  $\nu_{e,\text{th}}$  (line 4),  $\Delta_{e,\text{th}}$  (line 5), the thermal-like field  $t$  (line 6), the correlation length  $\ell_{\text{th}}$  (line 7), and the effective amplitude  $Z_{\chi,e}^+$  (line 8) of the susceptibility, using Eqs. (1) and (2), for the typical conditions given in line 2, respectively; (b): Corresponding physical values of the reduced temperature distance  $\Delta\tau^* = \frac{t}{\vartheta}$  (line 10), the dimensionless correlation length  $\frac{\xi}{\alpha_c} = \frac{\ell_{\text{th}}}{\mathbb{L}^{\{1f\}}}$  (line 11), and the effective amplitude  $\Gamma_{e,\text{th}}^+$  (line 12) of the dimensionless compressibility, using Eqs. (15), (21), and (23), for the xenon case, with  $\vartheta = 0.21069$ ,  $\mathbb{L}^{\{1f\}} = 25.6988$  and  $\psi_\rho = 3.2507 \cdot 10^{-4}$  (see text).

the quantum effects at the microscopic length scale (**author?**) [16] for the xenon case.

When  $t \rightarrow 0$  at  $h = 0$ ,  $t$  is analytically related to

$$\Delta\tau^* = \frac{T - T_c}{T_c} \rightarrow 0 \quad (12)$$

by the following linear approximation (**author?**) [19]

$$t = \vartheta \Delta\tau^* \quad (13)$$

The dimensionless scale factor  $\vartheta$  is a fluid-dependent parameter. The fluid critical temperature  $T_c$ , provides the energy unit

$$(\beta_c)^{-1} = k_B T_c \quad (14)$$

which links the dimensionless free energies of the  $\Phi^4$ -model and the selected fluid. Accordingly, the dimensionless form of the Hamiltonian of the  $\Phi^4$ -model results of the introduction of a finite (but arbitrary) wave number  $\Lambda_0$ , the so-called cutoff parameter (see I), whose inverse is related to the unknown finite short range of the microscopic molecular interaction. A convenient method at  $d = 3$  consists in replacing (unknown)  $\Lambda_0$  by  $g_0$  which is the adjustable critical coupling constant of the  $\Phi^4$  term having correct wave number dimension. The inverse  $(g_0)^{-1}$  acts as the physical length unit to link the theoretical dimensionless correlation length ( $\ell_{\text{th}}$ ) and the physical correlation length ( $\xi_{\text{exp}}$ ) of each one-component fluid, through the fitting equation

$$\ell_{\text{th}}(t) = g_0 \xi_{\text{exp}} (\Delta\tau^*) \quad (15)$$

The dimensionless ordering field for fluids is defined as (**author?**) [42, 43]

$$\Delta\tilde{\mu} = \tilde{\mu}_\rho - \tilde{\mu}_{\rho,c} \quad (16)$$

where  $\Delta\tilde{\mu}$  is written using practical dimensionless chemical potential  $\tilde{\mu} = \frac{\mu_\rho \rho_c}{p_c}$  (**author?**) [43].  $\mu_\rho$  ( $\mu_{\rho,c}$ ) is the (critical) chemical potential per mass unit,  $\rho$  ( $\rho_c$ ) is the (critical) mass density, and  $p$  ( $p_c$ ) is the (critical) pressure. Correspondingly, the practical dimensionless form  $\Delta\tilde{\rho}$  of the order parameter density reads as follows

$$\Delta\tilde{\rho} = \frac{\rho}{\rho_c} - 1 \quad (17)$$

using the practical dimensionless form  $\tilde{\rho} = \frac{\rho}{\rho_c}$  of the mass density (**author?**) [43].

When  $h \rightarrow 0$  and  $\Delta\tilde{\mu} \rightarrow 0$  at  $t = 0$ ,  $h$  is related to  $\Delta\tilde{\mu}$  as follows

$$h = \psi_\rho \Delta\tilde{\mu} \quad (18)$$

where  $\psi_\rho$  is the second (fluid-dependent) scale factor. However, the parameters  $T_c$ ,  $g_0$ ,  $\vartheta$ , and  $\psi_\rho$ , do not provide unequivocal link between theoretical and physical thermodynamics quantities. For example, the definition of  $\tilde{\mu}_\rho$  introduces a second unit  $\frac{\rho_c}{\rho_c} \sim \left[ \frac{\text{energy}}{\text{mass}} \right]$  for (specific) energy which differs from  $(m_{\bar{p}} \beta_c)^{-1}$  by the factor  $Z_c$  [ $m_{\bar{p}}$  is the mass of the fluid particle (i.e. the molecular mass)]. Correlatively, the critical mass unit of the one-component fluid introduces a critical specific volume  $\frac{1}{\rho_c}$  which differs from the volume  $\frac{k_B T_c}{p_c} = (\alpha_c)^d$  of the critical interaction cell [see below Eq. (19)]. The comparison between the two volumes introduces the extensivity of the system through the amount  $\frac{m_{\bar{p}}}{Z_c}$  of matter filling the volume of the critical interaction cell (**author?**) [12]. That provides alternative choice between two energy units and two length units originating from thermodynamics. Such noticeable differences in the system-dependent units of the dimensionless variables impose to have careful attention when comparing the dimensionless thermodynamics

potentials. Here, the selected length unit  $\alpha_c$  reads

$$\alpha_c = \left( \frac{k_B T_c}{p_c} \right)^{\frac{1}{d}} \quad (19)$$

and have physical meaning in terms of the range of intermolecular interaction in fluids. Therefore, in our notations, the superscript star labels a dimensionless variable which uses  $(\beta_c)^{-1}$  and  $\alpha_c$  as energy and length units in one self-consistent procedure to made dimensionless all the thermodynamic variables normalized per particle (**author?**) [12, 13], not per mass unit. The subscript  $\rho$  recalls for practical order parameter density defined by Eq. (17), and the related practical dimensionless variables are decorated by a tilde. For example, the experimental isothermal susceptibility  $\chi_{T,\rho}$  for fluids is defined by  $\chi_{T,\rho} = \left( \frac{\partial \rho}{\partial \mu_\rho} \right)_T \sim \left[ \frac{1}{\text{energy} \times \text{volume}} \right]$  when the fluid order parameter (respectively, the fluid ordering field) is proportional to the (mass) density  $\rho \sim \left[ \frac{\text{mass}}{\text{volume}} \right]$  (respectively, the chemical potential per mass unit  $\mu_\rho \sim \left[ \frac{\text{energy}}{\text{mass}} \right]$ ).  $\chi_{T,\rho}$  is related to the isothermal compressibility  $\kappa_T = \frac{1}{\rho} \left( \frac{\partial \rho}{\partial p} \right)_T \sim \left[ \frac{\text{volume}}{\text{energy}} \right]$  by  $\chi_{T,\rho} = \rho^2 \kappa_T$ . The practical fluid dimensionless variables are  $\tilde{\rho} = \frac{\rho}{\rho_c}$ ,  $\tilde{\mu} = \frac{\mu_\rho \rho_c}{p_c}$ , while  $\kappa_T^* = p_c \kappa_T$  (**author?**) [43]. Thus we obtain  $\tilde{\chi}_T \equiv \kappa_T^*$  only at  $\tilde{\rho} = 1$  for  $\Delta\tau^* > 0$ . Such a practical interrelation between the dimensionless variables results from the implicit use of these two ‘‘thermodynamic’’ length units previously defined from two distinct volumes  $v_{\tilde{\rho},c} = \frac{m\tilde{\rho}}{\rho_c}$  and  $(\alpha_c)^d$ . On the other hand, from the theoretical scheme applied to the  $\Phi_{d=3}^4$  ( $n=1$ )-model, after normalization of the free energies by  $k_B T \cong k_B T_c$ , the length dimensions of the Hamiltonian quantities  $r_0 - r_{0c} \sim (g_0)^2 t$ ,  $\langle \phi_0 \rangle \sim (g_0)^{\frac{5}{2}} m$ , and  $h_0 \sim (g_0)^{\frac{1}{2}} h$ , lead to  $\chi_{0,\text{th}} = (g_0)^2 \chi_{\text{th}} \sim \left[ \frac{1}{\text{surface}} \right]$  (see I for notations and definitions). We can then conclude that introducing the dimensionless scale factors  $\vartheta$  and  $\psi_\rho$  through Eqs. (13) and (18), provides a subtle critical combination (not discussed here) of the model units and the fluid units. The essential point is to guarantee the uniqueness of the energy unit and the length unit in the description of dimensionless singular behaviors (**author?**) [25]. Our selected length unit  $\alpha_c$  [see Eq. (19)] takes thermodynamic origin, while the wave number unit  $g_0$  [see Eq. (15)] has theoretical interest to fit the asymptotic singular divergence of  $\xi_{\text{exp}}^*(\Delta\tau^*) = \frac{\xi_{\text{exp}}(\Delta\tau^*)}{\alpha_c}$ . Then, by exchanging Eq. (15) and the following dimensionless form

$$\ell_{\text{th}}(t) = \mathbb{L}^{\{1f\}} \xi_{\text{exp}}^*(\Delta\tau^*), \quad (20)$$

we also introduce the supplementary scale factor

$$\mathbb{L}^{\{1f\}} = \alpha_c g_0 \quad (21)$$

as a dimensionless product between the two critical quantities (i.e., defined for  $t=0; h=0$  and  $\Delta\tau^*=0; \Delta\tilde{\mu}=0$ , respectively).

After all,  $m \rightarrow 0$  and  $\Delta\tilde{\rho} \rightarrow 0$  are related by the equation

$$m = \left( \mathbb{L}^{\{1f\}} \right)^{-d} (\psi_\rho)^{-1} \Delta\tilde{\rho}, \quad (22)$$

where  $m$  is the theoretical magnetization-like order parameter. Considering the theoretical susceptibility  $\chi_{\text{th}}(t) = \left( \frac{\partial m}{\partial h} \right)_t$  and the experimental isothermal susceptibility  $\tilde{\chi}_{T,\text{exp}}(\Delta\tau^*) = \left( \frac{\partial \Delta\tilde{\rho}}{\partial \Delta\tilde{\mu}} \right)_{\Delta\tau^*}$  for fluids, the second fitting equation is then obtained as follows

$$\chi_{\text{th}}(t) = \left( \mathbb{L}^{\{1f\}} \right)^{-d} (\psi_\rho)^{-2} \tilde{\chi}_{T,\text{exp}}(\Delta\tau^*), \quad (23)$$

with  $\tilde{\chi}_{T,\text{exp}}(\Delta\tau^*) \equiv \kappa_{T,\text{exp}}^*(\Delta\tau^*)$  when  $\Delta\tilde{\rho} = 0$ .

Finally, each one-component fluid is asymptotically characterized by the set (**author?**) [20]

$$\mathbb{Q}_c(\Delta\tau^* \rightarrow 0) = \left\{ (\beta_c)^{-1}; \alpha_c; g_0; \vartheta; \psi_\rho \right\} \quad (24)$$

which can be rewritten in an equivalent form

$$\mathbb{Q}_c(\Delta\tau^* \rightarrow 0) = \left\{ (\beta_c)^{-1}; \alpha_c; \mathbb{S}_{SF} \right\} \quad (25)$$

then introducing the following fluid set  $\mathbb{S}_{SF}$  made of three (asymptotic) dimensionless scale factors

$$\mathbb{S}_{SF}(\Delta\tau^* \rightarrow 0) = \left\{ \vartheta; \mathbb{L}^{\{1f\}}; \psi_\rho \right\} \quad (26)$$

The subscript  $SF$  recalls for the scale factor nature of the three fluid-dependent dimensionless numbers, while the condition  $\Delta\tau^* \rightarrow 0$  indicates the asymptotic nature of the hypotheses needed by the renormalization scheme. Within the Ising-like preasymptotic domain,  $\kappa_T^*(\Delta\tau^*)$  and  $\xi(\Delta\tau^*)$  can be approximated by

$$\kappa_{T,\text{exp}}^*(\Delta\tau^*) = \Gamma^+(\Delta\tau^*)^{-\gamma} \left[ 1 + a_\chi^+(\Delta\tau^*)^\Delta \right] \quad (27)$$

$$\frac{\xi_{\text{exp}}(\Delta\tau^*)}{\alpha_c} = \frac{\xi_0^+}{\alpha_c} (\Delta\tau^*)^{-\nu} \left[ 1 + a_\xi^+(\Delta\tau^*)^\Delta \right] \quad (28)$$

with (**author?**) [7]

$$\frac{a_\xi^+}{a_\chi^+} = \frac{\mathbb{Z}_\xi^{1,+}}{\mathbb{Z}_\chi^{1,+}} = 0.67919 \quad (29)$$

Hereabove, we have selected  $\Gamma^+$ ,  $\xi_0^+$  (or  $\xi^+ = \frac{\xi_0^+}{\alpha_c}$ ), and  $a_\chi^+$  as independent amplitudes to characterize each one-component fluid. The ‘‘experimental’’ parameter set written as

$$\mathbb{Q}_{c,\mathcal{L}_{\text{PAD}}^{\text{Xe}}} = \left\{ (\beta_c)^{-1}; \alpha_c; S_A \right\} \quad (30)$$

is then Ising-like equivalent to the set  $\mathbb{Q}_c(\Delta\tau^* \rightarrow 0)$  of Eq. (25) [here the subscript  $\mathcal{L}_{\text{PAD}}^{\text{Xe}}$  recalls for the fluid-dependent temperature domain of validity]. Its dimensionless part  $S_A$  (where the subscript  $A$  recalls for the

amplitude nature of the dimensionless numbers) is given as :

$$S_A = \{a_\chi^+; \xi^+; \Gamma^+\} \quad (31)$$

which is compared with Eq. (26) using the fitting equations (23) and (20) [or (15)]. The successive unequivocal determinations of the scale factors, first  $\vartheta$ , hence  $\mathbb{L}^{\{1f\}}$  (or  $g_0$ ), and finally  $\psi_\rho$ , are obtained from the following hierarchy of equations:

$$\vartheta = \left( \frac{a_\chi^+}{\mathbb{Z}_\chi^{1,+}} \right)^{\frac{1}{\Delta}} = \left( \frac{a_\xi^+}{\mathbb{Z}_\xi^{1,+}} \right)^{\frac{1}{\Delta}}, \quad (32)$$

$$\mathbb{L}^{\{1f\}} = \left[ \xi^+ \mathbb{Z}_\xi^+ \vartheta^\nu \right]^{-1} \text{ or } g_0 = \left[ \xi_0^+ \mathbb{Z}_\xi^+ \vartheta^\nu \right]^{-1}, \quad (33)$$

$$\psi_\rho = \left[ \left( \mathbb{L}^{\{1f\}} \right)^{-d} \Gamma^+ \mathbb{Z}_\chi^+ \vartheta^\gamma \right]^{\frac{1}{2}} \quad (34)$$

Each one-component fluid characterized by  $\mathbb{Q}_c$  of Eq. (25), has the Ising-like universal features of the  $\Phi_{d=3}^4$  ( $n=1$ )-model in the Ising-like preasymptotic domain  $\mathcal{L}_{\text{PAD}}^{\text{Xe}}$  given by

$$\Delta\tau^* < \mathcal{L}_{\text{PAD}}^{\text{Xe}} \simeq \frac{1}{\vartheta} \mathcal{L}_{\text{PAD}}^{\text{Ising}} \simeq \frac{1.9 \times 10^{-6}}{\vartheta} \quad (35)$$

Equation (35) demonstrates that the knowledge of the temperature-like scale factor  $\vartheta$  defines the extension of the Ising-like preasymptotic domain of each selected fluid, then providing an essential tool for analyzing experimental data. Correlatively, admitting a single  $\vartheta$  value whatever the property and the thermal field range, the (fluid dependent) crossover temperature  $\Delta\tau_\Delta^*$  is given by

$$\Delta\tau_\Delta^* \simeq \frac{1}{\vartheta} t_\Delta \simeq \frac{1.9 \times 10^{-3}}{\vartheta} \quad (36)$$

and the crucial problem of how to define the temperature range  $\Delta\tau^* \leq \mathcal{L}_{\text{PAD}}^{\text{Xe}}$  is solved. Appropriate rewriting of Eqs. (32) to (34), provides the following functional scaling form

$$\mathbb{S}_A^{MR} = S_A \mathbb{F}(\mathbb{S}_{SF}) \text{ with } \Delta\tau^* \lesssim \frac{1.9 \times 10^{-6}}{\vartheta} \quad (37)$$

where  $\mathbb{F}(\mathbb{S}_{SF})$  are universal functions. We note the ‘‘theoretical’’ (i.e. originating only from the MR scheme) nature of the l.h.s. of Eq. (37).

In next Section 3, we analyze the status of this expected three-scale-factor characterization for the xenon case, first, using the values inferred from the application of the scale dilatation method (**author?**) [13], and second, comparing the results (**author?**) [26, 28] obtained from the massive renormalization (MR) scheme (present work), the minimal subtraction renormalization (MSR) scheme (**author?**) [29], and the crossover parametric model (CPM) (**author?**) [40], with the experimental results of Güttinger and Cannell.

### 3. XENON CHARACTERIZATION WITHIN THE ISING-LIKE PREASYMPTOTIC DOMAIN.

#### 3.1. Hypothesized description of the Ising-like preasymptotic domain

We hypothesize that the two terms of the asymptotic Wegner-like expansion of  $\kappa_{T,\text{exp}}^*(\Delta\tau^*)$  and  $\xi_{\text{exp}}(\Delta\tau^*)$  are exactly known for critical xenon, provided by the application of the scale dilatation method given in Appendix A. In such a situation, all the needed information takes origin on four critical coordinates [see below Eq. (A2)] which localize the xenon critical point on the experimental phase surface of equation  $\Phi(p, v_{\bar{p}}, T) = 0$ . Accordingly, the (dimensional) values of Eqs. (14) and (19) are the following

$$\begin{aligned} T_c &= 289.733 \text{ K or } (\beta_c)^{-1} = 4.0002 \times 10^{-21} \text{ J} \\ \alpha_c &= 0.881508 \text{ nm} \end{aligned} \quad (38)$$

leading to the dimensionless amplitude set

$$S_A = \left\{ \begin{array}{l} a_\chi^+ = 1.23397 \\ \xi^+ = 0.209111 \quad (\xi_0^+ = 0.184333 \text{ nm}) \\ \Gamma^+ = 0.0578204 \end{array} \right\} \quad (39)$$

with  $a_\xi^+ = a_\chi^+ \frac{\mathbb{Z}_\xi^{1,+}}{\mathbb{Z}_\chi^{1,+}} = 0.83810$ . Obviously, the validation of our hypotheses and the justification of Eq. (39) require the detailed analysis of the isothermal compressibility data of xenon given in Appendix A. However, we note that the essential aspects for the following presentation are the Ising-like *nature* (since the fluid characterization originates from its critical point coordinates) and *quantity* (three) of the dimensionless amplitudes, while the quoted precision of their numerical values is of secondary importance. Using Eqs. (32) to (34), the three dimensionless scale factors for xenon are:

$$\mathbb{S}_{SF} = \left\{ \begin{array}{l} \vartheta = 0.021069 \\ \mathbb{L}^{\{1f\}} = 25.6936 \quad (g_0 = 29.1473 \text{ nm}^{-1}) \\ \psi_\rho = 3.2507 \cdot 10^{-4} \end{array} \right\} \quad (40)$$

The singular behavior of  $\xi^*(\Delta\tau^*)$  and  $\chi_T^*(\Delta\tau^*)$  of xenon can then be estimated by using Eqs. (1) to (3), (15), and (23), with xenon parameters of Eq. (39). Such an estimation of dimensionless susceptibility (or dimensionless isothermal compressibility) will be represented by a full black curve (with label MR) in the next figures.

As a most important result already underlined,  $\vartheta$  enables estimation of the extension of the Ising-like preasymptotic domain [see Eq. (35)]

$$\mathcal{L}_{\text{PAD}}^{\text{Xe}} \simeq 10^{-4} \quad (41)$$

and the reduced crossover temperature [see Eq. (36)]:

$$\Delta\tau_\Delta^* \simeq 10^{-1} \quad (42)$$

The temperature extension of the Ising-like preasymptotic domain of xenon corresponds to the temperature range  $T - T_c \lesssim 30$  mK [from Eq. (41)], while the Ising-like predominant nature for crossover estimated by the mean crossover functions cannot extend beyond  $\sim T_c + 30$  K [from Eq. (42)]. More generally, the knowledge of  $\vartheta$  also enables useful estimation of any relative temperature distance and any effective value attached to a specific condition of the mean crossover function on the complete  $\Delta\tau^*$  range, as reported for example in lines 7 to 9 of Table II.

Comparable values to the ones given by Eq. (39) can be found in several published papers *but without explicit reference to the effective temperature range of the Ising-like preasymptotic domain*.

For example, in upper part (a) of Table III, we have reported  $\Gamma^+$  (column 3) and  $a_\chi^+$  (column 5) values obtained by using different theoretical crossover functions calculated by several models labeled  $X = \{\text{GC}_{\text{RG4}}, \text{MR6}_{\text{max}}, \text{MR}, \text{MSR}, \text{CPM}, \text{LM}\}$  (column 1) of respective Refs. (author?) [22, 26, 27, 28] (column 9). These values result from fits of the isothermal susceptibility data of xenon published by Güttinger and Cannell (GC) (author?) [21], with  $\gamma$  (column 2) and  $\Delta$  (column 4) values fixed to their theoretical estimation. We note that the variations of the  $\Gamma^+$  values are on a few percent level when the change in  $\gamma$  values affects the third digit, while the variations of the  $a_\chi^+$  values cover a significant range such as  $0.9 \lesssim a_\chi^+ \lesssim 1.3$ , i.e.,  $a_\chi^+ \simeq 1.1$  with  $\sim 20\%$  deviation. Then, we have also reported in Table III, the calculated values of the asymptotic scale factors  $\vartheta$  (column 6),  $\mathbb{L}^{\{1f\}}$  (column 7), and  $\psi_\rho$  (column 8), by using Eqs. (32) to (34), respectively, and an available estimation of the leading amplitude  $\xi_0^+ = \alpha_c \xi^+$  of the correlation length (see column 7). We can observe a typical uncertainty of 25% in the  $\vartheta$  and  $\psi_\rho$  values. In addition, the theoretical error-bars and differences in the estimations of exponents  $\gamma$ ,  $\nu$ ,  $\Delta$ , and universal constants appearing in Eqs. (32) to (34), can have comparable effect on the estimation of  $\vartheta$ ,  $\psi_\rho$ , and  $g_0$  than the experimental uncertainties on the estimation of  $a_\chi^+$ ,  $\Gamma^+$ , and  $\xi^+$  and the critical coordinates (such as  $T_c$ ,  $\rho_c$ ,  $p_c$ , etc.).

Nevertheless, accounting for the above variations of the  $\vartheta$  values has no significant effect on the order of magnitude of  $\mathcal{L}_{\text{PAD}}^{\chi_e} \simeq 10^{-4}$  estimated from Eqs. (35) and (39). We can then note that the apparent amplitude agreement arises in spite of the *non overlap* between the estimated temperature range of the Ising-like preasymptotic domain [see Eq. (41)] and the temperature range  $10^{-4} \lesssim \Delta\tau^* \lesssim 10^{-1}$  [i.e.,  $30 \text{ mK} \lesssim T - T_c \lesssim 30 \text{ K}$ ], covered by the Güttinger and Cannell's measurements (see also Appendix A). Therefore, the asymptotic amplitude evaluation provided by these fitting results cannot be easily transformed in terms of the characteristic scale factors for two main reasons:

- i) measurements of the singular properties are made in a temperature range which do not reach the Ising-like preasymptotic domain;
- ii) fitting of the data is made with a Wegner-like expansion,

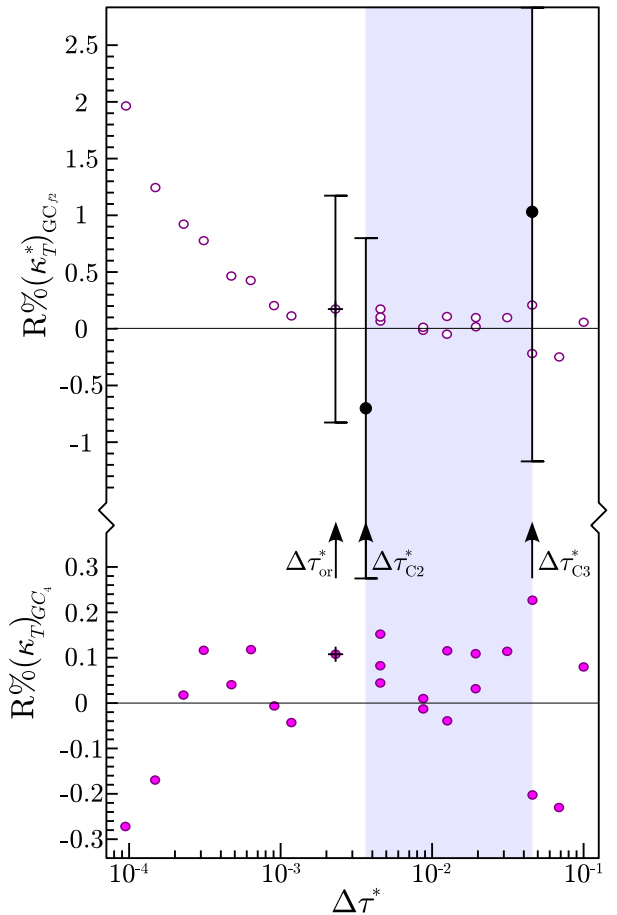


Figure 1: Residuals  $R\%(\kappa_T^*)_{\text{GC}_4}$  (expressed in %) between the dimensionless susceptibility data given in Table I of Ref. (author?) [21] and the fitting expression of Eq. (42); a) parameters given in line GC<sub>4</sub> of Table IV; b) after the  $T_c$  shift of 0.5 mK to retrieve the 0.2% numerical level illustrated in Fig. 3 of Ref. (author?) [21]; In (a) are also illustrated the respective deviations and related error-bars of the three “calibrated” values of the isothermal compressibility for the three temperature distances indicated by the respective vertical arrows labeled  $\Delta\tau_{\text{or}}^*$ ,  $\Delta\tau_{\text{C2}}^*$  and  $\Delta\tau_{\text{C3}}^*$  (see text and Appendix).

whose validity is questionable outside the Ising-like preasymptotic domain (see I).

Therefore, to replace with a suitable precision the independent amplitudes of Eqs. (39) by the independent scale factors of Eqs. (40), one needs to give the “rules” to interpolate from fitting results obtained in an experimental range *outside* the Ising-like preasymptotic domain, to the hypothesized ones, only valid *inside* the Ising-like preasymptotic domain.

$X$	$\gamma$	$\Delta$	$\Gamma^+$	$a_{\chi}^+$	$\vartheta$ Eq. (32)	$\mathbb{L}^{\{1f\}}$ Eq. (33)	$\psi_{\rho}$ Eq. (34)	$Ref$
GC <sub>RG4</sub> (pink)	1.241	0.496	0.0577	1.29	0.0230	24.305 $\xi_0^+ = 0.184$ nm		(author?) [21]
MR6 <sub>max</sub>	1.24194	0.491	0.057	1.1844	0.0194	24.305 $\xi_0^+ = 0.184$ nm	$3.25 \times 10^{-4}$	(author?) [22]
MR	1.2395935	0.50189	0.057821	1.23397	0.02107	25.6936 $\xi_0^+ = 0.184333$ nm	$3.25 \times 10^{-4}$	this work
MSR	1.2396	0.504	0.0587	1.11	0.0171	$\xi_0^+ = 0.184$ nm		(author?) [28]
CPM	1.239	0.51	n.a. (0.058)*	1.08	0.0162	30.382 $\xi_0^+ = 0.184$ nm (calculated)		(author?) [26]
LM	1.240	0.508	0.0594	n.a. (0.9)*		n.a.		(author?) [27]

Table III: Amplitude-exponent results (columns 3 to 6) of the fit of the isothermal compressibility data obtained from the turbidity measurements of Güttinger and Cannell (author?) [21], along the critical isochore, using different theoretical crossover models (labels  $X$ , column 1) proposed in references given in the last column. Corresponding scale factor values (columns 7 to 9) calculated from Eqs. (32) to (34) (see text for detail); n.a.: nonavailable. ; asterisk indicates a value used in the present work.

# (fit)	$\gamma$	$\Delta$	$\Gamma^+$	$a_{1\chi}^+ = a_{\chi}^+$	$a_{2\chi}^+$	$a_{3\chi}^+$	$T_c$ (16.64°C)	$Ref$
GC <sub>f2</sub> pink	$1.240 \pm 0.002$	(0.496)	$0.0584 \pm 0.0009$	$1.07 \pm 0.06$	(0)	(0)	$\pm 0.5$ mK	(author?) [21]
GC <sub>f4</sub> pink	$1.246 \pm 0.002$	(0.496)	$0.0551 \pm 0.0012$	$1.62 \pm 0.14$	$-2.7 \pm 0.5$	$3.6 \pm 0.8$	$\pm 0.5$ mK	(author?) [21]
GC <sub>4</sub> pink	(1.241)	(0.496)	$0.0577 \pm 0.0001$	$1.29 \pm 0.03$	$-1.55 \pm 0.2$	$1.9 \pm 0.5$	$\pm 0.5$ mK	(author?) [21]
G <sub>3</sub>	(1.240)	(0.5)	0.0574	1.55	-2.0	(0)		(author?) [12]

Table IV: Lines labeled GC<sub>f2</sub>, GC<sub>f4</sub>, GC<sub>4</sub>: Amplitude-exponent values obtained by Güttinger and Cannell from three representative fitting by Eq. (43) of the isothermal compressibility data for xenon along the critical isochore; Fixed values of the parameters are given between brackets; Line labeled G<sub>3</sub>: Amplitude-exponent values obtained by a three-point calibration method proposed in Ref. (author?) [12] and discussed in Appendix.

### 3.2. Present status of crossover modeling in critical xenon

#### 3.2.1. Güttinger and Cannell's analysis

Due to the primary importance of Eq. (32) in a scheme where a single confluent amplitude is readily expected independent, in the Table IV, we have recalled the main informations given from Güttinger and Cannell's experiment, which is the common support to compare theoretical fittings. Güttinger and Cannell observed that their susceptibility data systematically and continuously deviate from simple power-law behavior throughout the temperature range  $9.6 \times 10^{-5} \lesssim \Delta\tau^* \lesssim 10^{-1}$  with the effective exponent increasing from  $\gamma_e = 1.14$  to  $\gamma = 1.246 \pm 0.01$ . Thus the data appeared asymptotically consistent with the theoretical estimations provided at the end of the seventies, either using series calculation  $\gamma = 1.250 \pm 0.03$  for the Ising-model (author?) [57, 58], or the renormalization-group result  $\gamma = 1.241 \pm 0.002$  for the Landau-Ginzburg-Wilson Hamiltonian (author?) [59, 60]. To support this conclusion, their susceptibility data were fitted to the following (four

term) Wegner-like expansion

$$\kappa_{T,\text{exp}}^*(\Delta\tau^*) = \Gamma^+ (\Delta\tau^*)^{-\gamma} \left[ 1 + a_{1\chi}^+ (\Delta\tau^*)^{\Delta} + a_{2\chi}^+ (\Delta\tau^*)^{2\Delta} + a_{3\chi}^+ (\Delta\tau^*)^{3\Delta} \right] \quad (43)$$

with  $\Delta$  fixed at  $\Delta = 0.496$  (author?) [60] which was the theoretical value calculated at that time by the renormalization-group approach. In initial fittings, the parameters  $\Gamma^+$ ,  $\gamma$ ,  $a_{1\chi}^+$ ,  $a_{2\chi}^+$ ,  $a_{3\chi}^+$ , and  $T_c$  were independently adjusted, by variation of the data range in temperature. It was then shown that when the data range was narrowed to  $9.6 \times 10^{-5} \lesssim \Delta\tau^* \lesssim 8.8 \times 10^{-3}$  and the parameter  $a_{2\chi}^+$  and  $a_{3\chi}^+$  removed (i.e., with  $a_{2\chi}^+ = a_{3\chi}^+ = 0$ ), the fit resulted in  $\gamma = 1.240 \pm 0.002$  when  $\gamma$  was freely adjusted, and the results for  $\Gamma^+$ ,  $a_{1\chi}^+$  and  $T_c$  are in good agreement with all the other fits. This fit result is labeled GC<sub>f2</sub> and given in the corresponding line GC<sub>f2</sub> of Table IV where the error bars quoted are one standard deviation allowing for the correlation between parameters, not the experimental uncertainty which increases for the data nearest  $T_c$ , as discussed below. In fitting over the entire range, all the terms were required and the fit results (labeled GC<sub>f4</sub>) are given in line GC<sub>f4</sub> of Ta-

ble IV. The Güttinger and Cannell's analysis to examine the consistency with the predictions by renormalization-group calculations was then made with  $\gamma$  fixed at 1.241. The parameters for the fit result (labeled GC<sub>4</sub>) for the entire range in  $\Delta\tau^*$  are reported in line GC<sub>4</sub> of Table IV.

As noted by the authors, in all the fitting cases, the value of  $T_c$  found by the fitting procedure agreed to within 0.5 mK with the value observed by noting the temperature at which the meniscus formed upon cooling in small steps. It should be also noted that a shift of 0.5 mK in  $T_c$  amounts to a 2.5% change in fitted value at  $\Delta\tau^* = 9.6 \times 10^{-5}$ , which was a substantial effect in comparison to 0.2% deviations reported for all the fits (see Figure 3 in Ref. (author?) [21]). More generally, in the temperature range  $\Delta\tau^* \lesssim 9.1 \times 10^{-4}$ , the authors have accounted for the large uncertainty in the corrections due to all the possible effects which are not at the level of about 0.2%, by using a shift in  $T_c$  in the fitting program as a mean of compensating the systematic errors which increase for the points nearest  $T_c$ . However, for the present discussion, it is essential to account for the real level of the fit deviation attached to the systematic experimental uncertainties. Therefore, we have illustrated in Figure 1, the importance of the real uncertainty using the residuals (expressed in %)  $R\%(\kappa_T^*)_{GC_4} = 100 \left( \frac{\kappa_T^*}{\kappa_{T,GC_4}^*} - 1 \right)$  between the raw data of the dimensionless susceptibility given in Table 1 of Ref. (author?) [21] and the calculated ones from Eq. (43) with the parameters given in line GC<sub>4</sub>. The part a of Fig. 1, illustrates the 2% – 3% level of the true experimental error at  $\Delta\tau^* = 9.6 \times 10^{-5}$ , while the part b of Fig. 1 illustrates similar residuals, but after the  $T_c$  shift of 0.5 mK, then reproducing Figure 3 of Ref. (author?) [21] to show the 0.2% numerical level of the fit deviation.

In summary, comparing the three fit results of Table IV, Güttinger and Cannell have shown that the xenon susceptibility was correctly represented by a Wegner-like expansion whose the two first terms may be interpreted as proposed by the renormalization-group theory with  $\gamma = 1.241$  and  $\Delta = 0.496$  (author?) [60]. Despite a significative increase of experimental uncertainty as  $\Delta\tau^*$  decreases, the uncertainty on the “mean” determination of the free leading amplitude  $\Gamma^+$  value can be estimated of the order of 2% – 3%, while the first confluent amplitude  $a_\chi^+$  value was found in the range  $0.6 \lesssim a_\chi^+ \lesssim 1.45$  and seriously affected by the presence of the other two confluent parameters and the fitted temperature range. The comparison between  $\Gamma^+$  and  $a_\chi^+$  values given in Tables III and IV, especially the low dispersion of the  $\Gamma^+$ -values in a range  $0.0570 \lesssim \Gamma^+ \lesssim 0.0594$ , confirms an apparent reduction of the  $a_\chi^+$ -range, increasing the number of terms of the Wegner like expansion.

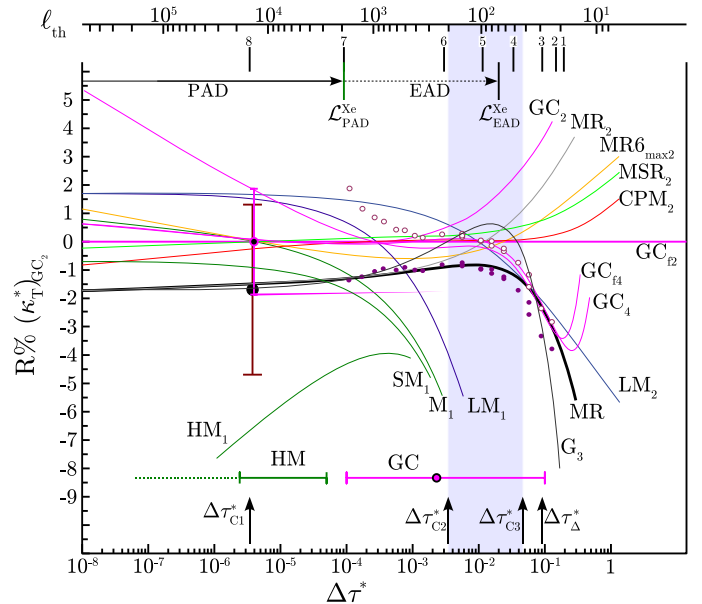


Figure 2: (Color on line) Residuals  $R\%(\kappa_T^*)_{GC_{f2}}$  (expressed in %), as a function of  $\Delta\tau^*$ , for the extrapolated description of the isothermal compressibility of xenon within the Ising-like preasymptotic domain  $\Delta\tau^* \lesssim \mathcal{L}_{PAD}^{Xe}$ . Each curve label  $X$  refers to the line  $X$  in Table III; subscript indicates the number of terms of Wegner-like expansion (see also the text); Arrows indicate the different extensions of the Ising like preasymptotic domain (see text); horizontal (pink) segment: Güttinger and Cannell experimental range (author?) [21]; open circle: temperature distance  $\Delta\tau_{or}^*$  (see Fig. 1) of the data calibration value; vertical (pink) segment: error bar of a calibrated value of the isothermal compressibility of xenon from Hocken and Moldover measurements (author?) [55, 56] (see text, Appendix A and Ref. (author?) [12]); upper horizontal axis: theoretical dimensionless correlation length calculated from the mean crossover function of Eq. (1); line indexation with labels 1 to 8:  $\gamma_e$ - or  $\ell_{th}$ -conditions reported in Table II (see text)

### 3.2.2. Crossover analyses

Since all the amplitude values given in Table III originate from the same experimental data, we consider that the extrapolation at  $\Delta\tau^* \rightarrow 0$  of the two-term expansion  $\kappa_{T,GC_{f2}}^*$  obtained with the free parameters given in line GC<sub>f2</sub> of Table III, can act as an “ideal” experimental result obtained *within* the Ising-like asymptotic domain. Making then reference to this extrapolated experimental behavior, the relative comparison with the predicted one using either a pure power law, or a two-term Wegner-like expansion, or finally a complete crossover function, associated to  $X = \{MR6_{max}, MR, MSR, CPM, LM\}$  models (see Table III), provides the required information to evaluate the Ising-like characterization in the ranges  $\Delta\tau^* < \mathcal{L}_{PAD}^{Xe} \simeq 10^{-4}$  and  $\Delta\tau^* \gtrsim \mathcal{L}_{PAD}^{Xe} \simeq 10^{-4}$ , separately. We use the subscript 1, 2, etc., to refer for

one-, two-, etc., terms in the Wegner like expansion, while the absence of this subscript indicates a complete crossover function (except for the MR6<sub>max</sub> case where the crossover function does not account for the classical behavior close to the Gaussian fixed point). So that, anticipating the discussion given in Appendix, we have systematically enlightened (using a grey-blue area in the next figures), the temperature range in between the two temperatures  $T = T_c + 1$  K (i.e.,  $\Delta\tau_{C_2}^* = 3.45137 \times 10^{-3}$ ) and  $T = T_c + 13.41$  K (i.e.,  $\Delta\tau_{C_3}^* = 4.62829 \times 10^{-2}$ ) where the  $pVT$  measurements can provide two “standard” values of the isothermal compressibility (see § A.3.b). These two temperatures are in the experimental range covered by the theoretical measurements of Güttinger and Cannell for  $\Delta\tau^* \gtrsim \mathcal{L}_{\text{PAD}}^{\text{Xe}} \simeq 10^{-4}$ .

Similarly, for  $\Delta\tau^* < \mathcal{L}_{\text{PAD}}^{\text{Xe}} \simeq 10^{-4}$ , we have also indicated in the following figures, the temperature  $T = T_c + 1$  mK (i.e.,  $\Delta\tau_{C_1}^* = 3.45137 \times 10^{-6}$ ) “closest” to  $T_c$ , where a careful analysis of the uncertainty on the theoretical estimations of the Ising-like exponent  $\gamma$  provides a calibrated value of the isothermal compressibility (see below and § A.3.a). This value is compatible with the interferometry measurements of Hocken and Moldover covering the temperature range  $-5$  mK  $< T - T_c < 15$  mK (i.e.,  $-1.5 \times 10^{-5} < \Delta\tau^* < 5 \times 10^{-5}$ ) (author?) [55]. As already shown, such a three point calibration can be used to define a practical three-term Wegner expansion with arbitrarily “fixed” values  $\gamma = \gamma_I = 1.240$  and  $\Delta = \Delta_I = 0.5$  for the exponents, which accounts for the isothermal compressibility of xenon in the experimental temperature range  $\Delta\tau^* < \Delta\tau_{C_3}^*$ , with  $\pm 1.5\%$  uncertainty on the “online” values produced by the distinct measurement methods around these three temperature of calibration. The corresponding amplitude parameters of Eq. (43) are given in line G<sub>3</sub> of Table IV, and each associated fitting curve will be labeled G<sub>3</sub> in the next figures.

In Figure 2, we have reported the residuals (expressed in %),  $R\%(\kappa_T^*)_{\text{GC}_{f_2}} = 100 \left( \frac{\kappa_{T,X}^*}{\kappa_{T,\text{GC}_{f_2}}^*} - 1 \right)$ , as a function of  $\Delta\tau^*$ . Note that the indexation of the (lower and upper) horizontal axes of this figure are conform with the discussion of Table II, while the experimental range of the GC measurements is given by the segment labeled GC where the open point indicates the temperature distance (noted  $\Delta\tau_{\text{or}}^*$  in the following) where light scattering data are calibrated by the authors. The specific analysis of the residuals obtained for the two-term expansion fitting (see all the curves labeled X<sub>2</sub> in Fig. 2) demonstrates that the deviations in the temperature range  $\mathcal{L}_{\text{PAD}}^{\text{Xe}} < \Delta\tau^* \lesssim 10^{-3} - 10^{-2}$ , induce a  $\pm (1\% - 2\%)$  uncertainty level in the estimation of the  $\Gamma^+$  value, which means that the value of the confluent amplitude  $a_\chi^+$  is “undetermined” due to the correlation between *free* leading amplitude and *fixed* theoretical value of  $\gamma$ .

More generally, Figure 2 is a well-defined tool to show the relative importance of each term of the Wegner like expansion as a function of each decade variation of the theoretical correlation length (see upper axis). For ex-

ample, the successive deviations at a 1% – 2% level of the curves X<sub>1</sub>, X<sub>2</sub>, ..., X, indicates that:

- i) the pure power law can be used in the range  $\ell_{\text{th}} \gtrsim (1 - 2) \times 10^4$ ,
- ii) the range  $\ell_{\text{th}} \gtrsim 1000 - 2000$  needs to add the first confluent term and effectively corresponds to the Ising-like preasymptotic domain,
- iii) a three-term-expansion seems sufficient to cover the range  $\ell_{\text{th}} \gtrsim 100 - 200$ , and, finally,
- iv) the range  $\ell_{\text{th}} \gtrsim 10 - 20$  needs to use at least four or more terms in the Wegner-like expansion.

To readily evaluate the relative importance of the effects due to the  $\gamma \Leftrightarrow \Gamma^+$  correlation, we note that the magnitude of the difference in  $\gamma$  values here considered affects only the third digit of the theoretical estimations and cannot be related to the realistic error-bar (one order of magnitude greater) provided by the experimental determination of this asymptotic exponent (see also below the related insert of Fig. 3). Therefore, in spite of the fact that measurements were performed beyond the Ising-like preasymptotic domain, the closest extrapolated Güttinger and Cannell’s fitting to  $T_c$  remains highly correlated to the theoretical value of  $\gamma$ , especially when  $T_c$  is fixed. This exponent-amplitude correlation was recently used by Luijten and Meyer (author?) [27] to re-evaluate the estimation of the leading amplitude for better agreement with the data for  $\Delta\tau^* < 0.2$  (see curve LM<sub>1</sub> in Fig. 2). However, such amplitude adjustment accounting for the data in a narrowed temperature range appears equivalent to the reverse effect of the theoretical min and max error-bar propagation outside the Ising-like preasymptotic domain clearly shown in reference I (or in the Fig. 7b of Appendix). Such an amplitude re-evaluation is then without gain on the Ising-like asymptotic quality of the crossover analysis. For example, only by addition of the first term for confluent corrections to scaling with  $a_\chi^+ = 0.86$  (see Table III, line LM), we can fit the experimental results (with deviations at a 0.5% level) on the complete experimental range (see curve LM<sub>2</sub> in Fig. 2). The comparison of the curves LM<sub>2</sub>, GC<sub>f<sub>4</sub></sub>, and GC<sub>4</sub> in Fig. 2 then shows that this “LM” fitting result which uses the parameters given in line LM of Table IV, agrees with the initial four-term fitting results given in lines GC<sub>f<sub>4</sub></sub>, and GC<sub>4</sub> of Table IV. The respective ranges of the amplitude variations,  $\Gamma^+ = 0.0584_{-0.0033}^{+0.0010}$  and  $a_\chi^+ = 1.07_{-0.25}^{+0.55}$ , illustrate the real difficulty to account for a single specific value of  $\gamma$  in the range  $\gamma = 1.24_{-0.001}^{+0.006}$ . More generally, as illustrated previously in Fig. 1, an “experimental” manner to account for each *fixed* value of  $\gamma$  is to use  $T_c$  as a *free parameter* in fitting the GC’s data. But, as observed by Güttinger and Cannell from their different fitting results, the true uncertainty on the free parameter  $\Gamma^+$  is then at a few percent level. Finally, we can conclude that, due to the 2% uncertainty of the GC’s measurements at the border of the Ising-like preasymptotic domain, the 1% – 2% magnitude of the residuals for extrapolated theoretical fittings at  $\Delta\tau^* (\lesssim \mathcal{L}_{\text{PAD}}^{\text{Xe}}) \rightarrow 0$ , is entirely related to the differences  $\gamma_X - 1.240$  between respective leading

exponents, while the apparent reduction of the uncertainty in the  $a_\chi^+$ -value results from the mandatory presence of (at least two) supplementary terms to correctly account ( $\sim 1\%$ -level) for the experimental results in the temperature range  $\Delta\tau^* \gtrsim 10^3 > \mathcal{L}_{\text{PAD}}^{\text{Xe}} \simeq 10^{-4}$ .

### 3.2.3. Analysis with $\gamma$ fixed

For a fixed theoretical value of  $\gamma$  with  $T_c$  fixed, the leading amplitude  $\Gamma^+$  can be obtained only using additional measurements performed well inside the Ising-like preasymptotic domain as defined by Eq. (9). The applicability of Eq. (34) [equivalently, Eq. (33) for the correlation length data] is then strictly limited within the Ising-like preasymptotic domain, *thus requiring a precision*  $< 0.1\%$ . In the absence of such an “ideal” experimental result, one alternative way to eliminate the “amplitude-exponent” correlation on the leading power law term, is to introduce a smallest temperature distance to the critical temperature where a single experimental data for the isothermal compressibility acts as a standard value (author?) [12]. We note  $\Delta\tau_{C_1}^*$  as this temperature distance such that  $\Delta\tau_{C_1}^* \ll \mathcal{L}_{\text{PAD}}^{\text{Xe}}$  (see column 9, Table II). For example, this method of calibration is detailed for xenon case in Appendix A, using the interferometric measurements of Hocken and Moldover (HM) (author?) [55] in the range  $2-3 \times 10^{-6} \lesssim \Delta\tau^* \lesssim 3-5 \times 10^{-5}$ . In Fig. 2, this experimental range is illustrated by the segment labeled HM. The selected smallest temperature distance is  $T - T_c = 1$  mK, or  $\Delta\tau_{C_1}^*(\text{Xe}) = 3.45 \times 10^{-6}$ , which effectively appears within the Ising-like preasymptotic domain, as evidenced by the corresponding vertical dashed line in Figure 2. Unfortunately, the required precision is not reached and here we only discuss the relative comparison between both (HM and GC) data measurements because there is no region of overlap between them and the two experiments rely on completely different effects. The interferometry measurements were performed in the very limited region of density and temperature quite close to the critical point such that the susceptibility data was represented by a pure power law with a highly correlated amplitude-exponent set. For example, the curve  $\text{HM}_1$  in Figure 2 illustrates the deviation obtained using the result  $\gamma = 1.23$  and  $\Gamma^+ = 0.062$  initially found by Hocken and Moldover. The Hocken and Moldover measurements, reanalyzed by Sengers and Moldover (SM) with  $\gamma = 1.24$ , yield  $\Gamma^+ = 0.058$ , leading to the curve  $\text{SM}_1$  in Figure 2. At  $\Delta\tau_{C_1}^*(\text{Xe}) = 3.45 \times 10^{-6}$  the deviation of  $\sim 6\%$  between  $\text{HM}_1$  and  $\text{SM}_1$  can be considered as representative of the experimental uncertainty. These results seem to systematically deviate from fitting the raw data (full pink points) of Güttinger and Cannell’s measurements. Moreover, accounting for the fitting results illustrated by the curves  $\text{LM}_2$  and/or  $\text{GC}_{f_4}$ , such a deviation appears to increase as the  $\gamma$  value increases (or as the  $\Gamma^+$  value increases, equivalently).

However, the Güttinger and Cannell’s data are rela-

tive to the isothermal compressibility value  $\kappa_T(\Delta\tau_{\text{or}}^*) = 1.9641 \times 10^{-5} \text{ Pa}^{-1}$  at  $\Delta\tau_{\text{or}}^* = 2.304 \times 10^{-3}$  (i.e.,  $T_{\text{or}} = T_c + 0.6677 \text{ K}$ ) (author?) [21], and the typical experimental uncertainty on the above reference value also is at a percent level. As a typical example, the difference on the GC value  $\rho_c(\text{GC}) = 1110 \text{ kg m}^{-3}$  and our present value  $\rho_c = 1113. \text{ kg m}^{-3}$  (see Eq. (A2) in Appendix) of the xenon critical density, contributes for a 0.6% difference on the calibration. It is then interesting to evaluate the cumulative effect of a 0.5 mK shift of  $T_c$  and a 1% change (uncertainty given by Güttinger and Cannell) of the reference value. The result is represented by the open pink points in Fig. 2. The fit deviation of these “corrected” points using our theoretical function is lower than 0.5%, as illustrated by the curve labeled MR in Fig. 2.

Subsidiarily, Fig. 2 also shows that the available fitting results of the Güttinger and Cannell’s data do not lead to the same standard value used to calibrate the mean crossover function. However, the attached relative difference appears compatible with an estimated error-bar of  $\pm 3\%$  for this standard value, which is comparable to the fitting uncertainty attached to the leading amplitude due to the theoretical uncertainty on the  $\gamma$  estimation. For example, considering the nine published pairs  $\gamma - \Gamma^+$  (see Tables III, IV and the interferometry result of Refs (author?) [56]) where  $1.239 \leq \gamma \leq 1.24194$  and  $0.056 \leq \Gamma^+ \leq 0.0594$ , the calculated mean value of the dimensionless isothermal compressibility at  $T = T_c + 1$  mK is  $\kappa_{T,\text{mean}}^* = 3.4330 \times 10^5$ , with  $3.3194 \times 10^5 \leq \kappa_{T,\text{mean}}^* \leq 3.5210 \times 10^5$ . Anticipating then the introduction of the calibrated value  $\kappa_{T,C_1}^* = 3.415 \times 10^5$  discussed in Appendix A, we note that the above mean value is 0.53% greater than the calibrated one, while the max and min values are 3.10% greater and 2.80% lower, respectively.

As an undeniable consequence of the differences  $\gamma_X - 1.240$ , (or the difference in leading amplitude, or the absence of one precise data inside the Ising-like preasymptotic domain, equivalently), the contribution of the highly correlated leading and first-confluent terms propagates in any fit procedure which uses a complete Wegner-like expansion outside the Ising-like preasymptotic domain, until a temperature distance of the order of  $\Delta\tau^* \simeq 10^{-3}$ . We can then reasonably estimate (and precisely demonstrate below, in § 4.2 and Fig. 4) that the fitting optimization occurs at finite temperature distance to the critical point (at least of the order of  $\Delta\tau^* \simeq 10^{-2}$ ), significantly outside the Ising-like preasymptotic domain (and such as  $\Delta\tau^* > \Delta\tau_{\text{or}}^*$ ). In such a situation already known as due to the low convergence of the Wegner-like expansion, it is not easy to define with the needed precision a *single* crossover parameter which must account simultaneously for two opposite roles:

1) it controls the asymptotic universal features of the Ising-like singular behavior which has the restricted form of Eq. (5), but without constraint due to the lack of experimental data in the corresponding validity range;

2) it detects the finite distance where classical-to-

critical behavior and/or non-critical behavior can occur, but may conjointly invalidate the use of the Wegner-like expansion with unique lowest confluent exponent.

Therefore, in the absence of the “ideal” experiment within the Ising-like preasymptotic domain, the universal form of Eq. (32) *can never be directly tested*. This has three correlative consequences:

i) the numerical value of  $\vartheta$  is undoubtedly related to the effects of many correction terms to scaling (for a more detailed illustration, see the discussion in terms of the effective exponent and Fig. 4 of Ref. (author?) [5]). To account for this essential result in the following, we note  $\vartheta_{\mathcal{L}}$  as the crossover parameter which is determined beyond the Ising-like preasymptotic domain, to distinguish it from  $\vartheta$  of Eq. (13) which is the scale factor needed to characterize the asymptotic critical crossover within the Ising-like preasymptotic domain;

ii) the use of Eqs. (32) to (34) needs to have supplementary information such as, for example, the unambiguous demonstration of the Ising-like uniqueness of the  $\vartheta_{\mathcal{L}}$ -value (i.e. a constant  $\vartheta_{\mathcal{L}}$ -value independent of the fitting domain and the fitted property);

iii) alternative equations valid beyond the Ising-like preasymptotic domain which provide the equivalent scaling information contained in Eqs. (32) to (34) are suitable to probe the identity  $\vartheta \equiv \vartheta_{\mathcal{L}}$  and the application of the linear Eq. (13) for  $\Delta\tau^* \rightarrow 0$ .

We recall that the first attempt (author?) [22] to understand the classical-to-critical crossover in xenon using the MR6<sub>max</sub> scheme, was made from such a global analysis of three singular properties (correlation length, susceptibility and heat capacity) of xenon in a rather large finite temperature range ( $T - T_c \lesssim 30$  K, i.e.  $\Delta\tau^* \lesssim 10^{-1}$ ). A rather well-defined value of  $\vartheta_{\mathcal{L}} = 0.0191 \pm 0.0095$  was then obtained, which was subsequently analyzed in terms of the influence of the corrections to scaling in real systems, even outside the Ising-like preasymptotic domain. The small difference with the present hypothesized value  $\vartheta = 0.021069$  [see Eq. (40)], only reflects the error-bar propagation of theoretical exponent and amplitude estimations in the respective fitting of the MR6<sub>max</sub> or MR discretized values, and not the true experimental uncertainty (see a detailed discussion of the experimental uncertainty in Appendix A). In other words, the hypothesized asymptotic value of  $\vartheta$  appears independent of the Ising-like Eq. (32). Similarly, in the other crossover modeling, the uniqueness of the crossover temperature scale appears independent of the theoretical approach in the sense where it is *de facto* obtained at a “single” finite temperature distance, noted  $\langle \Delta\tau^* \rangle_{\vartheta_{\mathcal{L}}}$ . Here *single* means that, in a log-log scale, the value of the free parameter  $\vartheta_{\mathcal{L}}$  is optimized on a *fine* temperature domain (covering typically less than one decade) centered on a large temperature distance  $\langle \Delta\tau^* \rangle_{\vartheta_{\mathcal{L}}}$ , such that  $\frac{\langle \Delta\tau^* \rangle_{\vartheta_{\mathcal{L}}}}{\Delta\tau_{C1}^*} \gg 1$ . For example considering the Güttinger and Cannell’s measurements in the next Section, we show clearly that  $\langle \Delta\tau^* \rangle_{\vartheta_{\mathcal{L}}}$  corresponds approximately to the “largest” experimental

value  $\langle \Delta\tau^* \rangle_{\vartheta_{\mathcal{L}}} \simeq 0.05 - 0.1 \lesssim \Delta\tau_{\Delta}^*$  of the fitted temperature range reported in Fig. 2. Then the ratio  $\frac{\langle \Delta\tau^* \rangle_{\vartheta_{\mathcal{L}}}}{\Delta\tau_{C1}^*}$  is greater than  $10^4$ . This value is *definitively* outside the Ising-like preasymptotic domain and similar to the value of crossover temperature scale  $\Delta\tau_{X,M}^* \simeq 0.23$  obtained from fitting using CPM and MSR crossover descriptions.

The above analysis limited to the results of Figure 2 extrapolated within the Ising-like preasymptotic domain, justify our special attention in the next section to methods which account for the calibrated contribution of the theoretical leading power law, in order to check in a self-consistent manner the  $\vartheta_{\mathcal{L}}$ -determination beyond the Ising-like preasymptotic domain.

## 4. XENON CHARACTERIZATION BEYOND THE ISING-LIKE PREASYMPTOTIC DOMAIN

### 4.1. Ising-like nature of the dimensionless scale factors

The finite and restricted  $\Delta\tau^*$  range where the mean crossover functions correctly represent  $\kappa_{T,\text{exp}}^*$  and  $\xi_{\text{exp}}$  data, determines the effective extension  $\mathcal{L}_{\text{EAD}}^{\text{Xe}}$  of the Ising-like extended asymptotic domain (EAD). Since the theoretical expressions of Eqs. (1) and (2), are in the form of a complete crossover,  $\mathcal{L}_{\text{EAD}}^{\text{Xe}}$  may involve correction-to-scaling terms higher than the first one. In such a situation, the following condition  $\mathcal{L}_{\text{PAD}}^{\text{Xe}} < \Delta\tau^* \leq \mathcal{L}_{\text{EAD}}^{\text{Xe}}$  occurs. This is precisely the case for the isothermal compressibility data of xenon obtained by Güttinger and Cannell. As a consequence, the value of  $\vartheta_{\mathcal{L}}$  introduced by the analytic relation  $t = \vartheta_{\mathcal{L}} \Delta\tau^*$ , is related to an “undefined” domain of extension  $\mathcal{L}_{\text{EAD}}^{\text{Xe}}$ . Here, “undefined” means “beyond the Ising-like preasymptotic domain”, so that we are not able to appreciate the effective influence of all the numerous corrections neglected in the massive renormalization scheme of the  $\Phi^4$  model (see I). We must solve new correlative difficulties concerning the effective number (which can thus be greater than 3) and the nature (which can originate from the neglected analytical and confluent effects in the critical massive renormalization scheme) of the fluid-dependent parameters.

Indeed, to complete  $T_c$  and  $\alpha_c$  knowledge in the absence of information concerning the true range of the Ising-like preasymptotic domain for an actual fluid, it is proposed (author?) [7, 17] to replace  $\vartheta$ ,  $\psi$ , and  $g_0$  by three new adjustable parameters  $\mathbb{X}_{0,\mathcal{L}}^*$ ,  $\mathbb{L}_{0,\mathcal{L}}^*$ , and  $\vartheta_{\mathcal{L}}$ , modifying Eqs. (23) and (20) in the following way:

$$\frac{1}{\kappa_{T,\text{exp}}^*(\Delta\tau^*)} = (\mathbb{X}_{0,\mathcal{L}}^*)^{-1} \mathbb{Z}_{\chi}^+ (\Delta\tau^*)^{\gamma} \prod_{i=1}^K (1 + X_{i,\chi}^+ t^{D(i)})^{Y_{i,\chi}^+} \quad (44)$$

$$\frac{\alpha_c}{\xi_{\text{exp}}^*(\Delta\tau^*)} = (\mathbb{L}_{0,\mathcal{L}}^*)^{-1} \mathbb{Z}_{\xi}^+ (\Delta\tau^*)^{\nu} \prod_{i=1}^K (1 + X_{i,\xi}^+ t^{D(i)})^{Y_{i,\xi}^+} \quad (45)$$

with

$$t = \vartheta_{\mathcal{L}} \Delta \tau^* \quad (46)$$

The new characteristic set

$$\mathbb{Q}_{c,\mathcal{L}} = \left\{ (\beta_c)^{-1}; \alpha_c; \mathbb{S}_{1CP,\mathcal{L}} \right\} \quad (47)$$

must substitute the set  $\mathbb{Q}_c (\Delta \tau^* \leq \mathcal{L}_{\text{EAD}}^{\text{Xe}})$  of Eq. (25), while the new dimensionless set

$$\mathbb{S}_{1CP,\mathcal{L}} = \left\{ \vartheta_{\mathcal{L}}; \mathbb{L}_{0,\mathcal{L}}^*; \mathbb{X}_{0,\mathcal{L}}^* \right\} \quad (48)$$

must substitute the set  $\mathbb{S}_{SF}$  of Eq. (26). The subscript  $1CP, \mathcal{L}$  recalls for a single crossover parameter to characterize the crossover behavior observed in the finite temperature range  $\mathcal{L}_{\text{PAD}}^{\text{Xe}} < \Delta \tau^* \lesssim \mathcal{L}_{\text{EAD}}^{\text{Xe}}$ .

In comparison to Eqs. (23) and (20), the noticeable modification of Eqs. (44) and (45) is the leading term in which  $\vartheta_{\mathcal{L}}$  is no longer involved in the asymptotic scaling part of the critical behavior expressed in terms of the physical field  $\Delta \tau^*$ . As introduced,  $\mathbb{X}_{0,\mathcal{L}}^*$  and  $\mathbb{L}_{0,\mathcal{L}}^*$  are prefactors for each corresponding property, here selected as independent and characteristic of the fluid by virtue of the two-scale-factor universality (provided that the same length unit was used to define the dimensionless quantities (**author?**) [25]). Correlatively,  $\vartheta_{\mathcal{L}}$  is a *pure* crossover parameter, with same value above and below  $T_c$ , which exclusively controls the magnitude of many correction terms to scaling. In addition,  $\vartheta_{\mathcal{L}}$  can also integrate some effects of the neglected terms linked to the supplementary confluent exponents, such as  $\Delta_2$  or  $\Delta_3$ , accounting for practical numerical approximations such as  $\Delta_2 \approx 2\Delta$  or  $\Delta_3 \approx 3\Delta$ , or the effects of using  $T$  to replace  $T_c$  in the energy unit and in the dimensionless form of the temperature distance to the critical temperature. For a fluid  $f$ , the determination of  $\vartheta_{\mathcal{L}}$  is then equivalent to the determination of  $\mathcal{L}_{\text{EAD}}^f$ . In this general case, the physical leading amplitudes can be calculated using:

$$\xi_{\mathcal{L}}^+ = \mathbb{L}_{0,\mathcal{L}}^* \left( \mathbb{Z}_{\xi}^+ \right)^{-1} \quad (49)$$

$$\Gamma_{\mathcal{L}}^+ = \mathbb{X}_{0,\mathcal{L}}^* \left( \mathbb{Z}_{\chi}^+ \right)^{-1} \quad (50)$$

i.e., without reference to  $\vartheta_{\mathcal{L}}$ . However, the subscript  $\mathcal{L}$  recalls for the determination of  $\vartheta_{\mathcal{L}}$ , then correlatively,  $\mathbb{L}_{0,\mathcal{L}}^*$  and  $\mathbb{X}_{0,\mathcal{L}}^*$ , made beyond the Ising-like preasymptotic domain. The single (system-dependent) first confluent amplitude can be calculated from  $\vartheta_{\mathcal{L}}$  uniquely, using one independent equation among the two following equations:

$$a_{\chi,\mathcal{L}}^+ = -(\vartheta_{\mathcal{L}})^{\Delta} \mathbb{Z}_{\chi}^{1,+} \quad (51)$$

$$a_{\xi,\mathcal{L}}^+ = -(\vartheta_{\mathcal{L}})^{\Delta} \mathbb{Z}_{\xi}^{1,+} \quad (52)$$

As suggested in Ref. (**author?**) [7], from similar fitting of the correlation length and the susceptibility in the inhomogeneous domain, the specific heat in the homogeneous and non homogeneous domains, and the coexisting density measurements in the inhomogeneous domain, one must verify the uniqueness of the  $\vartheta_{\mathcal{L}}$  value (along the critical isochore). Considering several properties allows then consistent tests for the determination of the set  $\mathbb{S}_{1CP,\mathcal{L}}$ , in coherence with the basic hypotheses of the renormalization group approach at the origin of the theoretical crossover functions.

To avoid this large task, in a first approach, we consider xenon for which we hypothesize the existence of a single scale factor  $\vartheta_{\mathcal{L}}$  in the temperature range  $\mathcal{L}_{\text{PAD}}^{\text{Xe}} < \Delta \tau^* \lesssim \mathcal{L}_{\text{EAD}}^{\text{Xe}}$ . Fitting then  $\kappa_{T,\text{exp}}^*$  and  $\xi_{\text{exp}}^*$  data in this temperature range with Eqs. (15) and (23), produces the set  $\mathbb{S}_{1CP,\mathcal{L}}$ , i.e., the determination of  $\vartheta_{\mathcal{L}}$ . Extrapolating the results for  $\Delta \tau^* \rightarrow 0$ , we can identify the value of the asymptotic scale factor  $\vartheta$  to

$$\vartheta \equiv \vartheta_{\mathcal{L}} \text{ for } \Delta \tau^* \leq \mathcal{L}_{\text{PAD}}^{\text{Xe}} \quad (53)$$

After that identification, we can introduce the dimensional prefactor  $\mathbb{L}_{0,\mathcal{L}} = \alpha_c \mathbb{L}_{0,\mathcal{L}}^*$  leading to define the asymptotic wave number  $g_0$  of Eq. (33) by the following parameter:

$$g_0 \equiv g_{0,\mathcal{L}} = (\mathbb{L}_{0,\mathcal{L}})^{-1} (\vartheta_{\mathcal{L}})^{-\nu} = [\alpha_c \mathbb{L}_{0,\mathcal{L}}^* (\vartheta_{\mathcal{L}})^{\nu}]^{-1} \quad (54)$$

The two remaining asymptotic scale factors  $\mathbb{L}^{\{1f\}}$  [see Eq. (21)], and  $\psi_{\rho}$  [see Eq. (18)], are then obtained by the hierarchical equations:

$$\mathbb{L}^{\{1f\}} = \alpha_c g_{0,\mathcal{L}} = [\mathbb{L}_{0,\mathcal{L}}^* (\vartheta_{\mathcal{L}})^{\nu}]^{-1} \quad (55)$$

$$\psi_{\rho,\mathcal{L}} = \left[ \left( \mathbb{L}^{\{1f\}} \right)^{-d} \mathbb{X}_{0,\mathcal{L}}^* (\vartheta_{\mathcal{L}})^{\gamma} \right]^{\frac{1}{2}} \quad (56)$$

Finally, for  $\Delta \tau^* \rightarrow 0$ , the scale factor set

$$\mathbb{S}_{SF,\mathcal{L}} = \left\{ \vartheta_{\mathcal{L}}; \mathbb{L}^{\{1f\}}; \psi_{\rho,\mathcal{L}} \right\} \text{ with } 0 < \Delta \tau^* < \mathcal{L}_{\text{EAD}}^{\text{Xe}} \quad (57)$$

has the appropriate asymptotic form to compare with  $\mathbb{S}_{SF}$  [Eq. (26)], except the noticeable subscript  $\mathcal{L}$  which recalls the “non-asymptotic” Ising-like nature of these numbers which originates *de facto* from the determination of  $\vartheta_{\mathcal{L}}$ ,  $\mathbb{L}_{0,\mathcal{L}}^*$  and  $\mathbb{X}_{0,\mathcal{L}}^*$  made *beyond* the Ising-like preasymptotic domain.

However, when this “hypothetical” xenon is characterized by Eq. (47) [or Eq. (57)], thus Eq. (55) is *true* and the following variable transformations

$$\xi \rightarrow \xi^* = \frac{\xi}{\alpha_c} \rightarrow \ell_{\text{th}} = \mathbb{L}^{\{1f\}} \xi^* \quad (58)$$

$$\Delta \tau^* \rightarrow t = \vartheta_{\mathcal{L}} \Delta \tau^* \quad (59)$$

result in the asymptotic collapse (over the extension  $\mathcal{L}_{\text{PAD}}^{\{1f\}}$  (**author?**) [10, 11]) of any physical curves of equation  $\xi(\Delta\tau^*)$  into the universal curve of equation

$$\ell_{\text{th}}(t) = \mathbb{L}^{\{1f\}} \xi^*(\Delta\tau^*) = g_{0,\mathcal{L}} \xi_{\text{exp}}(\Delta\tau^*) \quad (60)$$

We have used this universal feature due to the scale factor nature of  $\vartheta_{\mathcal{L}}$  to obtain the xenon values of lines 8 and 9 of Table II from theoretical values of lines 5 and 6, respectively. In such a numerical approach, the “hypothesized” xenon values of the characteristic set  $\mathcal{S}_{1CP,\mathcal{L}}$  are the following [see Eq. (A10) in Appendix]

$$\mathcal{S}_{1CP,\mathcal{L}} = \left\{ \begin{array}{l} \vartheta_{\mathcal{L}} = 0.021069 \\ \mathbb{L}_{0,\mathcal{L}}^* = 0.443526 \\ \mathbb{X}_{0,\mathcal{L}}^* = 0.214492 \end{array} \right\} \quad (61)$$

with

$$\mathbb{L}_{0,\mathcal{L}} = \alpha_c \mathbb{L}_{0,\mathcal{L}}^* = 0.390972 \text{ nm} \quad (62)$$

and, obviously

$$\mathbb{L}^{\{1f\}} \equiv \alpha_c g_{0,\mathcal{L}} = 25.6936 \quad (63)$$

More generally, our hypothesized values of Eq. (61) provide the (expected) identity  $\mathcal{S}_{SF,\mathcal{L}} \equiv \mathcal{S}_{SF}$ . Accordingly, the universal scaling form of the correlation length of xenon reads as follows

$$\mathbb{L}^{\{1f\}} \xi^*(\Delta\tau^*) = \frac{\xi_{\text{exp}}(\Delta\tau^*)}{\frac{0.0343085}{[\text{nm}]}} \equiv \ell_{\text{th}}(t) \quad (64)$$

with

$$t = 0.021069 \Delta\tau^* \quad (65)$$

Either the “theoretical” value  $0.0343085 \text{ nm} (= [g_{0,\mathcal{L}}]^{-1})$  of the length unit in Eq. (64), or the “measured” value  $0.184333 \text{ nm} (= \xi_{0,\mathcal{L}}^+)$  of the correlation length amplitude in Eq. (28), cannot easily be related to a real microscopic length of xenon atom, while the fact that the “fitting” value  $0.390972 \text{ nm} (= \mathbb{L}_{0,\mathcal{L}})$  of the dimensional prefactor is comparable to the size of the xenon atom can be considered as a fortuitous result (**author?**) [61].

As expected, more fundamental is the dimensionless nature of Eq. (63) which can then provide the needed uniqueness of the length unit for better understanding of universality. Indeed, the above asymptotic collapse of the correlation length implies equivalent asymptotic collapse of any other singular thermodynamic property, by virtue of hyperscaling. That means that, when the scale factors  $\mathbb{L}^{\{1f\}}$  and  $\vartheta_{\mathcal{L}}$  are determined in the Ising-like extended asymptotic domain  $\mathcal{L}_{\text{PAD}}^{\text{Xe}} < \Delta\tau^* \lesssim \mathcal{L}_{\text{EAD}}^{\text{Xe}}$ , the validity range where the universal collapse onto the theoretical thermodynamic behavior is expected, can be alternatively discussed in term of the value  $\ell_{\text{th}}(t) > \mathbb{L}^{\{1f\}}$ . In other words, all the crossover functions are “Ising-like” universal:

i) only over the temperature range where *the crossover parameter is unique*;

ii) only for a single dimensionless critical length  $\mathbb{L}^{\{1f\}}$  common for all the fluids which obey to this single parameter crossover description.

For example, looking back on our previous analysis of the residuals for the xenon isothermal compressibility case, by reversing Eq. (64), we can transform  $\Delta\tau^*$  in universal values of  $\ell_{\text{th}}$ , as illustrated in the upper axis of Figure 2. Simultaneously, as previously mentioned, we are also able to illustrate in this figure (or in any figure which use a xenon  $\Delta\tau^*$ -coordinate) all the conditions estimated in Table II. In the part of the Güttinger and Cannell’s experimental range which corresponds to the theoretical condition  $\ell_{\text{th}} \gtrsim (2.5 - 3) \mathbb{L}^{\{1f\}} \simeq 70$ , the universal behavior of the functional form  $\chi^*(\ell_{\text{th}})$  can then be analytically “tested” in this Ising-like extended asymptotic domain. Simultaneously, we will also confirm below the uniqueness of the crossover parameter by using an alternative facet of the universality accounted for by the mean crossover functions. As a matter of fact, to illustrate the asymptotic Ising-like transformation of each thermodynamic property  $P^*(\Delta\tau^*)$  attached to the uniqueness of the crossover parameter, we can also use the effective universal behavior of the local exponent  $e_{P,\text{th}}(t)$  to replace the one of the correlation length  $\ell_{\text{th}}(t)$ , in order to construct the “universal” scaling form  $F_P(e_{P,\text{th}})$ . Therefore, in a second approach with the objective to illustrate this transformation in a self-consistent manner for the susceptibility case, we consider the universal and experimental effective amplitudes attached to the local power laws with effective exponents, such as introduced in Ref. (**author?**) [41].

#### 4.2. Effective exponent and amplitude beyond the Ising-like PAD

From  $\chi_{\text{th}}(t)$  of Eq. (2), the related local values of the effective exponent  $\gamma_{e,\text{th}}(t)$  and effective amplitude  $\mathbb{Z}_{\chi,e}^+(t)$  are given by the equations

$$\gamma_{e,\text{th}}(t) = - \frac{\partial \text{Ln} [\chi_{\text{th}}(t)]}{\partial \text{Ln} t} \quad (66)$$

$$\mathbb{Z}_{\chi,e}^+(t) = \frac{\chi_{\text{th}}(t)}{t^{-\gamma_e}} \quad (67)$$

Eliminating  $t$  [then simultaneously eliminating the scale factor  $\vartheta_{\mathcal{L}}$ , since  $t = \vartheta_{\mathcal{L}} \Delta\tau^*$ ], the theoretical classical-to-critical crossover is characterized by a “universal” curve  $\mathbb{Z}_{\chi,e}^+(\gamma_{e,\text{th}})$  over the complete range  $\gamma_{\text{MF}} \leq \gamma_{e,\text{th}}(t) \leq \gamma$  (see curve labeled  $\Phi_3(1)$ -MR in Fig. 3).

Our present interest is restricted to the Ising-like range  $\gamma_{e,\text{th}}(t) \geq \gamma_{\frac{1}{2}} = \frac{\gamma + \gamma_{\text{MF}}}{2}$  (see the corresponding Ising-like range defined in the upper part of Fig. 3). The theoretical Ising-like limiting point takes universal coordinates

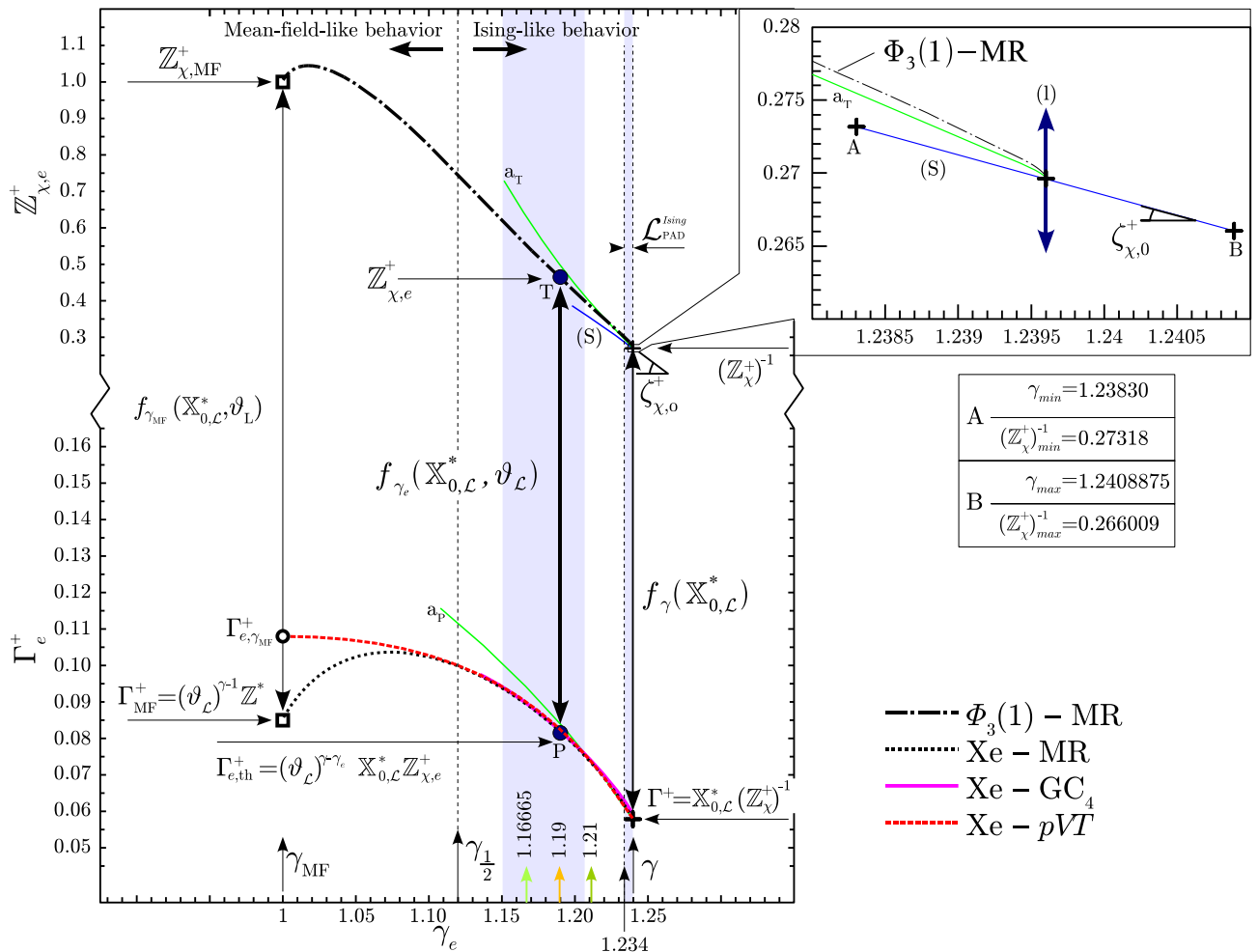


Figure 3: (Color on line) Two-parameter transformations  $f_{\gamma_e}(\mathbb{X}_{0,\mathcal{L}}^*, \vartheta_{\mathcal{L}})$  (see arrays), at  $\gamma_e = \text{constant value}$ , from the theoretical universal behavior of the susceptibility (upper curve), to the xenon effective behavior of the isothermal compressibility (lower curve) (in dimensionless variables);  $\mathbb{X}_{0,\mathcal{L}}^*$ : adjustable parameter for the general case of Eq. (44), unequivocally defined from comparison in positions of the two Ising limiting points (right crosses);  $\vartheta_{\mathcal{L}}$  adjustable parameter unequivocally defined by the two other points, either within the Ising-like preasymptotic domain (see the insert and the text), or outside the Ising-like preasymptotic domain (full black circles T and P on the two curves labeled  $\Phi_3(1) - \text{MR}$  and Xe - MR, respectively). Note the inversion of the relative position between the curve labeled  $\Phi_3(1) - \text{MR}$  and the curve labeled  $a_T$  which is related to the asymptotic (logarithmic) approximation of Eq. (68), beyond the Ising-like preasymptotic domain.

$\{\gamma; (Z_{\chi}^+)^{-1}\}$  (upper cross in Fig. 3). The “small” extension  $\gamma - \gamma_{e,th} \lesssim Z_{\chi}^{+,th} \Delta (\mathcal{L}_{\text{PAD}}^{\text{Ising}})^{\Delta} \approx 0.006$  of the Ising-like preasymptotic domain is magnified by the curve labeled  $\Phi_3(1) - \text{MR}$  in the insert of Fig. 3. On the other hand, the curve  $a_T$  corresponds to the asymptotic behavior of the derivative  $\left(\frac{\partial Z_{\chi,e}^+}{\partial \gamma_e}\right)_{\gamma_e \rightarrow \gamma}$  of equation

$$\left(\frac{\partial Z_{\chi,e}^+}{\partial \gamma_e}\right)_{\gamma_e,th \rightarrow \gamma} = (Z_{\chi}^+)^{-1} \left\{ 1 + \left(\frac{\gamma - \gamma_{e,th}}{\Delta |Z_{\chi}^{+,th}|}\right)^{-\left(\frac{\gamma - \gamma_{e,th}}{\Delta}\right)} \left(1 - \log \left[\frac{\gamma - \gamma_{e,th}}{\Delta |Z_{\chi}^{+,th}|}\right]\right) \left(\frac{\gamma - \gamma_{e,th}}{\Delta}\right) \right\} \quad (68)$$

The vertical double arrow with label(1) indicates the

above logarithmic divergence of  $\left(\frac{\partial Z_{\chi,e}^+}{\partial \gamma_e}\right)_{\gamma_e,th \rightarrow \gamma}$ . We note the significant difference between the curve  $a_T$  and the curve (S) which results from “analytic” error-bar correlation between the Ising values of  $\gamma$  and  $(Z_{\chi}^+)^{-1}$ . As a matter of fact, the curve (S) corresponds to the linearized slope  $\zeta_{\chi,0}^+ = \frac{(Z_{\chi}^+)_{max}^{-1} - (Z_{\chi}^+)_{min}^{-1}}{\gamma_{min} - \gamma_{max}}$  between the respective bounded coordinates of points A and B (see inserted table in Fig. 3 and Ref. (author?) [7] for data sources).

Since only two parameters ( $\mathbb{X}_{0,\mathcal{L}}^*$  and  $\vartheta_{\mathcal{L}}$ ) are free in fitting Eq. (44), Fig. 3 illustrates how the adjustable prefactor  $\mathbb{X}_{0,\mathcal{L}}^*$  acts at the exact value of the Ising exponent, since each Ising point of the fluid takes the coordinates  $\{\gamma; \Gamma^+ = \mathbb{X}_{0,\mathcal{L}}^* (\mathbb{Z}_{\chi}^+)^{-1}\}$ , as represented by the

lower cross in Fig. 3 for the critical xenon case. The resulting prefactor  $f_\gamma(\mathbb{X}_{0,\mathcal{L}}^*) \equiv \mathbb{X}_{0,\mathcal{L}}^*$  is schematized by the double array between two crosses in Fig. 3. Therefore, calibrating the  $\Gamma^+$  value as suggested in previous paragraph, fixes this prefactor value which governs the universal collapse of the Ising-like limiting point through Eq. (50).  $\mathbb{X}_{0,\mathcal{L}}^*$  acts in an equivalent manner to  $\mathbb{L}^{\{1f\}}$  [see Eq. (64)] for the correlation length case. In principle, the critical divergence in the initial slope at the limiting points provides the second “Ising-like constraint” which is needed to determine the asymptotic scale factor  $\vartheta$ . However, our previous description of the Ising-like preasymptotic domain and its above geometrical illustration underline the challenging (theoretical and experimental) difficulties to provide the exact characterization of the asymptotic scaling when a property reaches the Ising-like limiting point along a curve of “universal”, but *infinite*, slope for all the physical systems.

At contrario, the description of the  $\gamma_e$ -variation in the range  $\gamma - \gamma_e \gtrsim 0.015$  (i.e., in a temperature range significantly beyond the Ising-like preasymptotic domain), appears now simplified, using precisely the Güttinger and Cannell’s results of Eq. (43) to define the following effective exponent by :

$$\gamma_{e,\text{exp}}(\Delta\tau^*) = -\frac{\partial \text{Ln} [\kappa_{T,\text{exp}}^*(\Delta\tau^*)]}{\partial \text{Ln}(\Delta\tau^*)} \quad (69)$$

and its attached effective amplitude by :

$$\Gamma_e^+(\Delta\tau^*) = \frac{\kappa_{T,\text{exp}}^*(\Delta\tau^*)}{(\Delta\tau^*)^{-\gamma_{e,\text{exp}}}} \quad (70)$$

The resulting single curve  $\Gamma_e^+(\gamma_{e,\text{exp}})$  is illustrated in the lower part of Fig. 3 (see curve Xe – GC<sub>4</sub>), while the expected (two parameter) transformation  $f(\mathbb{X}_{0,\mathcal{L}}^*, \vartheta_{\mathcal{L}})$  able to insure the universal collapse between the theoretical curves (labeled Xe – MR and  $\Phi_3$  (1)-MR), is schematized by a double array between two points on each curve of well-defined *finite* slope. This transformation must contain the needed both constraints for the (point) position *and* the related (tangent) direction. Therefore, the scaling nature of the collapse beyond the Ising-like preasymptotic domain is significantly different in fitting procedure which either eliminates, or accounts for, the contribution of the leading term. In the latter situation, we can then replace the prefactor  $\mathbb{X}_{0,\mathcal{L}}^*$  by the calibrated leading amplitude  $\Gamma^+$ , as seen above.

In the first case, *at large temperature distance*, the fit procedure based on Eq. (44) is mainly equivalent to a dominant constraint in “direction” given by the following relation between the two effective exponents:

$$\gamma_{e,\text{exp}}(\Delta\tau^*) \equiv \gamma_{e,\text{th}}[\vartheta_{\mathcal{L}}(\Delta\tau^*)] \quad (71)$$

We *numerically* solve Eq. (71), using the Güttinger and Cannell’s fitting results given by Eq. (43), then providing the  $\gamma_e$   $[(\Delta\tau^*)]$  and  $\vartheta_{\mathcal{L}}(\Delta\tau^*)$  values as a function of  $\Delta\tau^*$ . Both results are reported as the curve labeled GC<sub>4</sub> in

Fig. 4a [ $\gamma_e$  as a function of  $\Delta\tau^*$ ], and the curve labeled 1 in Fig. 4b [ $\vartheta_{\mathcal{L}}$  as a function of  $\Delta\tau^*$ ], respectively.

In the second case, to account for the contribution of the leading term needs to use the following *scaling* relation between the two effective amplitudes

$$\Gamma_e^+ = (\vartheta_{\mathcal{L}})^{\gamma - \gamma_e} \mathbb{X}_{0,\mathcal{L}}^* \mathbb{Z}_{\chi,e}^+ \quad (72)$$

Now, the transformation  $f(\mathbb{X}_{0,\mathcal{L}}^*, \vartheta_{\mathcal{L}}) = (\vartheta_{\mathcal{L}})^{\gamma - \gamma_e} \mathbb{X}_{0,\mathcal{L}}^*$  is explicit in Eq. (72). It takes a convenient effective power law of the crossover parameter  $\vartheta_{\mathcal{L}}$ , while the prefactor  $\mathbb{X}_{0,\mathcal{L}}^*$  has (as expected above) the same value whatever the  $\gamma_e$  ( $= \gamma_{e,\text{exp}} = \gamma_{e,\text{th}}$ ) value is. The constrained “position and direction” are accounted for correctly. Therefore, using Eq. (50) to eliminate  $\mathbb{X}_{0,\mathcal{L}}^*$ , infers the *pure*  $\vartheta_{\mathcal{L}}$ -dependence of equation

$$\frac{\Gamma_e^+}{\Gamma^+} = (\vartheta_{\mathcal{L}})^{\gamma - \gamma_e} \frac{\mathbb{Z}_{\chi,e}^+}{(\mathbb{Z}_\chi^+)^{-1}} \quad (73)$$

By appropriate combination between the Güttinger and Cannell’s fitting results and the mean crossover function for susceptibility, we *numerically* calculate the local value of the crossover parameter over the complete experimental temperature range, using the equation

$$\vartheta_{\mathcal{L}} = \left( \frac{1}{\mathbb{Z}_\chi^+ \mathbb{Z}_{\chi,e}^+} \times \frac{\Gamma_e^+}{\Gamma^+} \right)^{\frac{1}{\gamma - \gamma_e}} \quad (74)$$

It is essential to note that for each fluid for which  $\Gamma^+$  is known, Eq. (74), applied in the extended asymptotic domain  $\Delta\tau^* \lesssim \mathcal{L}_{\text{EAD}}^{\text{Xe}}$ , takes equivalent “Ising-like” meaning to Eq. (32) applied within the Ising-like preasymptotic domain  $\Delta\tau^* \lesssim \mathcal{L}_{\text{PAD}}^{\text{Xe}}$ . In Figure 4b, we have reported as a curve labeled 2, the calculated value of  $\vartheta_{\mathcal{L}}$  as a function of  $\Delta\tau^*$ , using Eq. (74) with  $\Gamma^+ = 0.0578204$  [see Eq. (39)]. The available part of these curves 1 and 2 must be restricted to the experimental temperature range illustrated by the segment labeled GC.

For both cases, the  $\vartheta_{\mathcal{L}}$ -change as a function of  $\Delta\tau^*$  within the range  $10^{-3} \lesssim \Delta\tau^* \lesssim 10^{-1}$  of Fig. 4b, can be approximated by our hypothetical Ising-like asymptotic value  $\vartheta = 0.021069$  of Eq. (39). In Fig. 4c the corresponding curves (labeled 1 and 2) of the residuals  $R\%(\vartheta_{\mathcal{L}})_\vartheta = 100 \left( \frac{\vartheta_{\mathcal{L}}}{\vartheta} - 1 \right)$  (expressed in %), together with their mean curve (labeled *m*), are given. In the temperature range  $5 \times 10^{-3} \lesssim \Delta\tau^* \lesssim 10^{-1}$  of Fig. 4c, the green area corresponds to the error-bar of  $\pm 15\%$  for both determinations. Even at such large values of  $\Delta\tau^*$ , the main significant result obtained from the massive renormalization scheme, is the estimation of the temperature-like crossover parameter in conformity with the asymptotic two-scale-factor characterization of the fluid, especially using the true scaling Eq. (74).

Such a temperature range where a “measurable” value of the exponent difference  $\gamma - \gamma_e$  occurs, was largely investigated in the seventy’s (**author?**) [42], when the scaling approach of the fluid universality was based on the effective “universal” values of the critical exponents - as for

example  $\gamma_e = 1.211$  (author?) [43],  $\gamma_{eos} = 1.19$  (author?) [24, 42], and  $\gamma_e = 1.16665$  (author?) [13] - involved in effective power laws and/or effective “universal” form of a rescaled equation of state. Anticipating a more detailed discussion given in Appendix A, we can use the data reported on Table V for these  $\gamma_e$  values to easily demonstrate, using the corresponding arrows in Fig. 4a, the “Ising-like nature” of the covered temperature range  $\Delta\tau^* \lesssim 0.05 - 0.1 \ll \Delta\tau_{\Delta}^*$ , or alternatively but equivalently, the “Ising-like nature” of the covered correlation length range  $\ell_{th} \gtrsim 70 > 2.5L^{\{1f\}}$ . That also gives interest to revisit (author?) [17] the effective universal formulation of a parametric equation of state using the master crossover functions to validate the universal features observed in the well-defined Ising-like extended asymptotic domain of the fluid subclass.

Finally we note that, when  $T_c$  and  $\alpha_c$  are known, the mean crossover functions take a convenient controlled form to determine a single crossover parameter  $\vartheta_{\mathcal{L}}$  in a temperature range beyond the Ising-like preasymptotic domain. The Ising-like nature of this crossover parameter is then revealed by the dimensionless value of a single characteristic length. However, to define the “minimal” set of three characteristic parameters such as  $\{\vartheta_{\mathcal{L}}; \mathbb{X}_{0,\mathcal{L}}^*; \mathbb{L}_{0,\mathcal{L}}^*\}$ , or, alternatively but equivalently,  $\{\vartheta; \psi_{\rho}; g_0\}$ , and  $\{a_{\chi}^+; \Gamma^+; \xi_0^+\}$ , one needs a “data calibration” from measurements performed within the Ising-like preasymptotic domain. The practical interest of this data calibration is given in the Appendix A, without reference to the estimated precision of the experimental method able to provide such measurements in this closest temperature range.

In the absence of explicit thermodynamic definition for the prefactors  $\mathbb{L}_{0,\mathcal{L}}^*$ ,  $\mathbb{X}_{0,\mathcal{L}}^*$  and the crossover parameter  $\vartheta_{\mathcal{L}}$  [or for the scale factors  $g_0$ ,  $\vartheta$ , and  $\psi_{\rho}$ ], the remaining difficulty is to compare between distinct fluids which show differences in their fluid-dependent amplitudes  $\xi_0^+$ ,  $\Gamma^+$ , and  $a_{\chi}^+$ . This difficulty can be solved by application of the scale dilatation method when the localization of their liquid-vapor critical point is known, as shown in Appendix A for the xenon case.

## 5. CONCLUSION

Using xenon as a standard critical fluid, and the mean crossover function for susceptibility in the homogeneous phase as an illustrative example, we have estimated the values of the fluid-dependent parameters which are compatible with the universal features predicted by the massive renormalization scheme. A special mention for the three dimensionless parameter characterization *within* the Ising-like preasymptotic domain was given, in spite of the large theoretical and experimental uncertainties at such “closest” temperature distance to the critical temperature. Using the abundant literature now available from several fittings of Güttinger and Cannell’s data, we have demonstrated the great advantage of the mean

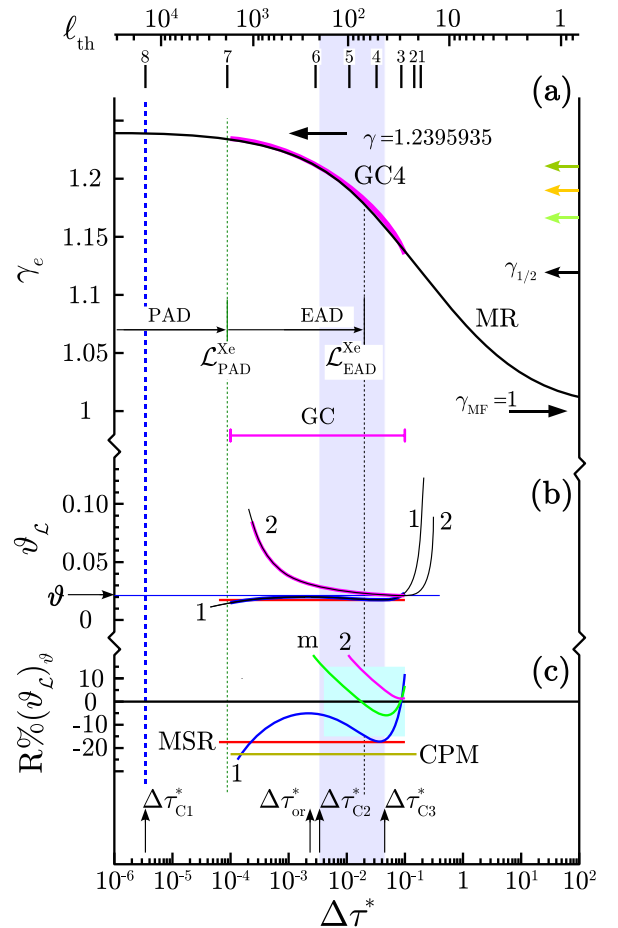


Figure 4: (Color on line) Ising-like asymptotic behaviors of: (a), the effective exponent  $\gamma_e$  for the xenon isothermal susceptibility, (b), the xenon crossover parameter  $\vartheta_{\mathcal{L}}$ , and (c), the percent deviation between  $\vartheta_{\mathcal{L}}$  and the xenon asymptotic scale factor  $\vartheta$  calculated from the scale dilatation method, as a function of the relative temperature  $\Delta\tau^*$  (lower horizontal axis) and the theoretical correlation length  $\ell_{th}$  (upper horizontal axis); curve labeled MR: from MR crossover function of Eq. (23) and xenon parameters of Eq. (40); curve GC4: from a fit of the Güttinger and Cannell’s data by Eq. (43) and xenon parameters in Table IV line GC<sub>4</sub>; curve 1: from Eq. (71); curve 2: from Eq. (74); Curve m: mean value of curves 1 and 2; lines labeled CPM and MSR: with  $\vartheta_{\mathcal{L}}$ -values of Table III obtained from the fitting results of the Güttinger and Cannell’s data by CPM and MSR crossover functions (see text).

crossover functions to provide an unambiguous determination of one fluid-dependent crossover parameter outside the Ising-like preasymptotic domain. Specifically, we have clearly shown that the value of this crossover parameter is entirely governed by fitting the data at “largest” distance to the critical point, leading for example to an apparent reduction of the uncertainty in the determination of the amplitude of the first confluent correction-to-scaling term. Finally, the magnitude of the resulting deviations and the range of temperature where it is to be

observed are exactly accounted for.

However, in the absence of controlled information about the Ising-like preasymptotic domain description, only the similar use of the complete set of mean crossover functions applied to several properties is able to demonstrate that the crossover parameter conserves its “Ising-like” nature, even outside the Ising-like preasymptotic domain. Alternatively, it was recently proposed in II and hereafter justified in the Appendix A for the xenon case, an appropriate modification of the mean crossover functions which only uses three master (i.e. constant) parameters. The modified crossover functions represent the master (i.e. unique) singular behaviors of the one component fluid subclass in a well-defined Ising-like extended asymptotic domain. In such a situation, the real extension and amplitude of the singular behavior of the fluid properties can be estimated for any one-component fluid for which the vapor-liquid critical point is localized in the  $pVT$  phase surface.

### Acknowledgments

The authors are indebted to C. Bervillier for valuable discussion and constructive comments during this work.

## Appendix A: ISOTHERMAL COMPRESSIBILITY OF XENON

In the first part of this Appendix we calculate the characteristic parameters of xenon involved in Eqs. (38) and (39), by using the scale dilatation method (author?) [13, 14]. The needed information is then given by the set  $Q_{c,a\bar{p}}^{min}$  made of four critical coordinates of the xenon critical point. Indeed, for any one-component fluid,  $Q_{c,a\bar{p}}^{min}$  reads as follows (II)

$$Q_{c,a\bar{p}}^{min} = \left\{ T_c; p_c; v_{\bar{p},c}; \gamma'_c \right\} \quad (\text{A1})$$

where  $v_{\bar{p},c} = \frac{m_{\bar{p}}}{\rho_c}$  is the critical molecular volume and  $\gamma'_c$  is the common critical direction at the critical temperature of the critical isochoric line and the saturation pressure curve in the  $p; T$  diagram.

The second part shows that the xenon parameters given by Eq. (40) can be used as entry data for the Eqs. (3) and (23) to represent accurately the singular behavior of the xenon isothermal compressibility in the temperature range such as  $T - T_c \lesssim 5 - 10$  K.

The last part discusses the data calibration and the uniqueness of the Ising-like crossover parameter within the extended asymptotic domain.

## 1. Xenon data sources from application of the scale dilatation method

### a. Xenon critical coordinates

The selected critical coordinates of xenon are:

$$\begin{aligned} T_c &= 289.733 \text{ K}; \\ p_c &= 5.84 \text{ MPa}; \\ \rho_c &= 1113 \text{ kg m}^{-3} \text{ or } v_{\bar{p},c} = 0.19596 \text{ nm}^3; \\ \gamma'_c &= 0.1192 \text{ MPa K}^{-1}; \\ \text{with } m_{\bar{p}} &= 2.181 \times 10^{-25} \text{ kg}. \end{aligned} \quad (\text{A2})$$

They result from the combined analysis (author?) [12, 13] of  $pVT$  measurements of Habgood and Schneider (author?) [46], and coexisting density measurements of Weinberger and Schneider (author?) [45], Cornfeld and Carr (author?) [63], Thoen and Garland (author?) [67], and Balzarini and coworkers (author?) [70, 71].

The xenon critical temperature and pressure were fixed to the values recently provided by Gillis et al (author?) [72] which are compatible with  $T_c = 289.740 \pm 0.003$  K and  $p_c = 5.8400 \pm 0.0005$  MPa obtained from Schneider et al's measurements.

The  $\rho_c$  value has an uncertainty of  $\pm 5 \text{ kg m}^{-3}$  ( $\sim 0.5\%$ ), which accounts for the  $\rho_c$  values of Schneider et al's ( $\rho_c = 1110 \pm 2 \text{ kg m}^{-3}$ ) (author?) [45, 46], Cornfeld and Carr's ( $\rho_c = 1111.2_{-3.4}^{+1.9} \text{ kg m}^{-3}$  for three different estimations) (author?) [63], Baidakov et al's ( $\rho_c = 1112.8 \pm n.a. \text{ kg m}^{-3}$ ) (author?) [64], and Balzarini et al's ( $\rho_c = 1099 \pm n.a. \text{ kg m}^{-3}$ ) (author?) [70],  $\rho_c = 1116.0 \pm 1.7 \text{ kg m}^{-3}$  and  $\rho_c = 1114.0 \pm 1.7 \text{ kg m}^{-3}$  (author?) [71]).

The value  $\gamma'_c = 0.1192 \pm 0.0005 \text{ MPa K}^{-1}$  ( $\sim 0.5\%$ ) was estimated by one of us (author?) [12] by graphical analysis of the  $pVT$  measurements of Habgood and Schneider, which agrees to other literature values  $\gamma'_c = 0.1192 \text{ MPa K}^{-1}$  (author?) [51],  $\gamma'_c = 0.1196 \text{ MPa K}^{-1}$  (author?) [52], and  $\gamma'_c = 0.120 \text{ MPa K}^{-1}$  (author?) [64]. The  $\gamma'_c$  value used in Ref. (author?) [72] differs by 0.19%.

More generally, we note the remarkable agreement with the critical set defined by Gillis et al (author?) [72] in their recent analysis of the sound attenuation (in the frequency range  $100 < f \text{ (Hz)} < 7500$ ) within thermoacoustic layers between solid surfaces and xenon at critical density.

### b. Physical and master amplitudes from the scale dilatation method

From Eq. (A2), the critical values [see Eq. (38)] of the energy  $(\beta_c)^{-1}$  and length  $\alpha_c$  units of xenon are the

following:

$$\begin{aligned} (\beta_c)^{-1} &= k_B T_c = 4.0003 \times 10^{-21} \text{ J} \\ \alpha_c &= \left( \frac{k_B T_c}{\rho_c} \right)^{\frac{1}{d}} = 0.881508 \text{ nm} \end{aligned} \quad (\text{A3})$$

while the values of two xenon scale factors  $Y_c$  and  $Z_c$  are the following:

$$\begin{aligned} Z_c &= \frac{\rho_c m_{\bar{p}}}{\rho_c k_B T_c} = 0.28601 \\ Y_c &= \gamma'_c \frac{T_c}{\rho_c} - 1 = 4.91373 \end{aligned} \quad (\text{A4})$$

We have calculated the values [see Eq. (39)] of the xenon amplitudes  $\Gamma^+$ ,  $\xi_0^+$ , and  $a_{\chi^+}$ , (or  $a_{\xi^+}$ ) by using the following relations :

$$\begin{aligned} a_{\chi^+} &= Z_{\chi^+}^{1,+} \left[ (Y_c)^{\Delta} \right] = 1.23399 \\ \xi^+ &= Z_{\xi^+}^+ \left[ (Y_c)^{-\nu} \right] = 0.209111 \\ \Gamma^+ &= Z_{\chi^+}^+ \left[ (Z_c)^{-1} (Y_c)^{-\gamma} \right] = 0.0578204 \end{aligned} \quad (\text{A5})$$

(with  $\alpha_c \xi^+ = 0.184333 \text{ nm}$ )

where the respective values of the master amplitudes  $Z_{\xi^+}^+$ ,  $Z_{\chi^+}^+$ , and  $Z_{\chi^+}^{1,+}$  (or  $Z_{\xi^+}^{1,+}$ ) are **(author?)** [17]

$$\begin{aligned} Z_{\xi^+}^+ &= 0.570481 \\ Z_{\chi^+}^+ &= 0.119 \\ Z_{\chi^+}^{1,+} &= 0.555 \end{aligned} \quad (\text{A6})$$

Hereabove, universal features within the Ising-like preasymptotic domain are correctly accounted for by the following equations

$$\begin{aligned} Z_{\xi^+}^{1,+} &= 0.37695 \\ a_{\xi^+}^+ &= Z_{\xi^+}^{1,+} \left[ (Y_c)^{\Delta} \right] = 0.83812 \\ \text{with } \frac{Z_{\xi^+}^{1,+}}{Z_{\chi^+}^{1,+}} &= \frac{a_{\xi^+}^+}{a_{\chi^+}^+} = 0.67919 \end{aligned} \quad (\text{A7})$$

The amplitude value  $\xi_0^+ = 0.184333 \text{ nm}$  estimated using the scale dilatation method, compares favorably with the one  $\xi_0^+ = 0.1866 \pm 0.001 \text{ nm}$  recently used by Gillis et al **(author?)** [72] to analyze sound attenuation within thermoacoustic layers between solid surfaces and xenon at critical density. Moreover, this amplitude value is also in agreement with the following ones obtained from analyses of (static and dynamic) light scattering measurements: (i)  $\xi_0^+ = 0.2 \text{ nm}$ , with  $\nu = 0.63$ , in the temperature range  $22 \text{ mK} \leq T - T_c \leq 3.3 \text{ K}$  [i.e.,  $8 \times 10^{-5} \lesssim \Delta\tau^* \lesssim 10^{-2}$ ] (see Refs. **(author?)** [49, 50, 52]); (ii)  $\xi_0^+ = 0.1934 \text{ nm}$ , with  $\nu = 0.62$ , in the temperature range  $2.6 \text{ mK} \leq T - T_c \leq 10 \text{ K}$  [i.e.,  $9 \times 10^{-6} \lesssim \Delta\tau^* \lesssim 3.4 \times 10^{-2}$ ] from Ref. **(author?)** [53]; (iii)  $\xi_0^+ = 0.184 \pm 0.009 \text{ nm}$  and one confluent correction term (with  $a_{\xi^+}^+ = 0.55$  and  $\Delta = 0.5$ ), in the temperature range  $28 \text{ mK} \leq T - T_c \leq 3.65 \text{ K}$  [i.e.,  $9.6 \times 10^{-5} \lesssim \Delta\tau^* \lesssim 1.26 \times 10^{-2}$ ] from Ref. **(author?)** [21].

Using the above xenon parameters in the theoretical estimation of the correlation length, we also underline that the agreement with the experimental measurements extends to the range  $\frac{\xi}{\alpha_c} \gtrsim 3$ , i.e., in a temperature range  $\Delta\tau^* \lesssim L_{EAD}^{\chi_c} \simeq (2 - 3) \times 10^{-2}$  which extends largely beyond the Ising-like preasymptotic domain (see Ref. **(author?)** [10]). For example, at the calibration temperature  $T = T_c + 1 \text{ K}$  ( $\Delta\tau_{C2}^* = 3.45137 \times 10^{-3}$ , see below), our calculated value of the correlation length is  $\xi = 68.6323 \text{ \AA}$  (i.e.,  $\frac{\xi}{\alpha_c} \simeq 7.8$ ), while the experimental values are  $\xi = 71.14 \text{ \AA}$  **(author?)** [50],  $\xi = 64.66 \text{ \AA}$  **(author?)** [53], and  $\xi = 67.56 \text{ \AA}$  **(author?)** [21]. Especially considering the light scattering measurements of the isothermal susceptibility and the turbidity of xenon reported by Güttinger and Cannell **(author?)** [21], we note that the turbidity data are fitted in the Orstein-Zernike approximation within a 1% precision in the temperature range  $28 \text{ mK} \leq T - T_c \leq 2.54 \text{ K}$  [i.e.,  $9.6 \times 10^{-5} \lesssim \Delta\tau^* \lesssim 8.76 \times 10^{-3}$ ], using the present theoretical estimation of the correlation length and isothermal compressibility. In particular, we estimate the reference value  $\tau (T_{\text{or}} = T_c + 0.6677 \text{ K}) = 4.1067 \text{ m}^{-1}$  of the turbidity, in excellent agreement with the Güttinger and Cannell's one  $\tau (T_{\text{or}}) = 4.1 \text{ m}^{-1}$  **(author?)** [21], without any adjustable parameter.

### c. Mean and master forms of a theoretical crossover function

The master modifications of the mean crossover functions of Eqs. (1) and (2) use the following values of three master (i.e., constant) factors **(author?)** [17]

$$\begin{aligned} \Theta^{\{1f\}} &= 4.288 \times 10^{-3} \\ \mathbb{L}^{\{1f\}} &= 25.6936 \\ \Psi^{\{1f\}} &= 1.73847 \times 10^{-4} \end{aligned} \quad (\text{A8})$$

The two scale factors  $\vartheta$  and  $\psi_{\rho}$  [see Eq. (40)] needed by the massive renormalization scheme are related to  $Y_c$  and  $Z_c$  through the equations

$$\begin{aligned} \vartheta &= Y_c \Theta^{\{1f\}} = 0.021069 \\ \psi_{\rho} &= (Z_c)^{-\frac{1}{2}} \Psi^{\{1f\}} = 3.2507 \times 10^{-4} \end{aligned} \quad (\text{A9})$$

In addition, the values of Eq. (61) for the metric prefactors  $\mathbb{L}_{0,\mathcal{L}}^*$  and  $\mathbb{X}_{0,\mathcal{L}}^*$  are calculated by using the following equations

$$\begin{aligned} \mathbb{L}_{0,\mathcal{L}}^* &= \frac{Z_{\xi^+}^{\pm} Z_{\xi^+}^{\pm} (Y_c)^{-\nu}}{(Y_c)^{-\nu}} \\ &= \frac{Z_{\xi^+}^{\pm} Z_{\xi^+}^{\pm} (Y_c)^{-\nu}}{[\mathbb{L}^{\{1f\}} \times (\Theta^{\{1f\}})^{\nu}]} = 0.443526 \\ \mathbb{X}_{0,\mathcal{L}}^* &= \frac{Z_{\chi^+}^{\pm} Z_{\chi^+}^{\pm} (Z_c)^{-1} (Y_c)^{-\gamma}}{(Z_c)^{-1} (Y_c)^{-\gamma}} \\ &= \frac{Z_{\chi^+}^{\pm} Z_{\chi^+}^{\pm} (Z_c)^{-1} (Y_c)^{-\gamma}}{[(\mathbb{L}^{\{1f\}})^{-d} (\Psi^{\{1f\}})^{-2} (\Theta^{\{1f\}})^{\gamma}]} = 0.214493 \end{aligned} \quad (\text{A10})$$

These two independent prefactors are two characteristic parameters of xenon, which permit to calculate all the

other xenon prefactors of the modified crossover functions, in conformity with the two-scale-factor universality.

## 2. Theoretical representation of the isothermal compressibility in the temperature range $T - T_c \lesssim 5 - 10 \text{ K}$

We can immediately compare all the published  $\kappa_T(\Delta T) = \frac{1}{\rho} \left( \frac{\partial \rho}{\partial p} \right)_T$  data for xenon at  $\rho = \rho_c$ , to the estimated values by using the mean crossover function of Eq. (2) and the xenon parameter set of Eq. (39). A complete view of the results is shown in Fig. 5 which covers about six decades on the temperature distance (the data sources are given below; see Table V). The related numerical resolution of this picture is such that the size of each data point (including the calibration data points defined below) corresponds to a relative error-bar of  $\pm 5\%$ , while the thickness of the theoretical curve (label MR) accounts for one of  $\pm 3\%$ . As expected from our previous analysis (author?) [10], no difference larger than  $\pm 5\%$  is visible between the curve and the experimental data points on the extended asymptotic domain (labeled EAD) such as  $T - T_c \lesssim 5 \text{ K}$ , i.e.,  $\Delta\tau^* \lesssim \mathcal{L}_{\text{EAD}}^{\text{Xe}} = \frac{\mathcal{L}_{\text{EAD}}^{\{1f\}}}{Y_c} \approx 2 \times 10^{-2}$  (see also below the Fig. 7 and the related discussion). In addition, the thickness of each (colored) line, having characteristic slope  $\gamma_{e,pVT}$ , amplitude  $\Gamma_{e,pVT}^+$ , and color indexation given in Table V, represents  $\pm 1.5\%$  relative error-bar.

### a. Data sources for xenon isothermal compressibility

As shown in the lower part of Figure 5, the complete temperature range  $1 \text{ mK} \lesssim \Delta T \lesssim 400 \text{ K}$  (i.e.  $3 \times 10^{-6} \lesssim \Delta\tau^* \lesssim 1$ ) is covered by successive overlap between  $\kappa_T$  data which originate from three distinct experimental methods:  $pVT$  measurements with labels  $pVT$  (B) (author?) [44], (M) (author?) [47], and (HS) (author?) [46]; light diffusion or turbidity measurements with label LS (GC) (author?) [21], and Franhauffer interferometry measurements with label IF (HM) (author?) [54, 55].

Within the main part of the temperature distance to  $T_c$  [typically  $0.1 \text{ K} \lesssim \Delta T \lesssim 400 \text{ K}$ , (i.e.,  $3 \times 10^{-3} \lesssim \Delta\tau^* \lesssim 1$ )],  $\kappa_T$  is obtained from  $pVT$  measurements (author?) [44, 46, 47], generally using graphical (author?) [12] or numerical fitting (author?) [42] of the  $[p(\rho)]_T$  isotherms to obtain the slope  $\left( \frac{\partial \rho}{\partial p} \right)_T$  at the selected critical density. We have also reported in Table V the  $\kappa_T$ -values obtained from  $pVT$  measurements which were used in our analysis. A noticeable specific situation occurs for xenon where the high precision of the  $pVT$  measurements of Habgood and Schneider (author?) [46], can be used to check carefully the overlap [in the temperature range  $0.2 \text{ K} \lesssim \Delta T \lesssim 1.8 \text{ K}$ , (i.e.  $6 \times 10^{-4} \lesssim \Delta\tau^* \lesssim 6 \times 10^{-3}$ )] with the optical

methods.

In the intermediate temperature range [typically  $30 \text{ mK} \lesssim \Delta T \lesssim 15 \text{ K}$ , (i.e.,  $10^{-4} \lesssim \Delta\tau^* \lesssim 5 \times 10^{-2}$ )], the analyses of the light (diffusion or transmission) intensity measurements (author?) [21], as a function of  $\Delta T = T - T_c$ , provide interrelated data of the correlation length  $\xi$  and isothermal susceptibility  $\chi_{\rho,T}$ .  $\kappa_T$  is related to  $\chi_{\rho,T}$  by  $\chi_{\rho,T} = \left( \frac{\partial \rho}{\partial \mu_\rho} \right)_T = \rho^2 \kappa_T$ .

In the closest temperature range [ $1 \text{ mK} \lesssim \Delta T \lesssim 10 \text{ K}$ , (i.e.,  $10^{-4} \lesssim \Delta\tau^* \lesssim 3 \times 10^{-2}$ )], the fluid density profile versus the cell height subjected to the gravitational field generates Franhauffer interferograms (author?) [54, 55] which are related to the isothermal compressibility (author?) [55, 56]. However, as already noted by Levelt-Sengers et al (author?) [43], the published results in Ref. (author?) [54] needs to be reconsidered before a quantitative comparison with other ones in overlapping temperature ranges.

In order to focus our attention in the restricted temperature range  $0.3 \text{ K} \lesssim \Delta T \lesssim 5 \text{ K}$ , around the central value  $T \simeq T_c + 1.25 K$  (see below next §), we have also used the isothermal compressibility data obtained from the dynamic lighth scattering data of Cannell and Benedek (author?) [51], and from the static lighth scattering data of Smith et al (author?) [50], as complementary data sources.

A realistic estimation of the experimental uncertainty is of the order of 10% when comparison is made between the data obtained from the different methods (the optical method being of high relative precision but lower absolute precision; see for example Fig. 6 below).

### b. Effective fitting results

To complete our analysis of the Güttinger and Cannell's measurements, we have also made a comparison with the published fitting results, obtained from  $pVT$  data, using the following effective power law with an adjustable *non-Ising* exponent,

$$\kappa_T^* = \Gamma_{e,pVT}^+ (\Delta\tau^*)^{-\gamma_{e,pVT}} \quad (\text{A11})$$

The  $\gamma_{e,pVT}$  and  $\Gamma_{e,pVT}^+$  values are reported in Table VI, in addition with the related finite extension  $\Delta\tau_{\min}^* - \Delta\tau_{\max}^*$  of the experimental temperature range. The labels #6, 5, 4, of the lines of Table VI correspond to the respective labels #6, 5, 4, of the columns of Table II. The typical error-bar values of these fitting results are given in line #6. At each restricted temperature range, we have attached the central value  $\langle \Delta\tau_{e,pVT}^* \rangle = \sqrt{\Delta\tau_{\min}^* \Delta\tau_{\max}^*}$  (in log scale). So that, in the next Fig. 7, each effective power law result is illustrated as a form of a (colored) point-segment (with  $\gamma_{e,pVT}$ -value as a label) covering the range  $\Delta\tau_{\min}^* \leq \Delta\tau^* \leq \Delta\tau_{\max}^*$ , around a central (full) point fixed at  $\langle \Delta\tau_{pVT}^* \rangle$ .

In this Table VI, results (author?) [12] given in line labeled # $\gamma_{\text{MF}}$  correspond to a fit of the  $pVT$  data of

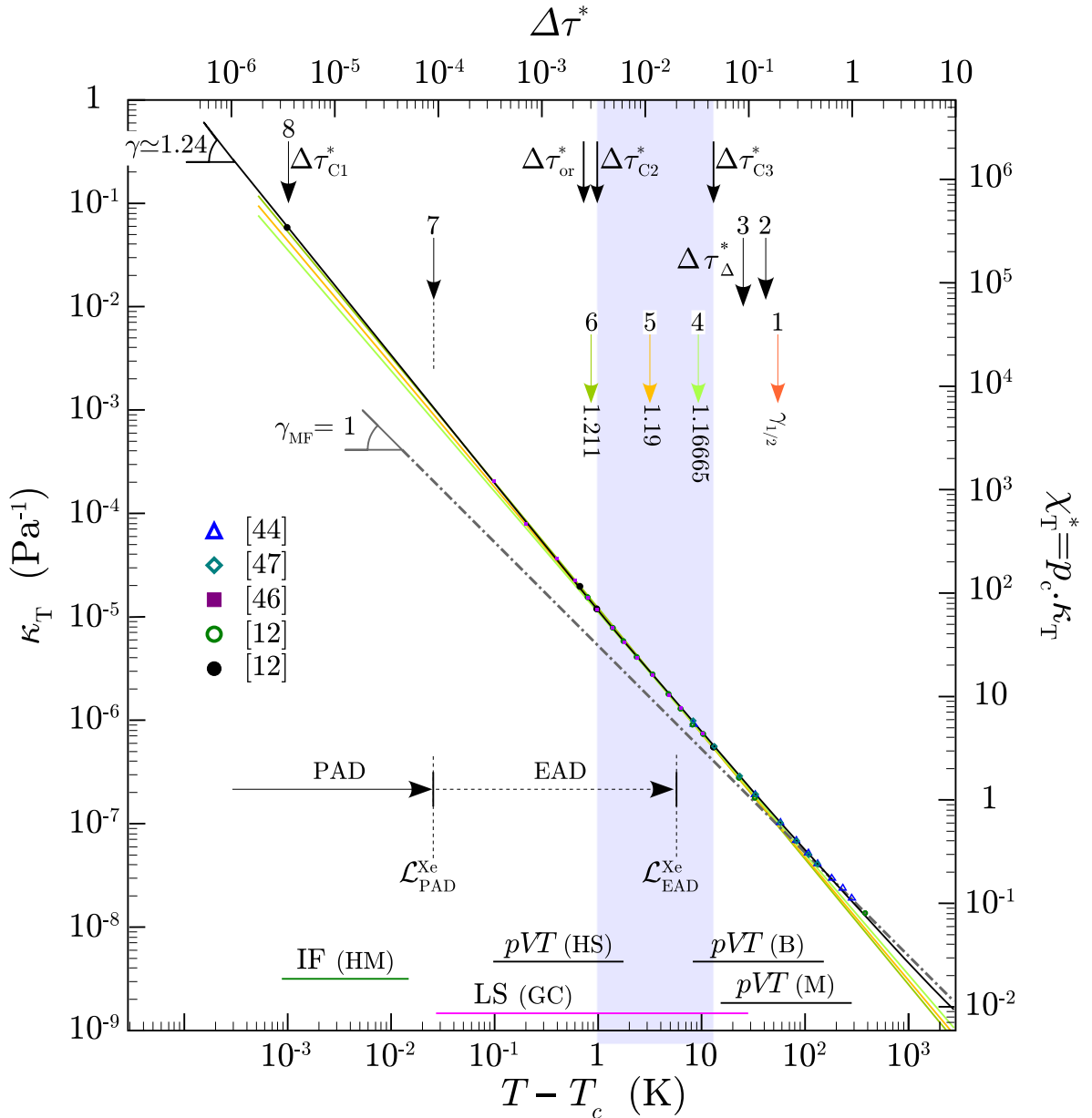


Figure 5: Isothermal compressibility of xenon along the critical isochore; Only the points corresponding to the  $pVT$  data given in Table V are reported; Inserted labels are common for all the figures (see text).

Beattie et al (author?) [44], where the mean-field value  $\gamma_e = \gamma_{MF} = 1$  of the effective exponent can be observed at large temperature distance from  $T_c$  (typically  $\Delta\tau^* > 0.5$ , see also Ref. (author?) [22]).

A similar introduction of the effective power law to analyse the results of light scattering experiments gives access to a quantitative comparison between the  $pVT$  and light scattering measurements of the isothermal compressibility. As a matter of fact, Güttinger and Cannell have claimed that the correction to scaling terms are important by demonstrating that the susceptibility deviates systematically from a simple power law behavior with the

effective exponent value  $\gamma_e = 1.206$ . More precisely, Fig. 2 of Ref. (author?) [21] shows that  $\gamma_e \simeq 1.206$  is the slope of the tangent line to the rough experimental behavior at  $\Delta\tau_{\gamma_e=1.206}^* \simeq 4.5 \times 10^{-3}$ , i.e., the temperature distance which corresponds to the minimum of the deviation curve in this Fig. 2. We have used this result to renew a fit of twelve compressibility data measured in the restricted temperature range  $9.115 \times 10^{-4} \leq \Delta\tau^* \leq 1.95 \times 10^{-2}$  (i.e.,  $0.26 \text{ K} \leq \Delta T \leq 6.90 \text{ K}$ ), i.e., a temperature range with a central value  $\langle \Delta\tau_{e,GC}^* \rangle = 4.215 \times 10^{-3}$ , very close to the  $\Delta\tau_{\gamma_e=1.206}^*$  one. As expected, our fitting values  $\gamma_e = 1.205879$  and  $\Gamma_e^+ = 0.07551466$  (re-

$T - T_c$	283.41	233.41	183.41	133.41	108.41	83.41	58.41	33.41	23.41	13.41	10.41	8.41	6.41	Ref.
$10^6 \kappa_T$	0.01883	0.02348	0.02912	0.04078	0.05095	0.06772	0.10074	0.18695				0.8961		(author?) [44]
				0.04145	0.05185	0.06904	0.10227	0.19268	0.29065	0.56344		1.0099		(author?) [47]
										0.54791	0.73594		1.3020	(author?) [12]
										0.555 ( $\pm 0.008$ )				(author?) [12]
$T - T_c$	4.91	3.41	2.41	1.80	1.4	1.0	0.6677*	0.8	0.6	0.4	0.2	0.1	0.001	
$10^6 \kappa_T$				5.7371	7.8543	11.858			22.701	36.640	79.11	204.86		(author?) [46]
	1.7835	2.7224	4.1139					15.432						(author?) [12]
						11.95 ( $\pm 0.15$ )	19.64* ( $\pm 1\%$ )						58562 ( $\pm 800$ )	(author?) [12]

Table V: Values of the isothermal compressibility  $\kappa_T$  (expressed in  $\text{Pa}^{-1}$ ) of xenon obtained from the  $pVT$  measurements along the critical isochore  $\rho_c = 1113 \text{ kg m}^{-3}$ , as a function of  $T - T_c$  (expressed in K); The lower part corresponds to data obtained within the Ising-like extended asymptotic domain; Asterisk indicates the reference values used by Güttinger and Cannell to calibrate their light scattering measurements of the isothermal compressibility; (see text).

	$\gamma_{e,pVT}$	$\Gamma_{e,pVT}^+$	Ref.	$\Delta\tau_{\min}^*$	$\Delta\tau_{\max}^*$	$\langle \Delta\tau_{pVT}^* \rangle$	$\Delta\tau_{\text{th}}^*$ (Table II)	$R\% (\Gamma_{e,pVT}^+)_{\Gamma_{e,\text{th}}^+}$	$\vartheta_{\mathcal{L}}$ Eq. (74)
#6	1.211 ( $\pm 0.02$ )	0.0743 ( $\pm 0.015$ )	(author?) [43]	$6.9 \times 10^{-4}$	$6.2 \times 10^{-3}$	$2.07 \times 10^{-3}$	$2.95 \times 10^{-3}$	2.3	0.04676
#5	1.190	0.0793	(author?) [42]	$2.8 \times 10^{-3}$	$4.6 \times 10^{-2}$	$1.13 \times 10^{-2}$	$1.135 \times 10^{-2}$	-1.9	0.01429
#4	1.1665	0.089	(author?) [14]	$6.2 \times 10^{-3}$	$8.1 \times 10^{-2}$	$2.24 \times 10^{-2}$	$3.338 \times 10^{-2}$	0.1	0.02618
# $\gamma_{\text{MF}}$	1	0.11	(author?) [12]	0.5	1	$7.1 \times 10^{-1}$	( $\infty$ )	30.	n.a.

Table VI: Lines with labels #6, 5, 4 (corresponding to the columns with same labels in Table II): Effective exponent  $\gamma_{e,pVT}$  (column 2) and amplitude  $\Gamma_{e,pVT}^+$  (column 3) of a power law description of Eq. (A11), for  $\kappa_T^*$  obtained from xenon  $pVT$  measurements in the temperature range and (geometrical) mean temperature  $\langle \Delta\tau_{pVT}^* \rangle = \sqrt{\Delta\tau_{\min}^* \Delta\tau_{\max}^*}$  (column 6); see references given in column 4; Calculated values of the local temperature distance  $\Delta\tau_{\text{th}}^*$  (column 7) are from Table II line10; Residuals  $R\% (\Gamma_{e,pVT}^+)_{\Gamma_{e,\text{th}}^+}$  (column 8), expressed in %, between experimental ( $\Gamma_{e,pVT}^+$ ) xenon amplitude and calculated ( $\Gamma_{e,\text{th}}^+$ ) xenon amplitude from Table II line 12; Calculated values of xenon crossover parameter  $\vartheta_{\mathcal{L}}$  (column 10) from Eq. (74); Line with label # $\gamma_{\text{MF}}$ : Equivalent results for  $\gamma_e = \gamma_{\text{MF}} = 1$  (see text); n.a.: non available.

ported in line #GC<sub>e</sub> of Table VII), are in excellent agreement with the Güttinger and Cannell's ones  $\gamma_e = 1.206$  and  $\Gamma_e^+ = 0.075135$ . The latter amplitude value was calculated applying a -4% correction (corresponding to the fit deviation observed in this restricted temperature range) to the effective amplitude of the published original fit. This resulting power law behavior may be seen from Fig. 6 which gives the % residual between the dimensionless isothermal compressibility and the fitting equation  $\kappa_{T,\text{GC}_e}^* = 0.07551466 (\Delta\tau^*)^{-1.205879}$ . For us, the most important consequence of the high *relative* precision of the Güttinger and Cannell's measurements is the demonstration that a well-defined local value  $\gamma_e \simeq 1.20588$  of the effective exponent can be measured at a well-defined local value ( $T - T_c \simeq 1.260 \text{ K}$ ) of the temperature distance to  $T_c$ . Accordingly, by expressing now the condition  $\gamma_{e,\text{th}} = 1.205879$  in complement to the similar eight conditions given in Table II for the theoretical crossover function of Eq. (2), such a local value of the effective exponent must be observed at  $\Delta\tau_{\text{th}}^* (\gamma_{e,\text{th}} = 1.2058) = 4.347 \times 10^{-3}$ , while the calculated local values of the effective theoretical and xenon ampli-

tudes are  $\mathbb{Z}_{\chi_e}^+ = 0.396926$  and  $\Gamma_{e,\text{th}}^+ (\gamma_{e,\text{th}} = 1.2058) = 0.0747481$ . We will exploit the noticeable agreement between the experimental and theoretical local value of the effective power law behavior in the last § of the Appendix. We note that the calculated value of the correlation length is then  $\frac{\xi(\gamma_e \simeq 1.20588)}{\alpha_c} \simeq 6.764$ , i.e., within our expected range for the Ising-like extended asymptotic domain previously defined by the condition  $\ell^* = \frac{\xi}{\alpha_c} \gtrsim 3$ .

Previously, in a first approach independent of any one-parameter crossover theory, it is necessary to control that the compressibility data obtained by any other measurement method covering a similar restricted temperature range, are satisfying this effective power law behavior with comparable values of the related effective amplitudes. This is the object of the results given in lines # $pVT$ ,  $CB$ ,  $SGB$  of Table VII (see also Fig. 6), where we have used:

i) line # $pVT$ , the  $pVT$  data of Table V covering the temperature range  $0.1 \text{ K} \leq T - T_c \leq 10.41 \text{ K}$  (i.e.,  $3.451 \times 10^{-4} \leq \Delta\tau^* \leq 3.593 \times 10^{-2}$ );

ii) lines # $CB$ , the dynamic lighth scattering data of Cannell and Benedek (author?) [51] covering the tem-

	$\gamma_e$	$\Gamma_e^+$	Ref.	$\frac{\Delta\tau_{\min}^*}{\Delta\tau_{\max}^*}$	$\langle \Delta\tau_{\gamma_e}^* \rangle$	$\Delta\tau_{\text{th}}^*$	$\Gamma_{e,\text{th}}^+$	$R\%(\Gamma_e^+)_{\Gamma_{e,\text{th}}^+}$	$Z_{\chi,e}^+$	$\vartheta_{\mathcal{L}}$	Eq. (
$GC_e$	1.205879	0.07551466	t.w.	$9.115 \times 10^{-4}$ $1.95 \times 10^{-2}$	$4.215 \times 10^{-3}$	$4.347 \times 10^{-3}$	0.0747481	1.03	0.396926	0.028	
$pVT$	1.204519	0.07590869	t.w.	$3.451 \times 10^{-4}$ $3.593 \times 10^{-2}$	$3.521 \times 10^{-3}$	$4.778 \times 10^{-3}$	0.075298	0.81	0.40195	0.026	
CB(a)	1.21	0.076845	(author?) [51]	$6.9 \times 10^{-4}$ $6.9 \times 10^{-2}$	$6.9 \times 10^{-3}$						
(b)	1.201586	0.0780485	t.w.	$3.451 \times 10^{-4}$ $2.5886 \times 10^{-2}$	$2.989 \times 10^{-3}$						
(c)	1.201586	0.0768207	t.w.			$5.804 \times 10^{-3}$	0.076466	0.46	0.41283	0.023	
SGB(a)	$1.21 \pm 0.03$	0.06742	(author?) [50]	$1.553 \times 10^{-4}$ $1.76 \times 10^{-2}$	$1.653 \times 10^{-3}$						
(b)	1.204381	0.0679096	t.w.	$1.5877 \times 10^{-4}$ $1.723 \times 10^{-2}$	$1.653 \times 10^{-3}$						
(c)	1.204381	0.0755227	t.w.			$4.823 \times 10^{-3}$	0.075354	0.22	0.40246	0.022	

Table VII: Fitting results using an effective power law equation  $\kappa_T^* = \Gamma_e^+ (\Delta\tau^*)^{-\gamma_e}$  in a restricted temperature range  $\Delta\tau_{\min}^* \leq \Delta\tau^* \leq \Delta\tau_{\max}^*$  (see text); The calculated local values of the temperature distance  $\Delta\tau_{\text{th}}^*$  (column 7), the xenon amplitude  $\Gamma_{e,\text{th}}^+$  (column 8), the universal amplitude  $Z_{\chi,e}^+$  (column 10), and the xenon crossover parameter  $\vartheta_{\mathcal{L}}$  (column 11), are for each condition  $\gamma_{e,\text{th}} = \gamma_e$ ; t.w.: this work.

perature range  $0.2 \text{ K} \leq T - T_c \leq 20 \text{ K}$ , i.e.,  $6.9 \times 10^{-4} \leq \Delta\tau^* \leq 6.9 \times 10^{-2}$ , and

iii) lines #*SGB*, the static lighth scattering data of Smith et al (author?) [50] covering the temperature range  $0.045 \text{ K} \leq T - T_c \leq 5.1 \text{ K}$ , i.e.,  $1.553 \times 10^{-4} \leq \Delta\tau^* \leq 1.76 \times 10^{-2}$ .

In the *pVT* case, the fitting values of the exponent-amplitude pair confirm the power law behavior observed from Güttinger and Cannell's measurements of high relative precision. On the other hand, we have reported the initial fitting results [lines #*CB*, *SGB*, (a)] of Refs. (author?) [50, 51]. They are only used to illustrate quantitatively the effects due to a large uncertainty on measurements of the geometrical factors in light scattering experiments (author?) [50], or to an indirect estimation of the magnitude of the compressibility from an elaborate and complex analysis of the Brillouin spectra of xenon (author?) [51]. For example, the numerical values found from Ref. (author?) [50] with  $\gamma_e = 1.21$  can be multiplied by a factor  $\frac{1.63}{1.43} = \frac{0.076845}{0.06742} \simeq 1.14$  to match those reported in Ref. (author?) [51]. However, in spite of the importance ( $\simeq (10 - 20)\%$ ) of these effects, we have confirmed with our fitting results [lines #*CB*, *SGB*, (b)] that the value of the effective exponent is well in the range  $\gamma_e \simeq 1.20 - 1.21$  for the restricted temperature range selected here. In addition, the large uncertainty on the experimental value of the effective amplitude can be decreased by using our calibrated value of the isothermal compressibility at  $T = T_c + 1 \text{ K}$ . For example, after calibration [lines #*CB*, *SGB*, (c)], the effective amplitude for Cannell and Benedek's data was lowered by 1.573%, while the one for Smith et al's data was increased by

11, 21%, in agreement with around  $\simeq 14\%$  initial deviation between these two data set.

Finally, as reported in column 9 of Table VII, the percent deviation  $\%R(\Gamma_e^+)_{\Gamma_{e,\text{th}}^+} = 100 \left( \frac{\Gamma_e^+}{\Gamma_{e,\text{th}}^+(\gamma_{e,\text{th}} = \gamma_e)} - 1 \right)$  between the experimental and theoretical effective amplitudes for the four experimental values of the effective exponent  $\gamma_e$  is on the 1%-level. In Fig. 6, we have also reported the residuals  $\%R(\kappa_T^*)_{GC_e} = 100 \left( \frac{\kappa_T^*}{\kappa_{T,GC_e}^*} - 1 \right)$  (expressed in %) between each experimental data  $\kappa_T^*$  and the calculated one  $\kappa_{T,GC_e}^*$  using the effective power law  $\kappa_{T,GC_e}^* = 0.07551466 (\Delta\tau^*)^{-1.205879}$  as reference (see line #*GC\_e* in Table VII). We note the data agreement at the same percent level that the precision on the calibrated values of the isothermal compressibility, which leads to a conclusion that the “experimental” values of the effective amplitude  $\Gamma_e^+$  are estimated with an uncertainty of 1%.

Therefore, in a second approach focussed on the validity test of the one-parameter crossover modelling in pure fluids, which will be discussed below in § A.3, all these fitting results with effective values of the exponents observed in a small restricted temperature range at large temperature distance to  $T_c$  are appropriate:

- i) to check the calibration of the leading asymptotic amplitude  $\Gamma^+$  (with  $\gamma$  fixed);
- ii) to verify the uniqueness of the scale factor  $\vartheta$  by estimating the related local values of  $\vartheta_{\mathcal{L}}$ , and then,
- iii) to control the master values of the leading amplitude  $Z_{\chi}^+ = 0.119$  [related to  $\Gamma^+$ , see Eq. (A5)] and the confluent amplitude  $Z_{\chi}^{1,+} = 0.555$ , [related to  $\vartheta$ , see Eq. (A5)].

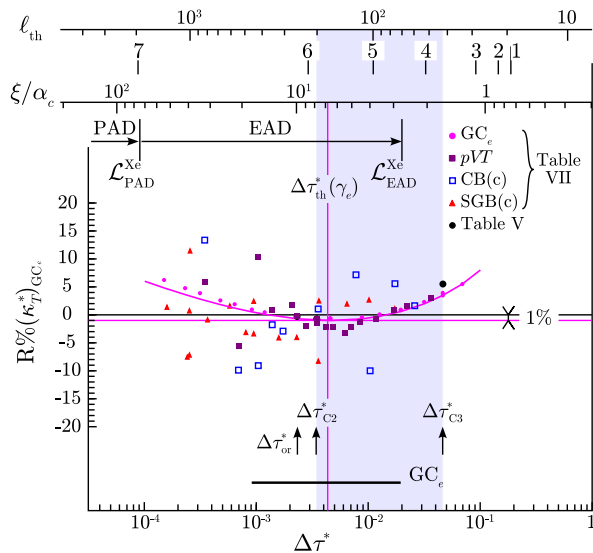


Figure 6: Residuals  $\%R(\kappa_T^*)_{GC_e}$  (expressed in %) of the  $\kappa_T^*$  data from the effective power law  $\kappa_{T,GC_e}^* = 0.07551466 (\Delta\tau^*)^{-1.205879}$  (see text); The horizontal and vertical (pink) lines permit to define the local values of the effective amplitude ( $\Gamma_{e,\gamma_e}^+ = 0.99 \times 0.07551466$ ) and the temperature distance [ $\Delta\tau_{th}^*(\gamma_e) = 4.347 \times 10^{-3}$ , see Table VII] where the line of slope  $\gamma_e = 1.205879$  and equation  $\kappa_T^* = \Gamma_{e,\gamma_e}^+ (\Delta\tau^*)^{-\gamma_e}$ , is tangent to the experimental singular behavior measured by Güttinger and Cannell, at the contact point of coordinates  $\{\Delta\tau_{th}^*(\gamma_e); 0.99\kappa_{T,GC_e}^*[\Delta\tau_{th}^*(\gamma_e)]\}$  (see also Table VII and text); Horizontal segment labeled  $GC_e$ : restricted temperature range of the fit by the effective power law  $\kappa_{T,GC_e}^* = 0.07551466 (\Delta\tau^*)^{-1.205879}$ ; (colored) symbols: see inserted legend and Tables V and VII; All the other inserted labels are identical to the ones previously used.

*c. Data comparison from reference to the master crossover function*

Data comparisons are magnified in the three parts (a), (b), and (c), of Figure 7 (in lin-log scale), either as a function of  $\Delta\tau^*$  in the lower horizontal axis, or as a function of the theoretical ( $\ell_{th}$ ) and master ( $\ell^* = \frac{\xi}{\alpha_c}$ ) correlation lengths (**author?**) [10] in the upper horizontal axis. The extensions of the Ising-like preasymptotic and extended asymptotic domains, the selected  $\gamma_e$ -conditions of Table II, and each experimental temperature range, are illustrated as in Fig. 2.

The asymptotic behavior of the quantity  $\frac{\kappa_T^*}{(\Delta\tau^*)^{-\gamma}}$  estimated from the crossover function [(black) curve MR] is given in Figure 7a. Such a presentation magnifies the role of the theoretical  $\gamma$ -value on the determination of the leading amplitude  $\Gamma^+$  close to  $T_c$  (given by an horizontal asymptotic limit for  $\Delta\tau^* \rightarrow 0$ ). Correlatively, at large values of  $\Delta\tau^*$ , the increasing contribution of the confluent corrections is well demonstrated by the decreasing  $\gamma_{e,pVT}$ -values, here given by the direction of each point-segment closely tangent to the MR curve (see Table VI). Only the published experimental data points

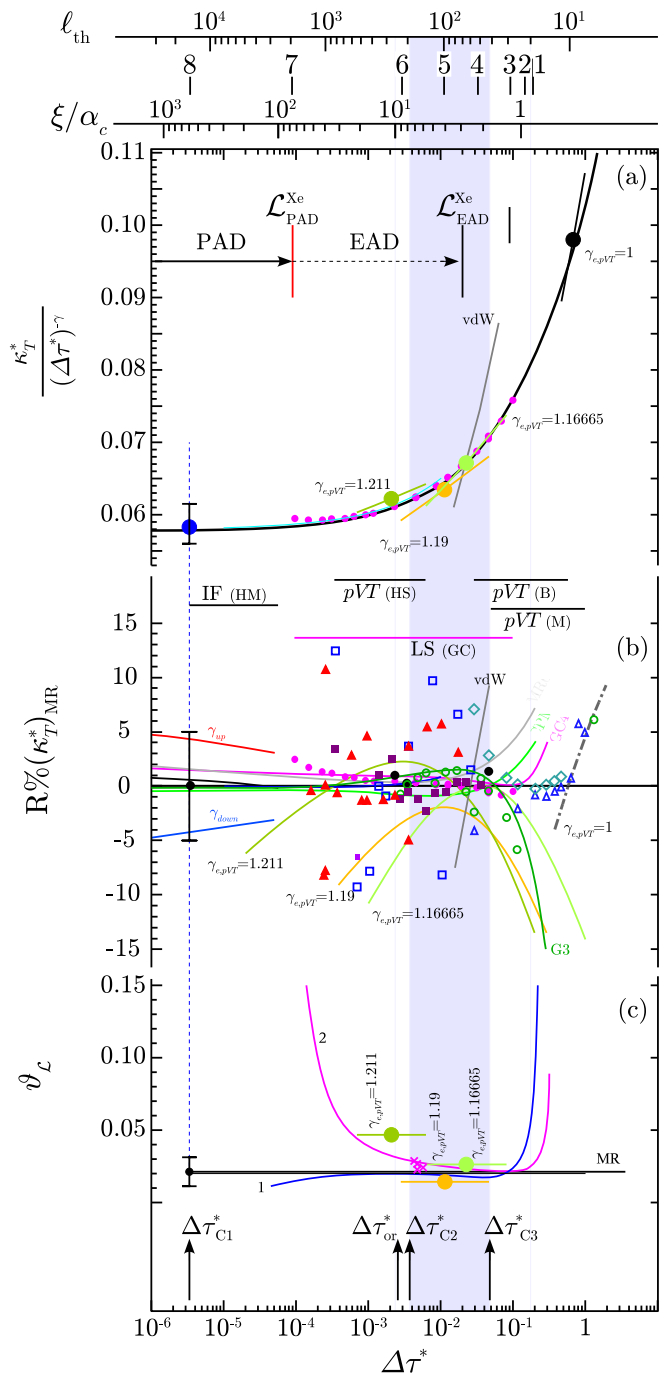


Figure 7: Fitting results of xenon isothermal compressibility  $\kappa_T^*$ , as a function of  $\Delta\tau^*$  (lower horizontal axis) or correlation lengths (upper horizontal axes), by using Eq. (23) with xenon parameters of Eq. (40); (a)  $\frac{\kappa_T^*}{(\Delta\tau^*)^{-\gamma}}$  (full black line: calculated confluent correction from the crossover function); (b) Residuals  $\%R(\kappa_T^*)_{MR}$  (expressed in %), for all the experimental data and fitting results selected in this work from reference to the theoretical estimation by the crossover function; (c) Same as Fig. 4(b), calculated  $\vartheta_L$  [line MR: using the scale dilation method; line 1: from Eq. (71); line 2: from Eq. (74)]; colored point-segments: from Table VI, column 10; crosses: from Table VII, column 11]; All the inserted labels and symbols are identical to the ones of the previous figures (see text).

[(pink) small circles] and fitting result [GC4 (pink) line] of Güttinger and Cannell's measurements are reported in this Fig. 7(a).

The residual  $R\% (\kappa_T^*)_{\text{MR}} = 100 \left[ \frac{\kappa_T^*}{\kappa_{T,\text{MR}}^*} - 1 \right]$ , expressed in %, for all the selected data, are reported in part (b). The accurate ( $\sim \pm 3\%$ ) theoretical representation of  $pVT$  data of Habgood and Schneider and light scattering data of Güttinger and Cannell confirms that the extended asymptotic domain is well such that  $\Delta\tau^* \lesssim \mathcal{L}_{\text{EAD}}^{\text{Xe}} \sim 0.02 - 0.03$ , which well corresponds to the range  $\ell^* = \frac{\xi}{\alpha_c} \gtrsim 2 - 3$  of accurate theoretical representation of the master singular behavior of the correlation length, as previously observed.

In Figs 7(a) and (b), a significant difference occurs in the case of the actual mean field like behavior represented by the segment  $\gamma_{pVT} = \gamma_{\text{MF}} = 1$  (see line 5 of Table II). In the temperature range  $90 \text{ K} \lesssim \Delta T \lesssim 300 \text{ K}$ , (i.e.,  $3 \times 10^{-1} \lesssim \Delta\tau^* \lesssim 1$ ), the effective classical-to-critical crossover for xenon is not accounted for by the mean crossover function. In addition, each part (a) and (b) also contains the relative position of a grey segment (labeled vdW) which corresponds to the mean-field-like equation  $\kappa_T^* \Delta\tau^* = \frac{1}{6}$ , where xenon is assimilated to a van der Waals fluid (i.e. with  $\gamma_{e,\text{vdW}} = 1$  and  $\Gamma_{e,\text{vdW}}^+ = \frac{1}{6}$ ). That clearly illustrates the failure of the van der Waals equation of state close to the liquid-gas critical point.

Figure 7(c) is similar to Figure 4(b). Now we have added the point-segment representation of the values of  $\vartheta_{\mathcal{L},pVT}$  calculated using Eq. (74) and the fitting results of the  $pVT$  measurements with Eq. (A11), as reported in Table V. We will return below to the discussion of these  $pVT$  results which confirm that the xenon crossover is characterized by a unique value [Eq. (61)] of the scale factor  $\vartheta(\text{Xe})$  over the temperature range where  $\frac{\xi}{\alpha_c} \gtrsim 2 - 3$ .

### 3. Data calibration and related discussion to the uniqueness of the crossover parameter

As already evidenced in the seventy's (author?) [42], fitting the experimental singular behavior using Wegner-like expansion with a limited number of terms generates large uncertainty in the amplitude determination, due to the low convergence of this expansion. Examining more carefully the isothermal compressibility data obtained from interferometry (author?) [55], light scattering (author?) [21], and  $pVT$  (author?) [44, 46, 47] measurements, it was noted by one of us (author?) [12], that a restricted three-term Wegner-like expansion, with fixed exponent values  $\gamma_I = 1.24 \pm 0.01$  and  $\Delta_I = \frac{1}{2} \pm 0.05$ , can provide satisfactory representation of the  $\kappa_T$  singular behavior in the range  $T - T_c \lesssim 13 \text{ K}$  (see for example the curve G3 in Figure 7b) which corresponds to Eq. (43) with  $\Gamma^+ = 0.0577$ ,  $a_{1\chi}^+ = a_{\chi}^+ = 1.55$ ,  $a_{2\chi}^+ = -1.3$ , and  $a_{3\chi}^+ = 0$ ; see Table IV, last line). It was conjointly shown that  $\Gamma^+$ ,  $a_{\chi}^+$ , and  $a_{2\chi}^+$  can also be calculated using three

calibrated values at three selected temperature distances (in logarithmic scale, see below). The correlative main results were the estimation of  $\min(a_{\chi,\text{min}}^+ \simeq 0.6)$  and  $\max(a_{\chi,\text{max}}^+ \simeq 1.8)$  values of  $a_{\chi}^+$  and the evaluation of the correlated error-bars which can then be controlled by a careful analysis of the residuals.

We recall the main advantages of such a three points calibration approach, first by examining the estimation of the leading amplitude and its attached uncertainty for the closest point to the critical point.

#### a. Calibration of the leading amplitude the closest to the critical point

At  $T - T_c = 1 \text{ mK}$  ( $\Delta\tau_{\text{C1}}^* = 3.45137 \times 10^{-6}$ ), which corresponds to the “lowest” temperature distance accessible by interferometry experiments of Hocken and Moldover (HM) (author?) [55], the standard dimensionless value of the isothermal compressibility was defined such that  $\kappa_{T,1}^* (\Delta\tau_{\text{C1}}^*) = \Gamma_I^+ (\Delta\tau_{\text{C1}}^*)^{-\gamma_I} = \Gamma_{\text{MR6max}}^+ (\Delta\tau_{\text{C1}}^*)^{-\gamma_{\text{MR6max}}} = (3.415 \pm 0.035) \times 10^5$  with  $\{\gamma_I = 1.240; \Gamma_I^+ = 0.0574 \pm 0.0006\}$  and  $\{\gamma_{\text{MR6max}} = 1.24194; \Gamma_{\text{MR6max}}^+ = 0.0563 \pm 0.0006\}$ . These initial values of the leading amplitude  $\Gamma^+$  were re-evaluated accounting for the small difference with  $\gamma = 1.2395935$ . Similar re-evaluation was conjointly made for the leading amplitudes  $\xi^+$  (of the dimensionless correlation length  $\xi^*$ ) and  $B$  (of the dimensionless order parameter density  $\Delta\rho_{LV}^*$ ) due to the small differences in  $\nu$  and  $\beta$  values. The updated values of the corresponding leading amplitudes (such as  $\Gamma^+(\text{Xe}) = 0.05782 \pm 0.0006$ ) were then used to optimize the new central values of the corresponding master amplitudes (such as  $Z_{\chi}^+ = 0.119$  reported here), using Eqs. (A6), corresponding values of the critical parameters [see Eq. (A2)], and the updated value of the universal amplitude combination  $(\xi^+)^{-d} \frac{\Gamma^+}{B^2} = (Z_{\xi}^+)^{-d} \frac{Z_{\chi}^+}{Z_M^2} = (Z_{\xi}^+)^d \frac{1}{Z_{\chi}^+ Z_M^2} = (R_{\xi}^+)^{-d} R_C^+ = 2.92638$  (with  $R_{\xi}^+ = 0.2696967$  and  $R_C^+ = 0.057406$  (author?) [7]). Finally, selecting  $Z_{\chi}^+ = 0.119$  and  $Z_M = 0.468$  (author?) [73] as “central” values for two independent master amplitudes, any other (master and physical) leading amplitude can be calculated with the numerical precision of the massive renormalization scheme. For example, the number of digits in the quoted value  $Z_{\xi}^+ = 0.570481$  is similar to the numerical precision of  $Z_{\xi}^+ = 2.121008$  (see Table Ia), and more generally, data of Eqs. (A6) to (A11) are obtained according to this scheme.

Considering now the  $\gamma$  differences between the theoretical estimations, we can admit that the mean value  $\gamma = 1.2395935$  (see Table Ib) is on the range  $\gamma_{\text{low}} \simeq 1.235 \leq \gamma \leq \gamma_{\text{high}} \simeq 1.242$ . The max value  $\gamma_{\text{high}} \simeq 1.242$  was used in our initial fitting of the GC data (see line 2 of Table III), while the min value  $\gamma_{\text{low}} \simeq 1.235$  was

recently estimated from the minimal subtraction scheme (**author?**) [29]. The correlative effect on the  $\Gamma^+$  value is of the order of  $\pm 3\%$ , as shown by the curves (labeled  $\gamma_{\text{high}}$  and  $\gamma_{\text{low}}$  in Fig. 7c) related to the power law  $\kappa_{\text{high,low}}^* = \Gamma_{\text{high,low}}^+ (\Delta\tau^*)^{-\gamma_{\text{up,down}}}$ , with  $\Gamma_{\text{high}}^+ = 0.056$  and  $\Gamma_{\text{low}}^+ = 0.062$ , respectively. This theoretical uncertainty level appears then comparable to the experimental one ( $\sim \pm 5\%$ ), when the  $\gamma$  and  $\Gamma^+$  values are obtained from interferometry measurements close to the critical point. For example, the initial “free” values are  $\gamma = 1.23$  and  $\Gamma^+ = 0.062 \pm 0.006$  (**author?**) [55], while a subsequent analysis made for fixed  $\gamma = 1.24$  gives  $\Gamma^+ = 0.058 \pm 0.002$  (**author?**) [56]. As a result, we note that the calibrated value of  $\kappa_{T,1}^*$  ( $\Delta\tau_{C1}^*$ ) =  $(3.415 \pm 0.035) \times 10^5$  remains well representative of the theoretical analyses of the interferometry measurements at this closest temperature distance to  $T_c$ . However, we also recall that the uncertainty associated to the experimental determination of the critical temperature (roughly estimated of the order of  $\pm 0.5$  mK) cannot be accounted for in the above analyses of the interferometry measurements.

To partly conclude, when the exponent  $\gamma$  is fixed to its *Ising-like* theoretical value  $\gamma = 1.2395935$ , the above standard value of the isothermal compressibility at  $T - T_c = 1$  mK is a realistic asymptotic constraint to fix the “central” value  $\Gamma^+(\text{Xe}) = 0.05782(\pm 0.0006)$  of the leading amplitude, before to analyse the isothermal compressibility data over larger temperature distances to the (known) critical temperature with the objective to estimate the contribution of the confluent corrections to scaling in the xenon case.

*b. Calibration of the first amplitude of the critical confluent correction to scaling beyond the Ising-like preasymptotic domain*

As indicated above, by using two other points of calibration properly selected to cover the temperature range of optical and  $pVT$  measurements, provides an analytical estimation of  $a_{\chi}^+ \equiv a_{1\chi}^+$  and  $a_{2\chi}^+$  in Eq. (43) [with  $\gamma$ ,  $\Delta$  fixed, and  $a_{3\chi}^+ = 0$ ]. Indeed, from the calibrated values  $\{\Delta\tau_{C2}^*; \kappa_{T,2}^*\}$  and  $\{\Delta\tau_{C3}^*; \kappa_{T,3}^*\}$ , we can define the pairs  $\left\{ \Delta\tau_2^* = \frac{\Delta\tau_{C2}^*}{R_{32}}; Y_2 = \frac{\kappa_{T,2}^*}{\Gamma^+(\Delta\tau_{C2}^*)^{-\gamma}} - 1 \right\}$  and  $\left\{ \Delta\tau_{C3}^*; Y_3 = \frac{\kappa_{T,3}^*}{\Gamma^+(\Delta\tau_{C3}^*)^{-\gamma}} - 1 \right\}$ . We obtain

$$a_{\chi}^+ \equiv a_{1\chi}^+ = \frac{Y_2 (R_{32})^{2\Delta} - Y_3}{\Delta\tau_{C3}^* \left[ (R_{32})^{\Delta} - 1 \right]} \quad (\text{A12})$$

and

$$a_{2\chi}^+ = \frac{Y_3 - Y_2 (R_{32})^{2\Delta}}{(\Delta\tau_{C2}^* \Delta\tau_{C3}^*)^{\Delta} \left[ (R_{32})^{\Delta} - 1 \right]} \quad (\text{A13})$$

Equations (A12) and (A13) have convenient analytic forms to check the influence of the selected values for

the exponents and calibrated points (**author?**) [12]. For example, we can choose the calibrated points at  $T_2 - T_c = 1$  K ( $\Delta\tau_{C2}^* = 3.45137 \times 10^{-3}$ ) with  $\kappa_{T,2} = (1.195 \pm 0.012) \times 10^{-5} \text{ Pa}^{-1}$  ( $\kappa_{T,2}^* = 69.8 \pm 0.7$ ), and  $T_3 - T_c = 13.41$  K ( $\Delta\tau_{C3}^* = 4.62829 \times 10^{-2}$ ) with  $\kappa_{T,3} = (5.55 \pm 0.08) \times 10^{-7} \text{ Pa}^{-1}$  ( $\kappa_{T,3}^* = 3.24 \pm 0.04$ ) (see Table V). Using the updated theoretical values  $\gamma = 1.2395935$ ,  $\Delta = 0.50189$  (see Table Ib),  $\Gamma^+(\text{Xe}) = 0.0578204$ , and the two calibrated pairs  $\{R_{32} = 13.41; Y_2 = 0.071051\}$  and  $\{\Delta\tau_{C3}^* = 4.62829 \times 10^{-2}; Y_3 = 0.242478\}$ , Eq. (A12) gives  $a_{\chi}^+ \equiv a_{1\chi}^+ = 1.25557$ , while Eq. (A13) gives  $a_{2\chi}^+ = -0.569934$ . The small difference with the value  $a_{\chi}^+ = 1.22961$  calculated using Eq. (39), is due to the similar “constrained” adjustment of the first amplitude  $a_M^+$  of the order parameter density (not reported here), which maintains the universal value  $\frac{a_M^+}{a_{\chi}^+} = 0.9$  of the related amplitude ratio (**author?**) [9]. In such an optimized result from two properties, the best central values of the master confluent amplitudes are  $Z_{\chi}^{1,+} = 0.555$  and  $Z_{\mathcal{M}}^1 = 0.4995$ , respectively. However, as previously indicated, a true error-bar of the order of  $\pm 35\%$  (at least) can be attached to these confluent amplitudes in the absence of data calibration closer to  $T_c$ .

*c. The uniqueness of the crossover parameter and the effective extension of the critical domain beyond the Ising-like preasymptotic domain*

Since the asymptotic amplitude  $\Gamma^+$  is now fixed, the effective exponent-amplitude pair  $\gamma_{e,pVT}; \Gamma_{e,pVT}^+$  reported in columns 2 and 3 of Table VI, can be used to calculate the value of a crossover parameter  $\vartheta_{\mathcal{L},pVT}$  at each “local” temperature distance  $\langle \Delta\tau_{pVT}^* \rangle$ , using the scale transformation of Eq. (73), and the theoretical values of  $Z_{\chi}^+$  and  $Z_{\chi,e}^+(\gamma_{e,pVT})$  given in Tables I and II. The corresponding values of  $\vartheta_{\mathcal{L},pVT}|_{\gamma_{pVT}=cte}$  are given in last column of Table VI. Each  $pVT$  result for  $\vartheta_{\mathcal{L},pVT}|_{\gamma_{pVT}}$  as a function of  $\Delta\tau^*$ , has then been illustrated in Fig. 7 (c) as a point-segment form. The “local” value  $\langle \Delta\tau_{pVT}^* \rangle$  is close to the calculated one  $\Delta\tau_{\text{th}}^*$  (see columns 6 and 7 in Table VI). In addition, the %-residuals  $R_{\Gamma_{e,\text{th}}^+} = 100 \left( \frac{\Gamma_{e,\text{th}}^+(\gamma_{e,pVT})}{\Gamma_{e,\text{th}}^+(\gamma_{e,pVT})} - 1 \right)$  between the effective amplitudes compare favorably with the estimated experimental precision (see column 8 in Table VI). Therefore, at large temperature distance from  $T_c$ , we obtain a significant confirmation that the values of the effective crossover parameter are close to the one of the asymptotic scale factor  $\vartheta = 0.021069$ , and can then be considered as independent of  $\Delta\tau^*$  in the Ising-like extended asymptotic domain.

Using in a similar manner the fitting results given in Table VII, we have obtained the corresponding values of  $\vartheta_{\mathcal{L}}$  given in column 11. However, we have now a better control of the related uncertainty, thanks to

the high precision of the light scattering experiment of Güttinger and Cannell. As a matter of fact, admitting in a first approach that the values of  $\Gamma^+$ ,  $\langle \Delta\tau_{\gamma_e}^* \rangle$ ,  $Z_{\chi}^+$  and  $Z_{\chi,e}^+(\gamma_e)$  are known with zero uncertainty, while  $\Gamma_e^+ = \Gamma_{e,\text{th}}^+(1 + \delta\Gamma)$ , with  $\delta\Gamma \sim 1 - 2\%$ , it is easy to show

from Eq. (74) and  $\vartheta = \left( \frac{1}{Z_{\chi}^+ Z_{\chi,e}^+} \times \frac{\Gamma_{e,\text{th}}^+}{\Gamma^+} \right)^{\frac{1}{\gamma - \gamma_e}}$  that

$$\vartheta = \frac{\theta_{\mathcal{L}}}{(1 + \delta\Gamma)^{\frac{1}{\gamma - \gamma_e}}} \simeq \frac{\theta_{\mathcal{L}}}{\left(1 + \frac{\delta\Gamma}{\gamma - \gamma_e}\right)} \quad (\text{A14})$$

Looking then to the percent deviation reported in Fig. 6, we can observe that the true tangent (pink) line of slope  $\gamma_e = 1.20588$  has an amplitude  $\simeq 1\%$  lower than the amplitude of the effective power law  $\kappa_{T,\text{GC}_e}^* = 0.07551466 (\Delta\tau^*)^{-1.205879}$  used as a reference (see also Table VII column 9, where the calculated value of the residual is  $-1\%$  in line #GC<sub>e</sub>). From Eq. (A14) with  $\delta\Gamma = 0.01$  and  $\vartheta_{\mathcal{L}} \simeq 0.02851$  (see line #GC<sub>e</sub>, column 11, Table VII), we obtain  $\vartheta \simeq 0.021988$  which is in excellent agreement (+4.38%) with our initial estimation  $\vartheta \simeq 0.21069$  from the scale dilatation method. As previously underlined, the precise description by a local exponent value defining the slope of the tangent line to the singular behavior of the isothermal compressibility of xenon at a well-defined temperature distance to  $T_c$ , is one of the major points of interest of the Güttinger and Cannell's results to validate the one-parameter crossover modelling predicted by the massive renormalization scheme. In a similar manner, using Eq. (A14) with  $\delta\Gamma$  and  $\vartheta_{\mathcal{L}}$  given in lines #pVT, CB(c), SGB(c) of Table VII, we obtain  $\vartheta \simeq 0.02160, 0.021232, 0.021136$ , and the corresponding deviations +2.52%, 0.77%, 0.32%, respectively for the three other fitting results reported in Table VII.

Obviously, similar effect is produced by the uncertainty level attached to the determination of the leading amplitude  $\Gamma^+$ , justifying oncemore its independent estimation from a "standard" value of the isothermal compressibility at a temperature distance well-inside the Ising-like preasymptotic domain.

Henceforth, the importance of the scaling form of Eq. (74) in the determination of a unique asymptotic value for the scale factor  $\vartheta$  is clearly established. Moreover,

Eq. (74) is valid in the range  $\frac{\xi}{\alpha_c} \gtrsim 2.5 - 3$ , or  $\Delta\tau^* \lesssim \mathcal{L}_{\text{EAD}}^{\text{Xe}} \simeq 0.02$  in xenon case.

One complementary remark can be formulated.

Outside the Ising-like extended asymptotic domain, i.e., typically for  $\Delta\tau^* \geq 10^{-1}$  in xenon case, it is well-established that the Ising-like universality is not valid. For example, increasing the temperature distance to  $T_c$  on the pVT data analyzes, we are able to observe the continuous decreasing behavior of  $\gamma_{e,pVT}$  until a value close to mean-field value  $\gamma_{e,pVT} \approx \gamma_{\text{MF}} = 1$  when  $\Delta\tau^* \lesssim 1$  (see Table VI). That unambiguously discriminates a sharp domain, i.e. typically  $0.3 \leq \Delta\tau^* \leq 0.5$ , where  $\gamma_{e,pVT}$  crosses the "mean" crossover value  $\gamma_{\frac{1}{2}} = \frac{\gamma + \gamma_{\text{MF}}}{2} \approx 1.12$  (as initially reported in Ref. (author?) [22]). For xenon, this classical-to-critical crossover "crossing" is expected close to  $\frac{\xi}{\alpha_c} \lesssim 1$ , that means that the correlation length is of the same order of magnitude or lower than the short-range molecular interaction. In Table VI, the non-defined value  $\vartheta_{\mathcal{L},pVT}|_{\gamma_{pVT}=1} (\sim \infty)$ , corroborates that the mean-field behavior predicted by the theoretical crossover function with  $\vartheta = 0.0210$ , is not compatible with the pVT experimental result  $\Gamma_{e,\gamma_{\text{MF}}}^+ \simeq 0.11$ . Such a typical limit of the mean-field-like range (see upper part of Figure 3) is well-illustrated by the corresponding transformation between the opened squares represented in Figure 3, which cannot account for the "experimental" location of the opened circle when  $\gamma_e = \gamma_{\text{MF}} = 1$ .

Finally, Figure 7 (c) confirms that the effective extended critical domain of xenon, corresponding to the condition  $\frac{\xi}{\alpha_c} \gtrsim 3$  discussed in a detailed manner in Ref. (author?) [10], is well characterized by a single crossover parameter whose value at the largest temperature range is comparable to the one of the asymptotic scale factor estimated from the scale dilatation method. We can conclude that singular behavior of any property in this extended critical domain of xenon can be calculated in conformity with the universal features predicted by the massive renormalization scheme, only using the required four critical coordinates to define the position and tangent surface of its actual liquid-gas critical point on the  $p, v_p, T$  phase surface, as expected by one of us two decades ago.

---

[1] M. A. Anisimov and J. V. Sengers, in *Equations of State for Fluids and Fluid Mixtures*, Part I, J.V. Sengers, R.F. Kayser, C.J. Peters, and H.J. White, Jr., Eds. (Elsevier, Amsterdam, UK, 2000) pp. 381-434.  
[2] see for example Zinn Justin, *Euclidean Field Theory and Critical Phenomena*, 3<sup>rd</sup> ed. (Oxford University Press, 1996).  
[3] A. Pellissetto, P. Rossi, and E. Vicari, Phys. Rev. E **58**, 7146 (1998).  
[4] C. Bagnuls and C. Bervillier, J. Phys. (Paris) Lett., **45**, L-95 (1984).

[5] C. Bagnuls and C. Bervillier, Phys. Rev. B **32**, 7209 (1985).  
[6] C. Bagnuls and C. Bervillier, D. Meiron, and B. Nickel, Phys. Rev. B **35**, 3585 (1987); **65**, 149901(E) (2002). Verifier la page 3585.  
[7] C. Bagnuls and C. Bervillier, Phys. Rev. E **65**, 066132 (2002).  
[8] R. Guida and J. Zinn-Justin, J. Phys. A: Math. Gen. **31**, 8103 (1998).  
[9] Y. Garrabos and C. Bervillier, Phys. Rev. E **74**, 021113 (2006).

- [10] Y. Garrabos, F. Palencia, C. Lecoutre-Chabot, C. J. Erkey, and B. Le Neindre, *Phys. Rev. E* **73**, 026125 (2006).
- [11] Y. Garrabos, C. Lecoutre-Chabot, F. Palencia, D. Brosetta, B. Le Neindre, and C. J. Erkey, *Phys. Rev. E* **75**, 061112 (2007).
- [12] Y. Garrabos, Ph. D. Thesis, University of Paris (1982).
- [13] Y. Garrabos, *J. Phys. (Paris)* **46**, 281 (1985) [for an english version see e-print/cond-mat/0512408].
- [14] Y. Garrabos, *J. Phys. (Paris)* **47**, 197 (1986).
- [15] Y. Garrabos, B. Le Neindre, R. Wunenburger, C. Lecoutre-Chabot, and D. Beysens, *Int. J. Thermophys.* **23**, 997 (2002).
- [16] Y. Garrabos, *Phys. Rev. E* **73**, 056110 (2006).
- [17] Y. Garrabos, C. Lecoutre-Chabot, F. Palencia, B. Le Neindre, and C. J. Erkey, preprint (2006) (see cond-mat/).
- [18] F. J. Wegner, *Phys. Rev. B* **5**, 4529 (1972).
- [19] K. G. Wilson and J. Kogut, *Phys. Rep.* **12 C**, 75 (1974).
- [20] In this approach of scaling, we use the correlation length and the susceptibility as independent properties in terms of the two-scale-factor universality. We can then ignore the universal features related to the additive universal constant of the heat capacity. Moreover, in a pure fluid case, the critical background constant is mixed with the non-universal contribution of the regular background terms.
- [21] H. Güttinger and D. S. Cannell, *Phys. Rev. A* **24**, 3188 (1981).
- [22] C. Bagnuls, C. Bervillier, and Y. Garrabos, *J. Phys. (Paris) Lett.* **45**, L-127 (1984).
- [23] C. Edwards, J. A. Lipa, and M. J. Buckingham, *Phys. Rev. Lett.* **20**, 496 (1968).
- [24] J. M. H. Levelt Sengers and J. V. Sengers, in “Progress in Liquid Physics”, Ed. C. A. Croxton (John Wiley & Sons, New York, 1978) pp. 103.
- [25] V. Privman, P. C. Hohenberg, and A. Aharony, Universal critical point amplitude relations, in “*Phase Transitions and Critical Phenomena*”, Vol. 14, Ed. C. Domb and J. B. Lebowitz (Academic Press, New York, 1991).
- [26] M. A. Anisimov, A. Povodyrev, V. Kulikov, and J. V. Sengers, *Phys. Rev. Lett.* **75**, 3146 (1995).
- [27] E. Luijten and H. Meyer, *Phys. Rev. E* **62**, 3257 (2000).
- [28] I. Hahn, F. Zhong, M. Barmatz, R. Haussmann, and J. Rudnick, *Phys. Rev. E* **63**, 055104(R) (2001).
- [29] F. Zhong, M. Barmatz, and I. Hahn, *Phys. Rev. E* **67**, 021106 (2003).
- [30] F. Zhong and M. Barmatz, *Phys. Rev. E* **70**, 066105 (2004).
- [31] V. Dohm, *Z. Phys. B: Condens. Matter* **60**, 61 (1985); R. Schloms and V. Dhom, *Europhys. Lett.* **3**, 413 (1987); *Nucl. Phys. B* **328**, 639 (1989); *Phys. Rev. B* **42**, 6142 (1990).
- [32] E. Luijten, H. W. J. Blöte, and K. Binder, *Phys. Rev. Lett.* **79**, 561 (1997).
- [33] E. Luijten and K. Binder, *Europhys. Lett.* **47**, 311 (1999).
- [34] E. Luijten and K. Binder, *Phys. Rev. E* **58**, R4060 (1998); **59**, 7254(E) (1999).
- [35] M. H. Müser and E. Luijten, *J. Chem. Phys.* **116**, 1621 (2002).
- [36] Z. Y. Chen, P. C. Albright, and J. V. Sengers, *Phys. Rev. A* **41**, 3161 (1990).
- [37] Z. Y. Chen, A. Abbaci, S. Tang, and J. V. Sengers, *Phys. Rev. A* **42**, 4470 (1990).
- [38] M. A. Anisimov, S. B. Kiselev, J. V. Sengers, and S. Tang, *Physica A* **188**, 487 (1992).
- [39] Belyakov and Kiselev, *Physica A* 190 (1992).
- [40] V. A. Agayan, M. A. Anisimov, and J. V. Sengers, *Phys. Rev. E* **64**, 026125 (2001).
- [41] J. S. Kouvel and M. E. Fisher, *Phys. Rev.* **136**, A 1626 (1964).
- [42] J. M. H. Levelt Sengers and J. V. Sengers, *Phys. Rev. A* **12**, 2622 (1975).
- [43] J. M. H. Levelt Sengers, W. L. Greer, and J. V. Sengers, *J. Phys. Chem. Ref. Data* **5**, 1 (1976).
- [44] J. A. Beattie, R. J. Barriault, and J. S. Brierley, *J. Chem. Phys.* **19**, 1219 (1951); **19**, 1222 (1951).
- [45] M. A. Weinberger and W. G. Schneider, *Can. J. Chem.* **30**, 422 (1952); **30**, 847 (1952).
- [46] H. W. Habgood and W. G. Schneider, *Can. J. Chem.* **32**, 98 (1954); **32**, 164 (1954).
- [47] A. Michels, T. Wassenaar, and P. Louwerse, *Physica* **20**, 99 (1954).
- [48] V. A. Rabinovich, L. A. Tokina, V. M. Berezin, *Teplo. Vys. Temp.* **11**, 64 (1973); V. A. Abovskii and V. A. Rabinovich, *Teploenerg.* **3**, 44-57 (1971); **6**, 45-93 (1973).
- [49] M. Giglio and G. B. Benedek, *Phys. Rev. Lett.* **23**, 1145 (1969).
- [50] I. W. Smith, M. Giglio, and G. B. Benedek, *Phys. Rev. Lett.* **27**, 1556 (1971).
- [51] D. S. Cannell and G. B. Benedek, *Phys. Rev. Lett.* **25**, 1157 (1970).
- [52] H. L. Swinney and D. L. Henry, *Phys. Rev. A* **8**, 2566 (1973).
- [53] H. Güttinger and D. S. Cannell, *Phys. Rev. A* **22**, 285 (1980).
- [54] W. T. Estler, R. Hocken, T. Charlton, and L. R. Wilcox, *Phys. Rev. A* **12**, 2118 (1975).
- [55] R. J. Hocken and M. R. Moldover, *Phys. Rev. Lett.* **37**, 29 (1976).
- [56] J. V. Sengers and M. R. Moldover, *Phys. Lett.* **66A**, 44 (1978).
- [57] W. J. Camp, D. M. Saul, J. P. Van Dyke, and M. Wortis, *Phys. Rev. B* **14**, 3990 (1976).
- [58] D. S. Gaunt and M. F. Sykes, *J. Phys. A* **12**, L25 (1979).
- [59] G.A. Baker, B. G. Nickel, M. S. Green, and D. I. Meiron, *Phys. Rev. Lett.* **36**, 1351 (1976); G.A. Baker, B. G. Nickel, and D. I. Meiron, *Phys. Rev. B* **17**, 1365 (1978).
- [60] J. C. Le Guillou and J. Zinn-Justin, *Phys. Rev. Lett.* **39**, 95 (1977).
- [61] For example, the microscopic spacing order in xenon fluid can be driven by the Lennard Jones like diameter  $\sigma^{LJ}$  of xenon atom, which typically is  $\sigma^{LJ}(\text{Xe}) \simeq 0.4 \text{ nm}$ , i.e. comparable in order of magnitude to the estimated value  $\mathbb{L}_{0,\mathcal{L}}(\text{Xe}) \simeq 0.391 \text{ nm}$ . However, this typical size of xenon atom is one order of magnitude greater than  $[g_{0,\mathcal{L}}(\text{Xe})]^{-1} \simeq 34.3 \cdot 10^{-3} \text{ nm}$  and also significantly greater than the critical thermal wavelength  $\Lambda_{T,c}(\text{Xe}) \simeq 8.95 \cdot 10^{-3} \text{ nm}$ .
- [62] L. M. Stacey, B. Pass, and H. Y. Carr, *Phys. Rev. Lett.* **23**, 1424 (1969).
- [63] A. B. Cornfeld and H. Y. Carr, *Phys. Rev. Lett.* **29**, 28 (1972); **29**, E320 (1972).
- [64] V. G. Baidakov, A. M. Rubshtein, V. R. Pomortsev, and I. J. Sulla, *Phys. Lett. A* **131**, 119 (1988).
- [69] C. E. Hayes and H. Y. Carr, *Phys. Rev. Lett.* **39**, 1558 (1977).
- [66] C. W. Garland and J. Thoen, *Phys. Rev. A* **13**, 1601,

- (1976).
- [67] J. Thoen and C. W. Garland, Phys. Rev. A **10**, 1311, (1974).
- [68] T. S. Chang, C. W. Garland, and J. Thoen, Phys. Rev. A **16**, 446, (1977).
- [69] C. E. Hayes and H. Y. Carr, Phys. Rev. Lett. **39**, 1558 (1977).
- [70] D. Balzarini and O. G. Mouritsen, Phys. Rev. A **28**, 3515 (1983).
- [71] U. Narger and D. A. Balzarini, Phys. Rev. B **42**, 6651 (1990).
- [72] K. A. Gillis, I. I. Shinder, and M. R. Moldover, Phys. Rev. E **70**, 021201 (2004); **72**, 051201 (2005).
- [73] As a typical example related to the master value  $\mathcal{Z}_M = 0.468$ , the leading amplitude  $B = \mathcal{Z}_M (Z_c)^{-\frac{1}{2}} (Y_c)^\beta$  (with  $\beta = 0.3258$ ) of the singular behavior of the order parameter density of xenon takes the value  $B = 1.46998$  which compare remarkably to the more recent experimental values  $B = 1.470 \pm 0.010$  and  $B = 1.479 \pm 0.011$  (with  $\beta = 0.327$ ) obtained in Ref. (author?) [71].